The Biogeochemistry of Marine Nitrous Oxide

By

Caitlin Frame

B.A. Harvard University, 2004

Submitted in partial fulfillment of the requirements for the degree of

Doctor of Philosophy

at the

Massachusetts Institute of Technology

and the

Woods Hole Oceanographic Institution

June 2011

© Caitlin Frame

All rights reserved

Signature of Author _____

Joint Program in Oceanography/Applied Ocean Science and Engineering
Massachusetts Institute of Techology
and Woods Hole Oceanographic Institution
March 1 2011

Certified by _____

Dr. Katen Casciotti
Thesis Surpervisor

_____

Dr. Mark Kurz
Interim Supervisor

Accepted by _____

Dr. Roger Summons
Chair, Joint Committee for Chemical Oceanography
Massachusetts Institute of Technology
Woods Hole Oceanographic Institution

THE BIOGEOCHEMISTRY OF MARINE NITROUS OXIDE

BY CAITLIN H FRAME

Submitted to the Department of Marine Chemistry and Geochemistry, Massachusetts
Institute of Technology-Woods Hole Oceanographic Institution Joint Program in
Chemical Oceanography on March 15, 2011
In partial fulfillment of the requirements for the degree of Doctor of Philosophy

Abstract

Atmospheric nitrous oxide N_2O concentrations have been rising steadily for the past century
as a result of human activities. In particular, human perturbation of the nitrogen cycle has
increased the N_2O production rates of the two major sources of this greenhouse gas, soil and
the ocean. Nitrification, and particularly ammonia oxidation, is one of the major processes
that produces N_2O in the ocean. In this thesis, a series of stable isotopic methods have been
used to characterize the biogeochemical controls on N_2O production by marine nitrification
as well as the natural abundance stable isotopic signatures of N_2O produced by marine
nitrifiers. This thesis shows that in addition to chemical controls on N_2O production rates
such as oxygen (O_2) and nitrite (NO_2^-) concentrations, there are also biological controls
such as nitrifier cell abundances and coastal phytoplankton blooms that may influence N_2O
production by ammonia oxidizers as well. Ammonia oxidizers can produce N_2O through
two separate biochemical mechanisms that have unique isotopic signatures. Using culture-
based measurements of these signatures, we conclude that one of these pathways, nitrifier-
denitrification, may be a significant source of N_2O produced in the South Atlantic Ocean
and possibly the global ocean.

Thesis Supervisor: Dr. Karen Casciotti

Assistant Professor, Stanford University

Acknowledgements

Thesis Supervisor: Dr. Karen Casciotti

Assistant Professor, Stanford University

TABLE OF CONTENTS

1. INTRODUCTION: NITROUS OXIDE IN THE OCEAN

1. INTRODUCTION

Nitrous oxide (N_2O) is the third most important greenhouse gas in terms of anthropogenic climate forcing (Solomon et al., 2007). Human activities have increased the flux of N_2O from the earth's surface by 40-50% since the industrial revolution (Hirsch et al., 2006), so that at 322 ppb, its current atmospheric concentration is 17% higher than the preindustrial concentration (Sowers et al., 2002; Prinn et al., 1990). Accelerating rates of microbial nitrogen cycling driven by agricultural use of nitrogen fertilizer have probably fed rising N_2O concentrations. Biomass burning, cattle farms, and fossil fuel combustion also make smaller contributions to the atmospheric N_2O budget (Solomon et al., 2007; Galloway et al., 2004). In the atmosphere, N_2O has a 120 year life span before reactions in the stratosphere destroy it (Prinn et al., 1990; Volk et al., 1997). These reactions include photolytic and photo-oxidation processes that also destroy ozone (O_3), increasing the earth surface's exposure to ultraviolet radiation (Crutzen, 1970; Johnston, 1971). With the phase out of industrially manufactured O_3-depleting substances, N_2O is now ranked as the most important O_3 depleting substance in the atmosphere (Ravishankara et al., 2009).

The oceans are an important source of N_2O, contributing up to 25% of global emissions (Nevison et al., 2004; Solomon et al., 2007). Marine N_2O is produced by cycling of the ocean's natural or baseline nitrogen inventory as well as growing amounts of nitrogen supplied to the ocean by human activities. Several microbial processes are involved in N_2O cycling. In oxic thermocline waters, nitrifying microorganisms are thought to produce N_2O, while in suboxic and anoxic waters, denitrification can both produce and consume N_2O (Cohen and Gordon, 1978; Naqvi et al., 2009). Nitrification is the sequential conversion of ammonia (NH_3) to nitrite (NO_2^-) and then nitrate (NO_3^-). This O_2 dependent two-step process is carried out by distinct groups of chemolithoautotrophic microorganisms: ammonia-oxidizing bacteria and archaea convert NH_3 to NO_2^- and nitrite oxidizing bacteria convert NO_2^- to NO_3^- (Martens-Habbena et al., 2009; Ward and O'Mullan, 2005). N_2O is a byproduct of ammonia oxidation, the first nitrification step. In contrast, denitrification is an anaerobic heterotrophic process that reduces NO_3^- to dinitrogen N_2 during organic

11

carbon respiration. The enzyme-mediated steps of this process reduce NO_3^- to NO_2^-, nitric oxide (NO), N_2O, and then N_2 (Figure 1).

Marine N_2O was originally attributed to nitrification or denitrification based on where its distributions were in relation to maxima and minima in O_2, NO_2^-, and NO_3^- concentration profiles. In aging, oxic water masses, decreasing O_2 concentrations and increasing NO_3^- concentrations are usually associated with increasing N_2O concentrations, producing especially tight linear correlations between N_2O and O_2 and implicating nitrification as the source of most marine N_2O (Elkins et al., 1978; Oudot et al., 1990; Naqvi and Noronha, 1991; Yoshinari, 1976; Nevison et al., 2003, 1995). However, in low O_2 ($<5\mu M$) environments, the linear relationship found in higher O_2 waters breaks down as more N_2O is produced relative to O_2 consumption (Codispoti and Christensen, 1985). Two different phenomena may explain this nonlinearity. The first is the increased production of N_2O by nitrifiers under low O_2 conditions (Goreau et al., 1980; Nevison et al., 2003). The second is denitrification interrupted by turbulent injections of O_2 that disrupt the full denitrification sequence (Figure 1) and allow the intermediate, N_2O, to escape further reduction (Firestone and Tiedje, 1979; Naqvi et al., 2000). There is also a sink for N_2O in anoxic waters such as those in the cores of the stable oxygen deficient zones (ODZs) in the Eastern Tropical North and South Pacific and the Arabian Sea where low N_2O concentrations are maintained, providing evidence that denitrification consumes N_2O in addition to NO_3^- and NO_2^- (Elkins et al., 1978; Cohen and Gordon, 1978; Naqvi and Noronha, 1991; Farias et al., 2009). Although N_2O is destroyed in these core anoxic waters, the ODZs are still net sources of N_2O because of high production rates above and below their main anoxic zones (Naqvi and Noronha, 1991).

Microbiological and enzymological research has provided a mechanistic understanding of how nitrification and denitrification produce N_2O (Payne et al., 1971; Poth and Focht, 1985; Ritchie and Nicholas, 1972; Hooper and Terry, 1979). A fraction of the NH_3 oxidized by ammonia oxidizers is released as N_2O rather than NO_2^- (Goreau et al., 1980; Ritchie and Nicholas, 1972). The size of this fraction, or yield, is variable and understanding what controls it is a primary focus of marine N_2O research. There are two pathways of N_2O

production in ammonia-oxidizing bacteria (Figure 1). The first occurs during the oxidation step, during which NH_3 and O_2 are converted to an intermediate, hydroxylamine (NH_2OH) that is then oxidized to NO_2^-. This intermediate can also decompose to N_2O through an unknown mechanism (Hooper and Terry, 1979; Ritchie and Nicholas, 1972). The second pathway is known as nitrifier-denitrification, which reduces NO_2^- to nitric oxide (NO) and then N_2O using enzymes that bear genetic similarity to those of certain denitrifiers (Poth and Focht, 1985; Ritchie and Nicholas, 1972; Casciotti and Ward, 2001, 2005). It is uncertain whether there is an adaptive significance of nitrifier-denitrification. It is thought to occur preferentially at low O_2 concentrations (Sutka et al., 2004) and in the presence of higher concentrations of NO_2^- (Beaumont et al., 2004). Some have proposed that when O_2 is scarce, NO_2^- acts as an alternative terminal electron acceptor, as it does during denitrification (Zumft, 1997). Others have concluded that the reaction is a means of removing accumulating NO_2^-, which can become toxic at high concentrations (Beaumont et al., 2004; Laanbroek et al., 2002; Ritchie and Nicholas, 1972). In either case, nitrifier-denitrification can significantly increase the amount of N_2O produced by nitrifiers.

Low O_2 environments such as coastal and continental shelf regions as well as the periferies of the ODZs are known to be large net sources of N_2O to the atmosphere (Naqvi et al., 2009). Although some of these suboxic regions occur naturally, several studies have noted that they are expanding and intensifying as a result of global climate change (Stramma et al., 2008). If these trends continue, marine emissions of N_2O may rise substantially (Codispoti, 2010). Low O_2 environments are unique in that aerobic nitrification and anaerobic denitrification may co-occur, leading to significant N_2O production. Identifying their individual contributions to the overall N_2O source is a necessary step before quantitative predictions can be made about the effects of eutrophication and expanding low O_2 zones on marine N_2O production. Stable isotopic measurements of N_2O can provide a way to distinguish between these two processes.

Measuring the amounts of the heavier stable isotopes (^{15}N, ^{18}O, ^{17}O) relative to the lighter stable isotopes (^{14}N, ^{16}O) of nitrogen and oxygen in N_2O provides a passive way to track them through the various nitrogen cycle transformations linked to N_2O. During

13

these transformations, molecules that contain different isotopes of the same element react at slightly different rates. The rate differences impart characteristic isotopic signatures on N_2O molecules as they are produced or consumed. Kinetic fraction factors, designated α_k, are used to keep track of these differences. For example, $\alpha_k = {}^{14}k/{}^{15}k$ and ${}^{14}k$ and ${}^{15}k$ are the respective rates of reaction of molecules containing the light and heavy nitrogen isotopes. When the kinetic fractionation factors are known for individual biological reactions they can be used to reconstruct or constrain the reaction's individual contribution to environmental N_2O distributions. With the development of techniques for measuring intramolecular nitrogen isotope distributions in N_2O (Toyoda and Yoshida, 1999), isotopomer ratios of N_2O are also used to interpret how production and consumption processes shape marine N_2O distributions.

If the isotopic signatures of N_2O from different environments (*e.g.* soil versus marine versus combustion) are unique and well constrained, they can be used to construct global atmospheric isotope budgets. Such budgets are typically used as a way of accounting for all of the known sources and sinks contributing to the net flux of N_2O into the atmosphere. In the ocean, a similar approach may also be taken towards accounting for the relative contributions of different biological processes (*e.g.* nitrification and denitrification) to the marine N_2O source. This thesis focuses on marine nitrification as a source of N_2O, a process whose environmental rates are typically slow, have high spatial and temporal variability, and produce a low yield of N_2O. As discussed below, stable isotopic measurements are particularly well suited to the study of this process because they are sensitive to low rates but can also integrate information about biological N_2O production over large temporal and spatial scales.

2. OVERVIEW

In the following three chapters, the stable isotopic composition of N_2O is used to answer three questions: how much marine N_2O is being produced?, how it is being produced?, and what environmental variables control the yield of N_2O? Stable isotopic methods provide a way to specifically track certain processes and also to integrate the effects of multiple

processes occurring at the same time or in the same location. Different stable isotopic approaches have different strengths and weaknesses. Here, three separate stable isotopic approaches have been adopted to address the same three questions.

In Chapter 2, pure cultures of ammonia-oxidizing bacteria were used to study the effects of basic biogeochemical variables like O_2 and NO_2^- concentrations, and cell density on the yields and isotopic signatures of N_2O that they produced. The advantage of culture based studies is that they allow experimental control over the chemical and isotopic composition of the growth environment and culture conditions for a single species of N_2O producing organisms. The drawback of such studies are that organisms that can be obtained in pure cultures are often not representative of the diversity of nitrifiers found in natural communities and culturing conditions are usually enriched in substrate (NH_3) relative to concentrations found in the ocean. Nevertheless, these effects were reduced by working with a marine strain of ammonia oxidizer and using relatively low substrate concentrations.

In Chapter 3, the motivating questions were whether coastal nitrification rates and the yields of N_2O from nitrification change as the overall productivity of the water increases. Here, the sensitivity of ^{15}N tracer-incubations was used to measure low *in situ* potential nitrification rates and N_2O production rates during a spring phytoplankton bloom in the coastal waters off Cape Cod, Massachusetts. While this technique achieves specificity and sensitivity in the rate measurements, they are potentially influenced by "bottle effects" that cause naturally occurring biological assemblages to behave differently in an incubation environment than they would in their natural environment. Whenever possible, we made an effort to minimize these effects by using large incubation volumes and by keeping incubation periods short (12 and 24 hours). In highly productive natural waters, nutrient regeneration can also have a significant impact on nitrification rate calculations by changing the isotopic composition of the ammonium (NH_4^+) pool over time. Here, the measurements necessary to correct this effect were made by adding NH_4^+ above ambient concentrations, possibly perturbing actual process rates.

In Chapter 4, the natural abundance stable isotope signatures of N_2O measured in the South Atlantic were used to identify the microbial sources and the yields of N_2O in this

15

region. While the process rates measured in the isotope tracer-incubations of Chapter 3 were subject to some experimental uncertainties and low spatial and temporal coverage, in Chapter 4 oceanographic isotopic measurements of dissolved N_2O were collected with high spatial resolution across the central South Atlantic. These data integrate the isotopic impacts of different biological and mixing processes, providing a more holistic view of what processes contribute to marine N_2O production and where in the water column they occur. The study region included the transition from the oligotrophic subtropical gyre to the low O_2 upwelling zone off the coast of southwestern Africa allowing us an opportunity to investigate how natural gradients in productivity, O_2, nutrients, and water mass distributions influence the concentration and isotopic compositions of dissolved N_2O.

Although different techniques are applied in each of the studies that follow, they target the same underlying question of what controls N_2O production by marine nitrifiers. The ultimate goal is to understand the present contribution of the ocean to the global N_2O source and how that contribution will change as human activities influence the climate and the marine nitrogen cycle. By pairing specific N_2O production mechanisms with their isotopic signatures as well as the chemical and biological variables that favor these mechanisms, we have expanded and refined the biogeochemical toolkit used to measure and model marine N_2O production.

REFERENCES

Beaumont, H. J. E., Lens, S., Reijnders, W. N. M., Westerhoff, H. V., and van Spanning, R. J. M. (2004). Expression of nitrite reductase in *Nitrosomonas europaea* involves nsrr, a novel nitrite-sensitive transcription repressor. *Molecular Microbiology*, 54(1):148–158.

Casciotti, K. L. and Ward, B. B. (2001). Dissimilatory nitrite reductase genes from autotrophic ammonia-oxidizing bacteria. *Applied and Environmental Microbiology*, 67(5):2213–2221.

Casciotti, K. L. and Ward, B. B. (2005). Phylogenetic analysis of nitric oxide reductase gene homologues from aerobic ammonia-oxidizing bacteria. *FEMS Microbiology Ecology*, 52:197–205.

Codispoti, L. A. (2010). Interesting times for marine N_2O. *Science*, 327:1339–1340.

Codispoti, L. A. and Christensen, J. P. (1985). Nitrification, denitrification and nitrous oxide cycling in the eastern tropic south pacific ocean. *Marine Chemistry*, 16:277–300.

Cohen, Y. and Gordon, L. I. (1978). Nitrous oxide in the oxygen minimum of the eastern tropical north pacific: evidence for its consumption during denitrification and possible mechanisms for its production. *Deep-Sea Research*, 25:509–524.

Crutzen, P. J. (1970). The influence of nitrogen oxides on the atmospheric ozone content. *Quarterly Journal Review of the Meteorological Society*, 96:320–325.

Elkins, J. W., Wofsy, S., McElroy, M. B., Kolb, C. E., and Kaplan, W. A. (1978). Aquatic sources and sinks for nitrous oxide. *Nature*, 275:602–606.

Farias, L., Castro-Gonsalez, M., Cornejo, M., Charpentier, J., Faundez, J., Boontanon, N., and Yoshida, N. (2009). Denitrification and nitrous oxide cycling within the upper oxycline of the eastern tropical south pacific oxygen minimum zone. *Limnology and Oceanography*, 54(1):132–144.

Firestone, M. K. and Tiedje, J. M. (1979). Temporal change in nitrous oxide and dinitrogen from denitrification following onset of anaerobiosis. *Applied and Environmental Microbiology*, 38(4):673–679.

Galloway, J. N., Dentener, F. J., Capone, D. G., Boyer, E. W., Howarth, R. W., Seitzinger, S. P., Asner, G. P., Cleveland, C. C., Green, P. A., Holland, E. A., Karl, D. M., Michaels, A. F., Porter, J. H., Townsend, A. R., and Vorosmarty, C. J. (2004). Nitrogen cycles: past, present, and future. *Biogeochemistry*, 70:153–226.

Goreau, T. J., Kaplan, W. A., Wofsy, S. C., McElroy, M. B., Valois, F. W., and Watson, S. W. (1980). Production of NO_2^- and N_2O by nitrifying bacteria at reduced concentrations of oxygen. *Applied and Environmental Microbiology*, 40(3):526–532.

Hirsch, A. I., Michalak, A. M., Bruhwiler, L. M., Peters, W., Dlugokencky, E. J., and Tans, P. P. (2006). Inverse modeling estimates of the global nitrous oxide surface flux from 1998-2001. *Global Biogeochemical Cycles*, 20(GB1008):doi:10.1029/2004GB002443.

Hooper, A. B. and Terry, K. R. (1979). Hydroxylamine oxidoreductase of *Nitrosomonas* production of nitric oxide from hydroxylamine. *Biochimica et Biophysica Acta*, 571:12–20.
17

Johnston, H. (1971). Reduction of stratospheric ozone by nitrogen oxide catalysts from supersonic transport exhaust. *Science*, 173(3996):517–522.

Laanbroek, H. J., Bar-Gilissen, M.-J., and Hoogveld, H. L. (2002). Nitrite as a stimulus for ammonia-starved *Nitrosomonas europaea*. *Applied and Environmental Microbiology*, 68(3):1454–1457.

Martens-Habbena, W., Berube, P. M., Urakawa, H., de la Torre, J. R., and Stahl, D. A. (2009). Ammonia oxidation kinetics determine niche separation of nitrifying archaea and bacteria. *Nature*, 461:976–981.

Naqvi, S. W. A., Bange, H. W., Farias, L., Monteiro, P. M. S., Scranton, M. I., and Zhang, J. (2009). Coastal hypoxia/anoxia as a source of CH_4 and N_2O. *Biogeosciences Discussions*, 6:9455–9523.

Naqvi, S. W. A., Jayakumar, D. A., Narvekar, P. V., Naik, H., Sarma, V. V. S. S., D'Souza, W., Joseph, S., and George, M. D. (2000). Increased marine production of N_2O due to intensifying anoxia on the indian continental shelf. *Nature*, 408:346–349.

Naqvi, S. W. A. and Noronha, R. J. (1991). Nitrous oxide in the arabian sea. *Deep-Sea Research*, 38(7):871–890.

Nevison, C., Butler, J. H., and Elkins, J. W. (2003). Global distribution of N_2O and the ΔN_2O - aou yield in the subsurface ocean. *Global Biogeochemical Cycles*, 17(4):30-1–18.

Nevison, C. D., Lueker, T. J., and Weiss, R. F. (2004). Quantifying the nitrous oxide source from coastal upwelling. *Global Biogeochemical Cycles*, 18(GB1018):doi:10.1029/2003GB002110.

Nevison, C. D., Weiss, R. F., and Erickson III, D. J. (1995). Global oceanic emissions of nitrous oxide. *Journal of Geophysical Research*, 100(C8):15809–15820.

Oudot, C., Andrie, C., and Montel, Y. (1990). Nitrous oxide production in the tropical atlantic ocean. *Deep-Sea Research*, 37(2):183–202.

Payne, W. J., Riley, P. S., and Cox, C. D. J. (1971). Separate nitrite, nitric oxide, and nitrous oxide reducing fractions from *Pseudomonas perfectomarinus*. *Journal of Bacteriology*, 106(2):356–361.

Poth, M. and Focht, D. (1985). ^{15}N kinetic analysis of N_2O production by *Nitrosomonas europaea*: an examination of nitrifier denitrification. *Applied and Environmental Microbiology*, 49(5):1134–1141.

Prinn, R., Cunnold, D., Rasmussen, R., Simmonds, P., Alyea, F., Crawford, A., Fraser, P., and Rosen, R. (1990). Atmospheric emissions and trends of nitrous oxide deduced from 10 years of ALE − GAGE data. *Journal of Geophysical Research*, 95(D11):18369–18385.

Ravishankara, A. R., Daniel, J. S., and Portmann, R. W. (2009). Nitrous oxide (N_2O: the dominant ozone-depleting substance emitted in the 21st century. *Science*, 326:123–125.

Ritchie, G. A. F. and Nicholas, D. J. D. (1972). Identification of the sources of nitrous oxide produced by oxidative and reductive processes in *Nitrosomonas europaea*. *Biochemistry Journal*, 126:1181–1191.

Solomon, S., Qin, M., Manning, M., Chen, Z., Marquis, M., Averyt, K., Tignor, M., and Miller, H. (2007). *Climate Change 2007: The Physical Science Basis*. Cambridge University Press, New York, NY, USA.

Sowers, T., Rodebaugh, A., Yoshida, N., and Toyoda, S. (2002). Extending records of the isotopic composition of atmospheric N_2O back to 1800 a.d. from air trapped in snow at the south pole and the greenland ice sheet project ii ice core. *Global Biogeochemical Cycles*, 16(4):doi:10.1029/2002GB001911.

Stramma, L., Johnson, G. C., Sprintall, J., and Mohrholz, V. (2008). Expanding oxygen-minimum zones in the tropical oceans. *Science*, 320:655–658.

Sutka, R. L., Ostrom, N. E., Ostrom, P. H., Gandhi, H., and Breznak, J. A. (2004). Nitrogen isotopomer site preference of N_2O produced by *Nitrosomonas europaea* and *Methylococcus capsulatus* bath. *Rapid Communications in Mass Spectrometry*, 18:1411–1412.

Toyoda, S. and Yoshida, N. (1999). Determination of nitrogen isotopomers of nitrous oxide on a modified isotope ratio mass spectrometer. *Analytical Chemistry*, 71:4711–4718.

Volk, C. M., Elkins, J. W., Fahey, D. W., Dutton, G. S., Gilligan, J. M., Loewenstein, M., Podolske, J. R., Chan, K. R., and Gunson, M. R. (1997). Evaluation of source gas lifetimes from stratospheric observations. *Journal of Geophysical Research*, 102(D21):25543–25564.

Ward, B. B. and O'Mullan, G. D. (2005). Community level analysis: genetic and bio-geochemical approaches to investigate community composition and function in aerobic ammonia oxidation. *Methods in Enzymology*, 397:395–413.

Yoshinari, T. (1976). Nitrous oxide in the sea. *Marine Chemistry*, 4:189–202.

Zumft, W. G. (1997). Cell biology and molecular basis of denitrification. *Microbiology and molecular biology reviews*, 61(4):533–616.

$$NO_2\text{-} \rightarrow NO \rightarrow N_2O \rightarrow N_2$$

$$\uparrow$$

$$N_2O \qquad NO_3\text{-} \qquad \text{Denitrification}$$

Nitrification

$$NH_3 \rightarrow NH_2OH \rightarrow NO_2\text{-} \rightarrow NO \rightarrow N_2O$$
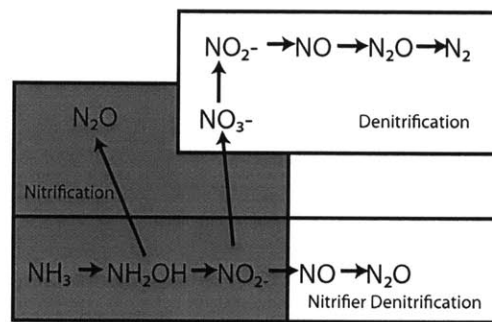
Nitrifier Denitrification

FIGURE 1. The steps in the nitrogen cycle that produce N_2O are nitrification, nitrifier-denitrification, and denitrification. Denitrification can also consume N_2O, converting it to N_2

2. BIOGEOCHEMICAL CONTROLS AND ISOTOPIC SIGNATURES OF NITROUS OXIDE PRODUCTION BY A MARINE AMMONIA-OXIDIZING BACTERIUM

Biogeosciences

Biogeochemical controls and isotopic signatures of nitrous oxide production by a marine ammonia-oxidizing bacterium

C. H. Frame[1,2] and K. L. Casciotti[1]

[1]Marine Chemistry and Geochemistry, Woods Hole Oceanographic Institution, Woods Hole, Massachusetts, USA
[2]Joint Program in Chemical Oceanography, MIT Woods Hole Oceanographic Institution, Woods Hole, Massachusetts, USA

Abstract. Nitrous oxide (N_2O) is a trace gas that contributes to the greenhouse effect and stratospheric ozone depletion. The N_2O yield from nitrification (moles N_2O-N produced per mole ammonium-N consumed) has been used to estimate marine N_2O production rates from measured nitrification rates and global estimates of oceanic export production. However, the N_2O yield from nitrification is not constant. Previous culture-based measurements indicate that N_2O yield increases as oxygen (O_2) concentration decreases and as nitrite (NO_2^-) concentration increases. Here, we have measured yields of N_2O from cultures of the marine β-proteobacterium *Nitrosomonas marina* C-113a as they grew on low-ammonium ($50 \mu M$) media. These yields, which were typically between 4×10^{-4} and 7×10^{-4} for cultures with cell densities between 2×10^2 and 2.1×10^4 cells ml^{-1}, were lower than previous reports for ammonia-oxidizing bacteria. The observed impact of O_2 concentration on yield was also smaller than previously reported under all conditions except at high starting cell densities (1.5×10^6 cells ml^{-1}), where 160-fold higher yields were observed at 0.5% O_2 ($5.1 \mu M$ dissolved O_2) compared with 20% O_2 ($203 \mu M$ dissolved O_2). At lower cell densities (2×10^2 and 2.1×10^4 cells ml^{-1}), cultures grown under 0.5% O_2 had yields that were only 1.25- to 1.73-fold higher than cultures grown under 20% O_2. Thus, previously reported many-fold increases in N_2O yield with dropping O_2 could be reproduced only at cell densities that far exceeded those of ammonia oxidizers in the ocean. The presence of excess NO_2^- (up to 1 mM) in the growth medium also increased N_2O yields by an average of 70% to 87% depending on O_2 concentration. We made stable isotopic measurements on N_2O from these cultures to identify the biochemical mechanisms behind variations in N_2O yield. Based on measurements of $\delta^{15}N^{bulk}$, site preference ($SP = \delta^{15}N^\alpha - \delta^{15}N^\beta$), and $\delta^{18}O$ of N_2O ($\delta^{18}O$-N_2O), we estimate that nitrifier-denitrification produced between 11% and 26% of N_2O from cultures grown under 20% O_2 and 43% to 87% under 0.5% O_2. We also demonstrate that a positive correlation between SP and $\delta^{18}O$-N_2O is expected when nitrifying bacteria produce N_2O. A positive relationship between SP and $\delta^{18}O$-N_2O has been observed in environmental N_2O datasets, but until now, explanations for the observation invoked only denitrification. Such interpretations may overestimate the role of heterotrophic denitrification and underestimate the role of ammonia oxidation in environmental N_2O production.

1 Introduction

The atmospheric concentration of the greenhouse gas nitrous oxide (N_2O) has risen steadily over the last century. Processes in the microbial nitrogen cycle are the largest source of atmospheric N_2O and 20% of this source may come from the oceans (IPCC, 2007). Humans have greatly increased the amount of fixed nitrogen entering the oceans (Galloway et al., 1995), and the functioning of marine microbial ecosystems is shifting in response (Fulweiler et al., 2007; Beman et al., 2005; Naqvi et al., 2000). Understanding the impact of anthropogenic activity on the size of the marine N_2O source requires knowledge of which microbes are involved in N_2O production and how the production is controlled by chemical variables.

Correspondence to: C. H. Frame
(cframe@whoi.edu)

Nitrification, and in particular ammonia oxidation, is thought to dominate N_2O production in oxic water columns (Elkins et al., 1978; Cohen and Gordon, 1979; Goreau et al., 1980; Ostrom et al., 2000; Popp et al., 2002). Over-saturations of dissolved N_2O ($\boxtimes N_2O$, $nmol\,L^{-1}$) are often positively correlated with apparent oxygen utilization (AOU, $\mu mol\,L^{-1}$) (Yoshinari, 1976; Cohen and Gordon, 1978; Elkins et al., 1978). AOU is a tracer of organic matter remineralization. Therefore, the direct relationship between AOU and $\boxtimes N_2O$ is taken as evidence that N_2O is produced as nitrifying organisms convert regenerated NH_3 to NO_2^- and NO_3^-.

Stoichiometric relationships among N_2O production, NO_3^- regeneration, and AOU have been used to convert oceanographic nutrient and O_2 data to estimates of N_2O production (e.g., Codispoti and Christensen, 1985; Fuhrman and Capone, 1991; Jin and Gruber, 2003; Suntharalingam and Sarmiento, 2000) or to use N_2O concentration data to calculate nitrification rates (e.g., Law and Ling, 2001). However, there is not a universal $AOU:N_2O$ ratio and linear $AOU:N_2O$ relationships break down unpredictably in low-O_2 environments (Cohen and Gordon, 1979). Several different factors may contribute to this break-down: 1) at low O_2 concentrations, ammonia-oxidizing bacteria produce higher yields of N_2O per mole of NH_3 oxidized (Goreau et al., 1980; Lipschultz et al., 1981; Jorgensen et al., 1984), 2) heterotrophic denitrifying bacteria produce more N_2O in low-O_2 conditions (Knowles et al., 1981; Payne et al., 1971), 3) in stably anoxic environments denitrifying bacteria are net consumers of N_2O, which they reduce to nitrogen gas (N_2) (Cline et al., 1987), and 4) mixing between waters with different chemical properties influences the slopes of $AOU:N_2O$ linear regressions (Nevison et al., 2003). There is also potential niche overlap among nitrifiers and denitrifiers in low-O_2 environments, making it especially difficult to distinguish between these two N_2O sources. Ammonia-oxidizing bacteria are able to thrive at low O_2 concentrations (Carlucci and Mc-Nally, 1969; Goreau et al., 1980; Codispoti and Christensen, 1985) and it has been suggested that denitrification occurs in oxic ocean waters in the anaerobic interiors of organic particles (Yoshida et al., 1989; Alldredge and Cohen, 1987). To understand how the N_2O budget may respond to global change, we need methods for determining the individual contributions of nitrification and denitrification to the N_2O budget.

Understanding the N_2O source from ammonia-oxidizing bacteria is particularly complicated because these organisms contain two distinct N_2O-producing pathways that may respond differently to geochemical controls. One pathway is the oxidative decomposition of hydroxylamine (NH_2OH), or one of its derivatives, during the conversion of NH_3 to NO_2^- (Hooper and Terry, 1979). The other mechanism, known as nitrifier-denitrification, is the sequential reduction of NO_2^- to NO and then N_2O by the action of the nitrite reductase (NIR, encoded by the gene *nirK*) and the nitric oxide reduc-

tase (NOR, encoded by the gene *norB*). All of the ammonia-oxidizing bacteria that have been screened to date contain the *nirK* and *norB* genes (Casciotti and Ward, 2001; Shaw et al., 2006; Casciotti and Ward, 2005; Cantera and Stein, 2007; Norton et al., 2008; Arp et al., 2007), and the conversion of $^{15}NO_2^-$ to $^{15}N_2O$ has been demonstrated in several genera (Poth and Focht, 1985; Shaw et al., 2006). Archaeal ammonia oxidizers also appear to possess *nirK* and *norB* homologs (Treusch et al., 2005; Hallam et al., 2006; Walker et al., 2010) but it is not known whether the proteins encoded by these genes are involved in N_2O production.

The enzymes involved in nitrifier-denitrification are homologous to those found in a subset of heterotrophic denitrifying bacteria. However, unlike heterotrophic denitrification, nitrifier-denitrification may not be a strictly anaerobic process (Shaw et al., 2006). Ammonia-oxidizing bacteria express *nirK* in aerobic environments in response to NO_2^- (Beaumont et al., 2004) and it has been hypothesized that NIR's main role is in detoxifying NO_2^- (Poth and Focht, 1985; Beaumont et al., 2002). Nevertheless, a role for O_2 is suggested by the fact that *nirK* expression increases in low-O_2 conditions (Beaumont et al., 2004), and yields of N_2O from cultures of ammonia-oxidizing bacteria increase more than 40-fold when O_2 concentrations drop below $5\,\mu M$ (Goreau et al., 1980).

N_2O with biologically distinct origins can be identified using stable isotopic signatures. The oxygen isotopic signature ($\delta^{18}O$-N_2O) has been used to distinguish nitrification and denitrification N_2O sources (Ostrom et al., 2000; Toyoda et al., 2005; Wrage et al., 2005; Kool et al., 2007). The $\delta^{18}O$ of N_2O depends on the proportion of oxygen in N_2O that is derived from O_2 vs. H_2O, as well as any fractionation factors associated with incorporation or loss of the oxygen atoms in the metabolic precursors of N_2O (Fig. 1) (Casciotti et al., 2010). N_2O derived from NH_2OH contains only oxygen atoms from O_2 whereas N_2O produced by nitrifier-denitrification or heterotrophic denitrification depends on the $\delta^{18}O$ of NO_2^- (and the $\delta^{18}O$ of NO_3^-, in the case of heterotrophic denitrification), which is derived from both O_2 and H_2O (Andersson et al., 1982; Casciotti et al., 2010; Buchwald and Casciotti, 2010). Since the $\delta^{18}O$ values of marine H_2O are typically at least $20\%o$ less than those of dissolved O_2 (Kroopnick and Craig, 1976), marine N_2O produced with different amounts of oxygen from H_2O and O_2 will reflect this in the $\delta^{18}O$ signature. Indeed, positive correlations between oceanographic $\delta^{18}O$-O_2 and $\delta^{18}O$-N_2O data have been interpreted as evidence that the N_2O is a product of nitrification because oxygen from O_2 is most directly incorporated into N_2O through NH_2OH during NH_3 oxidation (Ostrom et al., 2000; Andersson and Hooper, 1983).

However, there may be isotope effects associated with the incorporation of oxygen atoms from O_2 and H_2O into N_2O (Casciotti et al., 2010). If these isotope effects are significant and variable among different species of ammonia oxidizers, it may prove difficult to extract source information
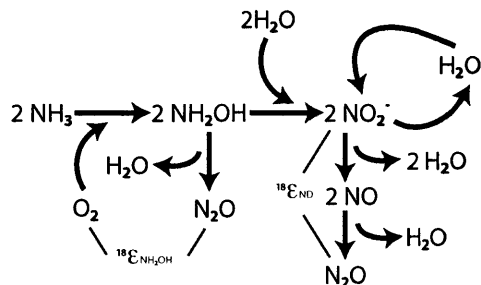
Fig. 1. During ammonia oxidation, the oxygen atoms incorporated into N_2O come from either O_2 or H_2O. The $\delta^{18}O$-N_2O depends upon the isotopic signatures of these two substrates as well as isotope effects ($^{18}\varepsilon$) that may be associated with the individual formation mechanisms, hydroxylamine ($^{18}\varepsilon_{NH2OH}$) decomposition and nitrifier-denitrification of nitrite ($^{18}\varepsilon_{ND}$).

based on oxygen isotopes alone. Furthermore, the $\delta^{18}O$ of N_2O produced by ammonia-oxidizing bacteria may change depending on what fraction of the oxygen atoms are derived from O_2 (via NH_2OH decomposition and nitrifier-denitrification) vs. H_2O (via nitrifier-denitrification) (Fig. 1).

The ^{15}N site preference (SP) is another isotopic signature used to interpret environmental N_2O data (Toyoda et al., 2002; Sutka et al., 2003, 2004; Toyoda et al., 2005; Sutka et al., 2006; Koba et al., 2009). SP as defined by Toyoda and Yoshida (1999) is the difference in the isotopic enrichment of the internal (α) and external (β) nitrogen atoms in the linear N_2O molecule:

$$SP = \delta^{15}N^{\alpha} - \delta^{15}N^{\beta}.$$

Unlike $\delta^{18}O$ and $\delta^{15}N^{bulk}$ values, SP is thought to reflect the N_2O production mechanism while remaining independent of the substrate's isotopic signature. This is because the reactions that produce N_2O involve two identical precursor molecules (either NO or NH_2OH) (Toyoda et al., 2002; Schmidt et al., 2004) that are presumably drawn simultaneously from the same substrate pool. SP measurements made on N_2O produced by ammonia-oxidizing bacteria and denitrifying bacteria support this idea (Sutka et al., 2006). Cultures of ammonia-oxidizing bacteria produce N_2O with a SP of about 33.5‰ via NH_2OH decomposition. However, in the presence of NO_2^- and low O_2 concentrations, the same bacteria make N_2O with a SP that is closer to that of denitrifying bacteria (−0.8‰) (Sutka et al., 2003, 2004, 2006).

Previous workers have estimated the "end-member" SP signatures for the two different sources of N_2O in ammonia oxidizer cultures by manipulating O_2 concentrations in order to favor production via one process over the other (Sutka et al., 2003, 2004, 2006). However, since NH_2OH decomposition and nitrifier-denitrification can give rise to N_2O simul-

taneously, failure to account for this mixing may cause errors in these end-member SP estimates. If N_2O from NH_2OH decomposition has a SP that is much higher than the SP of N_2O from nitrifier-denitrification, as proposed by Sutka et al. (2003, 2004, 2006), then source mixing would cause underestimation of the SP of NH_2OH decomposition and overestimation of the SP of nitrifier-denitrification.

Here we have used $\delta^{18}O$-N_2O and SP measurements to make mixing-corrected estimates of the end-member SP values for N_2O produced by NH_2OH decomposition and nitrifier-denitrification by the marine ammonia-oxidizing bacterium *Nitrosomonas marina* C-113a. These end-member values were then used to calculate the N_2O yields from nitrification and nitrifier-denitrification in different growth conditions, including a range of O_2 headspace concentrations (20%, 2%, and 0.5%), excess NO_2^- (0.2 to 1 mM), at different cell densities, and in the presence of nitrite-oxidizing bacteria. Each experiment was carried out with an eye towards simulating environmental conditions more closely than previous studies by using growth medium that contains a fraction of the NH_4^+ present in commonly used recipes for ammonia oxidizer media (50 μM vs. 5 to 10 mM NH_4^+), and lower cell densities.

2 Materials and methods

2.1 Culture maintenance and experimental setup

Nitrosomonas marina C-113a cultures were maintained semi-continuously in Watson medium containing 5 mM NH_4^+ (Watson, 1965). All maintenance cultures were kept in the dark at 22 °C with shaking at 100 rpm. The cultures used to inoculate experiments were periodically tested for heterotrophic contamination as follows: 1 ml of each culture was added to 2 ml of a sterile 1:4 mixture of tryptic soy broth and artificial seawater and incubated 3 to 4 weeks in aerated culture tubes. Contamination was of particular concern during experiments on high density C-113a cultures because the abundance of cellular material was a potential source of organic substrate for the growth of heterotrophic denitrifiers, which can also produce N_2O at low O_2 concentrations. For this reason, additional purity tests were done by inoculating 5 ml of each high density culture (10^5 – 10^6 cells ml^{-1}) into 10 ml of the sterile tryptic soy/artificial seawater mixture amended with 1 mM $NaNO_2$. These cultures were incubated in closed, inverted 15 ml centrifuge tubes for 3 to 4 weeks. All tubes remained free of turbidity and showed no production of gas bubbles that would indicate heterotrophic denitrification.

Experiments were carried out in 545 ml glass serum bottles (Wheaton, 223952) that contained 100 ml sterile Watson medium with 50 μM NH_4^+. Parallel experiments in ^{18}O-enriched water were set up by adding 1 ml of 5000‰ $\delta^{18}O$-H_2O into each bottle. The headspace of each bottle

was sealed using 30 mm gray butyl rubber septa (Wheaton, 224100-331) and aluminum crimps (Wheaton, 224187-01). Atmospheric O_2 and N_2O were removed by purging for 3 h with N_2 flowing at > 60 ml min^{-1} and appropriate amounts of high-purity O_2 ($\delta^{18}O = +25.3\permil$) were injected back into each headspace to achieve 20%, 2%, or 0.5% O_2 (v/v) (203, 20, or 5 μM dissolved O_2, respectively). Headspace O_2 and N_2O concentrations were checked before and after each experiment by electron capture gas chromatography (see below). The ratio of headspace to liquid volumes was such that complete NH_3 oxidation consumed less than 10% of the total O_2 in the lowest O_2 headspaces.

Immediately before each experiment, 1–2 l of late exponential or early stationary phase cultures were centrifuged at 10 000 g for 30 min, washed to remove residual NH_4^+ and NO_2^-, and re-suspended in 30 ml sterile media without NH_4^+. Experiments were initiated by the injection of 500 μl of washed and resuspended cells into each bottle. In the co-culture experiments, ammonia oxidizers with cell densities of approximately 2×10^5 cells ml^{-1} were added with washed and resuspended cells of the nitrite oxidizer *Nitrococcus mobilis* (10^6 cells ml^{-1}).

Initial and final cell densities were measured in samples preserved with 2% formalin (0.22-μm filtered) by making microscopic counts of DAPI-stained cells, or by using fluorescence assisted flow cytometry (FACS) to count SYBR green-stained cells on a FACS Calibur flow cytometer (Becton Dickinson). Uninoculated bottles served as a control for abiotic N_2O production and were analyzed in parallel with experimental bottles. All bottles were incubated in the dark at room temperature with constant shaking. The progress of NH_3 oxidation was monitored by measuring accumulation of NO_2^- and disappearance of NH_4^+ from the medium (see below). Once NH_3 oxidation was complete, experiments were terminated by injecting each bottle with 1 ml of 6 M NaOH, lysing the cells.

2.2 Chemical analyses

The concentrations of NH_4^+ were determined colorimetrically by the phenol-hypochlorite method (Solorzano, 1969) and NO_2^- concentrations were determined by the Griess-Ilosvay colorimetric method (Pai and Yang, 1990) using a 1 cm path-length flow cell. Headspace O_2 concentrations were determined using a gas chromatograph with a ^{63}Ni electron capture detector (Shimadzu GC-8A). The O_2 peaks from 20 to 250 μl injections of sample headspace were recorded and integrated using Shimadzu EZStart software (v. 7.2.1). Sample peak areas were calibrated with standard injections of air. Headspace N_2O concentrations were also measured before and after each experiment using the GC-8A. Sample peak areas were calibrated against commercial N_2O mixtures (10, 1, and 0.1 ppm) and fresh atmospheric air (approximately 320 ppb). When total headspace N_2O was less than 20 nmol, N_2O was quantified by analyzing the whole

bottle (by purging and trapping, see below) on a Finnigan Delta^{PLUS} Isotope ratio mass spectrometer (IRMS) and using the linear relationship between peak area of m/z 44 and nanomoles of N_2O to determine total N_2O. The average blank determined by analyzing bottles flushed with high-purity N_2 was 0.08 ± 0.04 nmol N_2O.

2.3 Isotopic analyses

Isotopic analyses of N_2O were conducted using a Finnigan Delta^{PLUS} XP IRMS. Bottles were purged with He and N_2O was cryo-trapped on-line with a custom-built purge and trap system (McIlvin and Casciotti, 2010) operated manually with 545 ml serum bottles. The following modifications made large volume gas extraction possible: bottles were loaded manually, the helium flow rate was increased to 60 ml min^{-1}, and the purge time was extended to 45 min. As described in McIlvin and Casciotti (2010), CO_2 was largely removed from the gas stream by passage through a Carbosorb trap, then N_2O was separated from residual CO_2 using a capillary column (25 m × 0.32 mm) lined with Poraplot-Q before injection into the mass spectrometer through an open split. Mass/charge *(m/z)* peak areas were automatically integrated using Isodat 2.0 software. Values for $\delta^{18}O$-N_2O, $\delta^{15}N^{bulk}$, $\delta^{15}N^\alpha$, and $\delta^{15}N^\beta$ were obtained from the 45/44, 46/44, and 31/30 peak area ratios and referenced to our laboratory's N_2O tank as described in Appendix A. This reference tank has been calibrated for $\delta^{18}O$-N_2O (‰ vs. VSMOW), $\delta^{15}N^{bulk}$, $\delta^{15}N^\alpha$, and $\delta^{15}N^\beta$ (‰ vs. AIR) by S. Toyoda (Tokyo Institute of Technology). Furthermore, the isotopomer-specific NO^+ fragment ion yields for our Delta^{PLUS} XP were determined for the ion source conditions used in these measurements (see Appendix B). For quality-control, two or three tropospheric N_2O samples were analyzed between every 7 to 10 experimental samples to check the consistency of our isotopomer analyses. These samples were created by allowing 100 ml of artificial seawater to equilibrate with outside air in 545 mL serum bottles, sealing the bottles, and analyzing them as described above. Triplicate samples of tropospheric N_2O from Woods Hole, MA analyzed during a typical run had $\delta^{15}N^\alpha = 15.0 \pm 0.1\permil$, $\delta^{15}N^\beta = -1.9 \pm 0.1\permil$, $\delta^{18}O = 44.4 \pm 0.2\permil$, $\delta^{15}N^{bulk} = 6.5 \pm 0.1\permil$, SP = 16.9 ± 0.1‰, and m/z 44 peak area = 15.6 ± 0.2 mV-s (7.8 ± 0.1 nmol).

We also measured the $\delta^{18}O$ and $\delta^{15}N$ of NO_2^- that was produced by cultures as NH_3 oxidation progressed. NO_2^- was converted to N_2O using the azide method developed by McIlvin and Altabet (2005). The conversion to N_2O was carried out immediately after sampling to avoid shifts in the oxygen isotopic values by abiotic exchange with water (Casciotti et al., 2007) or continued biological production of NO_2^- from residual NH_3. Individual sample volumes were adjusted so that a consistent amount of N_2O (5 or 10 nmol) was produced for each set of azide reactions. Each sample set included at least three sets of three different NO_2^- standards (N-23,

N-7373, and N-10219; Casciotti et al., 2007) that were used to calculate sample δ^{15}-NO_2^- (‰ vs. AIR) and δ^{18}O-NO_2^- (‰ vs. VSMOW) values. These samples were analyzed in 20 ml headspace vials using the autosampler setup described by Casciotti et al. (2002), modified with the addition of an $-60\,^\circ$C ethanol trap and column backflush (McIlvin and Casciotti, 2010).

3 Results and discussion

Nitrifier-denitrification depends on the presence of NO_2^- to produce N_2O (Ritchie and Nicholas, 1972; Poth and Focht, 1985; Yoshida, 1988), and the accumulation of NO_2^- in environments such as oxygen deficient zones (ODZs) could contribute to increased N_2O production in these regions. To date, the roles of substrate concentration and cell density in determining N_2O yield have not been systematically investigated. This study was designed to test the impact of O_2 and NO_2^- concentrations on the N_2O yield of marine ammonia-oxidizing bacteria at a lower substrate (NH_3) concentration, and at a broader and lower range of cell densities than any previous work. N_2O yield data are presented in the same form used in oceanographic N_2O studies so that yields are the fraction of N-atoms converted to N_2O out of the total amount of NH_3 that is oxidized (i.e. $2 \times$ moles N_2O/moles NH_3). In other words, a yield of 5×10^{-4} indicates that 1 in every 2000 N-atoms from oxidized NH_3 will go into an N_2O molecule.

3.1 Cell density and O_2 concentration

Cell density influenced the observed N_2O yields in both low O_2 (0.5% and 2%) and high O_2 (20%) conditions. O_2 concentration had the greatest impact on N_2O yield at the highest starting cell density tested (1.5×10^6 cells ml^{-1}) (Fig. 2). At 20% O_2, the high density cultures had the lowest average yields observed, ($1.3 \pm 0.4 \times 10^{-4}$) while at 0.5% O_2 the high density cultures had the highest average yields observed ($220 \pm 40 \times 10^{-4}$). In contrast, O_2 had a much smaller impact on N_2O yield in the medium density cultures (starting density $= 2.1 \times 10^4$ cells ml^{-1}) and the low density cultures (starting density $= 2 \times 10^2$ cells ml^{-1}). In fact, the N_2O yields of the medium density cultures were not significantly different among the high and low O_2 treatments (at 20% O_2, $5.1 \pm 0.5 \times 10^{-4}$, at 2% O_2, $5.5 \pm 0.8 \times 10^{-4}$, and at 0.5% O_2, $6.4 \pm 1.4 \times 10^{-4}$). Low density cultures produced average yields of $3.9 \pm 0.3 \times 10^{-4}$ at 20% O_2, $4.7 \pm 0.1 \times 10^{-4}$ at 2% O_2, and $6.7 \pm 0.5 \times 10^{-4}$ at 0.5% O_2.

The average yields of the cultures at 20% O_2 were comparable to the production yields ($0.8 - 5.4 \times 10^{-4}$) measured by Yoshida et al. (1989) in the oxic surface waters of the western North Pacific using $^{15}NH_4^+$ tracer techniques. However, they are lower than previously reported yields for *Nitrosomonas* cultures at 20% O_2 ($26 - 30 \times 10^{-4}$ in Goreau et al. (1980) and $10 - 390 \times 10^{-4}$ in Remde and Conrad, 1990).
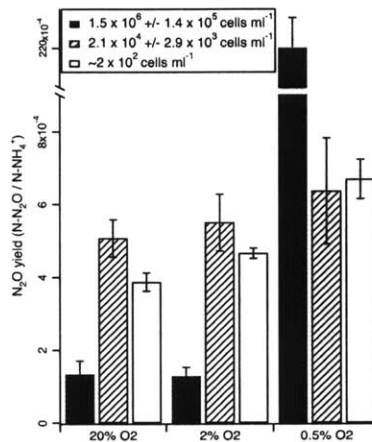

Fig. 2. N_2O yields vs. cell density. Each bar represents the average of 5 replicate cultures. Error bars are for one standard deviation among replicates.

In this study, low-O_2 conditions only resulted in substantial increases in N_2O yield when cell densities were greater than 10^6 cells ml^{-1}. N_2O yields were relatively low and less sensitive to O_2 when cell densities were closer to those observed in the ocean ($10^3 - 10^4$ cells l^{-1}; Ward et al., 1982). This draws into question the oceanographic applicability of previous culture-based yield measurements, where a many-fold increase in N_2O yield was observed as O_2 dropped from 20% to 0.5% (Goreau et al., 1980). Goreau et al. (1980) worked with a marine *Nitrosomonas* strain at cell densities (1×10^6 cells ml^{-1}) comparable to our high density experiments and observed N_2O yields of $800 - 1000 \times 10^{-4}$ for cultures grown at 0.5% O_2 on 24 mM NH_4^+. The implication of the present study is that factors such as cell density can influence the relationship between N_2O yield and O_2 concentration.

The mechanisms that explain the high N_2O yields of high density cultures at low O_2 could be chemical or biological. O_2 has a major influence on the half-life of nitric oxide (NO), the gaseous precursor of N_2O during nitrifier-denitrification. Therefore, concentration-dependent changes in the rate of N_2O-production could be related to O_2 as a consequence of the abiotic oxidation of NO:

$$2NO + O_2 \rightarrow 2NO_2$$

$$2NO_2 + H_2O \rightarrow HNO_2 + HNO_3, \text{ (Ritchie and Nicholas, 1972),}$$
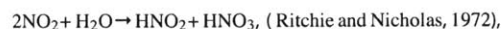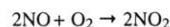
where nitrous acid (HNO_2), is the major decomposition product of the second reaction (Ignarro et al., 1993). In aerobic environments, O_2 is the major reactant and any NO present reacts away soon after it is produced (Lewis and

Deen, 1994). However, in low-O_2 environments the half-life of NO increases, so that during bacterial NH_3 oxidation, it can accumulate to concentrations that are similar to N_2O (Remde and Conrad, 1990; Lipschultz et al., 1981). This may allow the enzymes that carry out NO reduction to compete for NO with the above O_2-dependent reaction. Studies of *N. europaea* have also shown that the expression of *nirK* during nitrifier-denitrification is controlled by a repressor protein (Beaumont et al., 2002, 2004) that belongs to a family of NO-sensitive transcription regulators (Rodionov et al., 2005). If NO induces *nirK* transcription, the abiotic reaction of O_2 with NO could reduce NIR-dependent N_2O production by consuming the inducer. Finally, high cell densities may be necessary for either of these effects to become important because the ability of NO-reducing enzymes to compete with O_2 for NO will depend on the diffusivities of O_2 and NO relative to the average distance between cells.

It is unclear why cultures with the highest cell densities had significantly lower N_2O yields at 20% O_2 than cultures with lower densities (Fig. 2). Time, NO_2^- (or NO), and increasing cell numbers could all enhance N_2O production by nitrifier-denitrification. There were significant differences in the amount of time that it took cultures of each density to oxidize all the NH_4^+ present. The low and medium density cultures took 14 and 3.5 d to oxidize $50\,\mu M$ NH_4^+, respectively, while the high density cultures took only 7 h. Cell numbers also doubled approximately 7, 2, and 0 times, in the low, medium, and high density cultures, respectively. Thus, in the low and medium density cultures, NO_2^- and cells accumulated over longer periods of time than they did in the high density cultures. Further research is needed to determine the behavioral and/or kinetic effects that influence the N_2O yields from ammonia oxidizers.

3.2 NO_2^- and O_2 concentration

In pure batch cultures of ammonia oxidizers, NO_2^- exposure is an unavoidable result of growth because NO_2^- accumulates up to the initial NH_4^+ concentration. Excess NO_2^- may increase N_2O yields if ammonia oxidizers convert NO_2^- to N_2O to avoid the toxic effects of NO_2^- (Poth and Focht, 1985; Beaumont et al., 2002, 2004). To test the impact of NO_2^- on N_2O yields, we increased NO_2^- concentrations by adding 0.2 or 1 mM NO_2^- to some cultures, and decreased accumulated NO_2^- concentrations in others by adding the nitrite-oxidizing bacterium *Nitrococcus mobilis* to create a co-culture.

In the co-cultures, NO_2^- concentrations remained below detection at 20% O_2 and below $17\,\mu M$ at 0.5% O_2. Although co-culturing kept NO_2^- concentrations lower than they were in the pure cultures, N_2O yields were not significantly lower in the presence of the nitrite-oxidizing bacteria (Fig. 3a). The insignificant differences between the yields with and without nitrite oxidizers suggests that the $50\,\mu M$ NO_2^- that accumulated in our pure cultures did not have a major impact on

the N_2O yields measured for those cultures. However, we were unable to entirely eliminate NO_2^- accumulation in the low-O_2 experiments. Future work should focus on identifying the impact of NO_2^- on N_2O production by nitrifiers in low-O_2 environments.

The addition of 1 mM NO_2^- had a greater impact on N_2O yield than the differences in O_2 concentration did (Fig. 3b). The increase due to the additional NO_2^- was apparent in both low and high O_2 conditions. Furthermore, the average N_2O yields increased as the amount of added NO_2^- increased. Cultures under 20% O_2 with no added NO_2^- had an average yield of $4.0 \pm 0.03 \times 10^{-4}$ while those with 1 mM added NO_2^- had an average yield of $7.6 \pm 0.5 \times 10^{-4}$. Cultures under 0.5% O_2 with no added NO_2^- had an average yield of $6.0 \pm 0.5 \times 10^{-4}$ and those with 1 mM added NO_2^- had an average yield of $10.2 \pm 0.3 \times 10^{-4}$. N_2O yields were calculated as a fraction of the total N in NH_4^+ consumed during the experiment ($\boxtimes$ 5×10^{-6} moles).

From this work, it is clear that increased NO_2^- concentrations enhance N_2O production in cultures of ammonia-oxidizing bacteria. This is consistent with a detoxification role for nitrite reductase in nitrifying bacteria, as suggested by previous work (Beaumont et al., 2004). The relationship between NO_2^-, nitrifier-denitrification, and N_2O production is also complex. Aerobic *nirK* expression occurs in response to increasing NO_2^- concentrations (Beaumont et al., 2004), but *nirK* knock-out mutants actually produce more N_2O than the wild-type strain. The authors suggest that the NH_2OH-dependent pathway has a role in this increase (Beaumont et al., 2002).

Oceanic O_2 concentrations may influence a number of different biogeochemical variables that enhance N_2O production by ammonia oxidizers. For example, low dissolved O_2 concentrations are often associated with elevated NO_2^- concentrations (Codispoti et al., 2001). When dissolved O_2 concentrations are low, the biological turnover time of NO_2^- also increases (Hashimoto et al., 1983) in part because the activity of nitrite-oxidizing bacteria ceases at a higher O_2 concentration than the activity of ammonia-oxidizing bacteria (Helder and de Vries, 1983). Charpentier et al. (2007) also suggest that high concentrations of organic particles found in certain productive waters enhance N_2O production by creating high-NO_2^-, low-O_2 microenvironments necessary to support nitrifier-denitrification. Future oceanographic work should investigate how N_2O production rates in oxygen deficient zones (ODZs) relate to these different biogeochemical variables.

3.3 Pathway dependence of $\delta^{15}N^{bulk}$-N_2O

Ammonia-oxidizing bacteria make N_2O through two different pathways, so that the observed isotopic signatures of N_2O are a function of the pathways' mixing fractions, the isotopic signatures of their different substrate molecules,
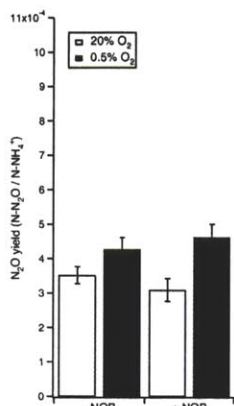
Fig. 3a. N_2O yields in the presence and absence of nitrite-oxidizing bacteria (NOB). Starting NH_4^+ concentrations were $50\,\mu M$.
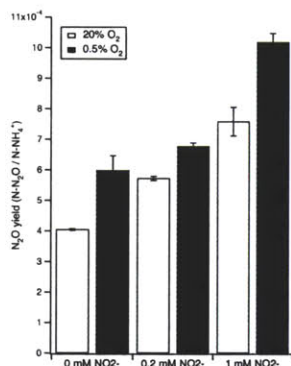

Fig. 3b. N_2O yields increased when NO_2^- was added to the starting media. Initial NH_4^+ concentrations were $50\,\mu M$. Added NO_2^- was either $0, 0.2\,mM$, or $1\,mM$.

and the different isotope effects associated with those pathways. Complete biochemical decoupling of the nitrifier-denitrification pathway from the NH_2OH decomposition pathway is difficult to achieve with intact C-113a cells because the bacteria require NH_3 to support their respiratory electron transport chain, and N_2O production stops once NH_3 oxidation is complete (Supplementary Fig. S.3). Therefore, while we manipulated growth conditions such as O_2 concentration and cell density in order to favor one N_2O production mechanism over another, in interpreting the results we account for N_2O contributions from both sources.
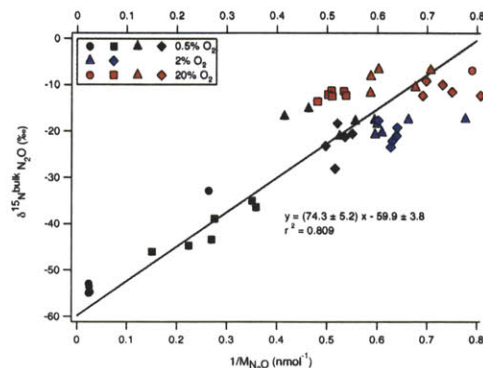

Fig. 4. Pathway dependence of $\delta^{15}N^{bulk}$ N_2O. Symbol shapes correspond to different starting cell densities: circles correspond to 1.5×10^6 cells ml^{-1}, squares to 2×10^5 cells ml^{-1}, triangles to 2.1×10^4 cells ml^{-1}, and diamonds to 2×10^2 cells ml^{-1}. Colors correspond to headspace O_2 levels, with black symbols representing 0.5% O_2, blue symbols 2% O_2, and red symbols 20% O_2. The slope and intercept of a Type II linear regression of $\delta^{15}N^{bulk}$ and $1/M_{N_2O}$ are given $\pm$ one standard deviation. In making a linear fit to the data, we assume that any differences in total N_2O are due to nitrifier-denitrification. The y-intercept of the line is equal to the $\delta^{15}N^{bulk}$ of N_2O from nitrifier-denitrification. Data points that were less than 1 nmol N_2O were not included.

N_2O produced by all C-113a cultures was depleted in ^{15}N relative to the substrate ($\delta^{15}N$-$NH_4^+ = -3$‰), although the range varied widely ($\delta^{15}N^{bulk}$-$N_2O = -54.9$‰ to -6.6‰, Fig. 4). Culture conditions affected the degree of ^{15}N depletion, with cultures grown under 0.5% O_2 producing the most depleted N_2O (-54.9‰ to -15.2‰), while cultures grown with 20% O_2 generally produced N_2O with higher $\delta^{15}N$ values (-13.6‰ to -6.7‰). The low-O_2 cultures that produced the most depleted N_2O also produced the most N_2O (the highest yield). We interpret the observed variation in $\delta^{15}N^{bulk}$-N_2O to have arisen from pathway-dependent mixing, which implies that a single isotope effect will not adequately relate the $\delta^{15}N^{bulk}$-N_2O to the substrate nitrogen compounds.

We assume that each datapoint ($\delta^{15}N^{bulk}_{total}$, M_{total}, where M refers to moles of N_2O) represents a two-component mixture of a constant or "basal" N_2O source from NH_2OH decomposition (M_{NH_2OH}) and a variable source of N_2O from nitrifier-denitrification (M_{ND}) that tended to be larger in low-O_2 cultures. This is the basis for performing the type II linear regression of $\delta^{15}N^{bulk}$ vs. $\frac{1}{M_{N_2O}}$ in Fig. 4. Equation (3b), the model for the linear regression was developed using the mass balance Eqs. (1 and 2) (Table 1).

According to Eq. (3b), the y-intercept of the regression is the $\delta^{15}N^{bulk}$ of the more depleted nitrifier-denitrification

29

Table 1. Equations used to model the $\delta^{15}N^{bulk}N_2O$ data in Fig. 4.

---

(1) $\delta^{15}N^{bulk}_{total} \times M_{total} = \delta^{15}N^{bulk}_{ND} \times M_{ND} + \delta^{15}N^{bulk}_{NH_2OH} \times M_{NH_2OH}$

(2) $M_{ND} = M_{total} - M_{NH_2OH}$

(3a) $\delta^{15}N^{bulk}_{total} = \dfrac{\delta^{15}N^{bulk}_{ND} \times (M_{total} - M_{NH_2OH}) + \delta^{15}N^{bulk}_{NH_2OH} \times M_{NH_2OH}}{M_{total}}$

(3b) $\delta^{15}N^{bulk}_{total} = (\delta^{15}N^{bulk}_{NH_2OH} \times M_{NH_2OH} - \delta^{15}N^{bulk}_{ND} \times M_{NH_2OH}) \times \frac{1}{M_{total}} + \delta^{15}N^{bulk}_{ND}$

---

end-member ($\delta^{15}N^{bulk}_{ND}$). This is because as the amount of N_2O approaches infinity, the $\delta^{15}N^{bulk}_{ND}$ should overwhelm the basal end-member signature, $\delta^{15}N^{bulk}_{NH_2OH}$.

The value of $\delta^{15}N^{bulk}_{ND}$ obtained in this way is -59.9%, $\pm 3.8\%$ (errors are given as one standard deviation of the y-intercept). The difference between the $\delta^{15}N^{bulk}$ of the product N_2O and the $\delta^{15}N$ of the substrate NH_3 is the overall isotope effect associated with N_2O formation by nitrifier-denitrification ($^{15}\varepsilon_{ND} = -56.9\%$). The most enriched N_2O produced in these experiments had a $\delta^{15}N^{bulk}$ of -6.7%, providing a minimum for $\delta^{15}N^{bulk}_{NH_2OH}$. This is a minimum because if a fraction of this N_2O was produced by nitrifier-denitrification, we would not observe the heaviest possible value for the NH_2OH end-member.

This end-member mixing model does not account for the Rayleigh effects that kinetic isotopic fractionation has in closed systems such as batch cultures. These effects change the isotopic signatures of the NH_3 that is consumed and the NO_2^- that accumulates as NH_3 oxidation proceeds (Mariotti et al., 1981) so that at any instant during the reaction, the $\delta^{15}N$ of N_2O produced from these substrates will also reflect these isotopic shifts. However in this study, the end-member mixing model is not a serious violation of Rayleigh assumptions because all cultures were allowed to oxidize the same amount of NH_3 to completion before the total N_2O was analyzed. Abrupt changes in N_2O production rates during the NH_3 oxidation reaction could also make this model problematic in a Rayleigh system. In these experiments, however, N_2O accumulated steadily as NH_3 oxidation progressed and NO_2^- accumulated (Supplementary Fig. S.3).

3.4 Covariation of SP and $\delta^{18}O$-N_2O

The $\delta^{18}O$ of N_2O is like the $\delta^{15}N^{bulk}$ in that these signatures are both process-dependent and substrate-dependent. That is, the $\delta^{18}O$ of N_2O produced by ammonia-oxidizing bacteria depends on the mixing fraction of the two N_2O-producing pathways as well as the isotopic signatures of the substrates (O_2 and H_2O) that contribute oxygen atoms to those pathways and isotopic fractionation during oxygen atom incorporation or loss in the reactions that make N_2O (Fig. 1) (Cas-

ciotti et al., 2010). The conversion of NH_3 to NO_2^- incorporates oxygen atoms from O_2 in the first step and H_2O in the second step (Andersson et al., 1982; Andersson and Hooper, 1983):

$$NH_3 + \frac{1}{2}O_2 \rightarrow NH_2OH$$

$$NH_2OH + H_2O \rightarrow HNO_2 + 4H\cdot$$
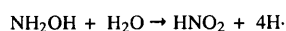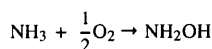
We expect the $\delta^{18}O$ of N_2O derived from NH_2OH decomposition to be independent of the $\delta^{18}O$ of H_2O because O_2 is the sole contributor of oxygen during the first reaction. However, the $\delta^{18}O$ of N_2O produced by NO_2^- reduction during nitrifier-denitrification depends upon both the $\delta^{18}O$-O_2 and $\delta^{18}O$-H_2O, in proportions that are affected by the amount of oxygen atom exchange between NO_2^- and H_2O (Andersson and Hooper, 1983; Casciotti et al., 2002; Kool et al., 2007; Casciotti et al., 2010). The fact that the $\delta^{18}O$ of N_2O produced by nitrifier-denitrification is sensitive to changes in $\delta^{18}O$-H_2O is the basis for a technique that uses parallel experiments in ^{18}O-labeled and unlabeled H_2O to identify the proportion of N_2O produced by nitrifier-denitrification (Wrage et al., 2005).

The impact of the $\delta^{18}O$-H_2O on the $\delta^{18}O$ of N_2O produced by C-113a is demonstrated in Fig. 5, where cultures grown in water with a $\delta^{18}O$ of $+40\%$ (labeled) produced N_2O that was 5% to 40% more enriched in ^{18}O than cultures grown in H_2O with a $\delta^{18}O$ of -5% (unlabeled). The difference in $\delta^{18}O$-N_2O between labeled and unlabeled cultures was greatest at 0.5% O_2, when more N_2O was produced. At higher O_2 concentrations, less N_2O was produced and there was convergence of the $\delta^{18}O$-N_2O values from labeled and unlabeled experiments. The difference in $\delta^{18}O$-N_2O from ammonia oxidizers grown in labeled and unlabeled H_2O is directly proportional to the fraction of the total N_2O that is produced by nitrifier-denitrification. The pattern is consistent with relatively more N_2O production by nitrifier-denitrification as the O_2 concentration drops and H_2O contributes more to the overall $\delta^{18}O$-N_2O. Note that in these experiments, side-by-side comparisons between labeled and unlabeled replicates assume that nitrifier-denitrification and NH_2OH decomposition contribute the same proportion of N_2O to both labeled

30

Table 2. Equations used to model the SP and δ^{18}O-N$_2$O data in Figure 5.

$$(4a)\ SP_{total} = F_{ND} \times SP_{ND} + (1 - F_{ND}) \times SP_{NH_2OH}$$

$$(4b)\ F_{ND} = \frac{SP_{total} - SP_{NH_2OH}}{SP_{ND} - SP_{NH_2OH}}$$

$$(5)\ \delta^{18}O\text{-}N_2O_{total} = F_{ND} \times (\delta^{18}O\text{-}NO_2^- - {}^{18}\varepsilon_{ND}) + (1 - F_{ND}) \times (\delta^{18}O\text{-}O_2 - {}^{18}\varepsilon_{NH_2OH})$$

$$(6)\ \delta^{18}O\text{-}N_2O_{total} = \frac{SP_{total} - SP_{NH_2OH}}{SP_{ND} - SP_{NH_2OH}} \times (\delta^{18}O\text{-}NO_2^- - \varepsilon_{ND}) + (1 - \frac{SP_{total} - SP_{NH_2OH}}{SP_{ND} - SP_{NH2OH}}) \times (\delta^{18}O\text{-}O_2 - \varepsilon_{NH_2OH})$$

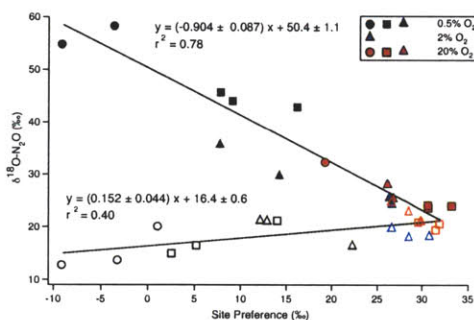**Fig. 5.** Pathway dependence of δ^{18}O-N$_2$O and SP. Filled symbols are data from cultures grown in labeled water (about 40‰) while open symbols are data from cultures in unlabeled water (about -5‰). Circles correspond to cultures with cell densities of 1.5×10^6 cells ml^{-1}, squares to 2×10^5 cells ml^{-1}, and triangles to 2.1×10^4 cells ml^{-1}. Colors correspond to headspace O$_2$ levels, with black symbols representing 0.5% O$_2$, blue symbols 2% O$_2$, and red symbols 20% O$_2$. Regression slopes and intercepts are given ± one standard deviation. Data from low-density cultures were not included to avoid the impact of relaxation of the δ^{18}O-NO$_2^-$ towards equilibrium with H$_2$O over the course of the NH$_3$ oxidation reaction. Data points that were less than 1 nmol N$_2$O were not included. All δ^{18}O values are referenced to VSMOW.

and unlabeled replicates and that the N$_2$O from NH$_2$OH decomposition has the same ^{18}O signature in both labeled and unlabeled experiments. This will be addressed in more detail below.

In contrast to δ^{18}O-N$_2$O, SP signatures of N$_2$O from ammonia oxidizers are thought to be process-dependent and substrate-independent: SP signatures vary as a result of mixing among N$_2$O sources with distinct SP values (Sutka et al., 2003, 2004, 2006), but they do not depend on the δ^{15}N values of the N$_2$O precursor molecules (Toyoda et al., 2002). In the present study, C-113a produced high-SP N$_2$O (up to 33.2‰) under 20% O$_2$ and low-SP N$_2$O (down to -9.1‰) under 0.5% O$_2$ (Fig. 5). Similar results have been observed for *N. europaea*, which produces high-SP N$_2$O (31.4 ± 4.2‰)

when growing aerobically on NH$_3$, (Sutka et al., 2006) but can also produce low-SP N$_2$O (-0.8 ± 5.8‰) in the presence of NO$_2^-$ and anaerobic conditions (Sutka et al., 2003, 2004).

Knowing the end-member SP signatures of N$_2$O from NH$_2$OH decomposition and nitrifier-denitrification is powerful because these values can then be used to calculate the size of each pathway's contribution to a culture's total N$_2$O output based on its SP signature (SP$_{total}$) (Charpentier et al., 2007). We developed the following model in order to extract these end-member SP signatures from our data while accounting for the fact that the SP of the N$_2$O from each culture is a mixture of these end-members. Following Charpentier et al. (2007), we set up a system of isotopic mass balance equations (Table 2) that describe isotopic mixing between low-SP N$_2$O from nitrifier-denitrification (SP$_{ND}$) and high-SP N$_2$O from NH$_2$OH decomposition (SP$_{NH_2OH}$), where F$_{ND}$ is the fraction of total N$_2$O that is produced by nitrifier-denitrification. Solving Eq. (4a) for F$_{ND}$ produces Eq. (4b) which cannot be solved for F$_{ND}$ without knowing the end-member values, SP$_{ND}$ and SP$_{NH_2OH}$, or having additional information about the value of F$_{ND}$ for each data point. Therefore, we develop a complementary mixing equation based on the δ^{18}O-N$_2$O in Eq. (5) (Table 2).

As discussed above, the measured δ^{18}O-N$_2$O (δ^{18}O-N$_2$O$_{total}$) depends not only on the mixing fraction F$_{ND}$, but also the isotopic signatures of the substrate molecules (δ^{18}O-O$_2$ and δ^{18}O-NO$_2^-$) and kinetic and/or branching isotope effects associated with either reaction ($^{18}\varepsilon_{NH_2OH}$ and $^{18}\varepsilon_{ND}$). In these equations, $^{18}\varepsilon_{NH_2OH}$ and $^{18}\varepsilon_{ND}$ are the respective net isotope effects expressed during oxygen incorporation from O$_2$ or NO$_2^-$ into N$_2$O. Here we do not consider the impact of Rayleigh fractionation on the δ^{18}O-O$_2$ because the O$_2$ pool is large relative to the fraction that is consumed (< 10%) and is expected to raise the δ^{18}O-O$_2$ less than 2‰. Substituting (4b) into (5) produces Eq. (6) (Table 2), which includes both SP values and oxygen isotopic signatures.

The best-fit values of the parameters SP$_{NH_2OH}$, SP$_{ND}$, $^{18}\varepsilon_{NH_2OH}$, and $^{18}\varepsilon_{ND}$ (Table 3) were obtained by fitting Eq. (6) to our dataset (n = 33) using a Levenberg-Marquardt non-linear regression program (Draper and Smith, 1981).

Table 3. Isotope effects and signatures derived in this paper for N_2O production by *N. marina* C-113a. Best fit values of model parameters for Eq. (6) are given with standard deviations based on covariance estimates in Bard (1974).

parameter	value	σ	description
$^{15}\varepsilon_{ND}$	56.9‰	3.8‰	N isotope effect of nitrifier-denitrification
$^{18}\varepsilon_{ND}$	-8.4‰	1.4‰	O isotope effect of nitrifier-denitrification
$^{18}\varepsilon_{NH_2OH}$	2.9‰	0.8‰	effective O isotope effect of NH_2OH decomposition
SP_{ND}	-10.7‰	2.9‰	site preference of N_2O from nitrifier-denitrification
SP_{NH_2OH}	36.3‰	2.4‰	site preference of N_2O from NH_2OH decomposition

Inputs were the values of SP_{total}, $\delta^{18}O$-N_2O, and $\delta^{18}O$-NO_2^- measured for each culture, as well as the known $\delta^{18}O$ of the high-purity O_2 used in the headspaces ($+25.3$‰). Our estimates of the end-member SP values of N_2O are significantly lower for N_2O produced by nitrifier-denitrification (-10.7 ± 2.9‰) and higher for N_2O produced by NH_2OH decomposition (36.3 ± 2.4‰) than previous estimates (Sutka et al., 2003, 2004, 2006). A sensitivity analysis of the model reveals that the value of SP_{ND} is sensitive to the values of the isotope effects $^{18}\varepsilon_{NH_2OH}$ (Supplementary Fig. S.4A and S.4C and Supplementary Table 1) and $^{18}\varepsilon_{ND}$ (Supplementary Fig. S.4A) but that this sensitivity decreases in labeled water (Supplementary Fig. S.4B and S.4D and Supplementary Table 2). Drawing data from both labeled and unlabeled experiments, as we have done here, leads to acceptable levels of uncertainty (Table 3).

These results expand the range of SP values produced by ammonia oxidizers by more than 10‰. This has an impact when Eq. (4b) is used to calculate the fraction of N_2O from nitrifier-denitrification using oceanographic SP data (Charpentier et al., 2007). We used the new end-member SP values to calculate that nitrifier-denitrification by C-113a accounted for 11% to 26% of N_2O production under 20% O_2 and 43% to 87% of production under 0.5% O_2 (Table 4). The variability for a given O_2 level occurred among cultures with different cell densities; on average, the denser cultures produced relatively more N_2O by nitrifier-denitrification at low-O_2 and less at high-O_2 concentrations (also see Fig. 5).

Our estimated values of $^{18}\varepsilon_{ND}$ and $^{18}\varepsilon_{NH_2OH}$ were -8.4 ± 1.4‰ and $+2.9 \pm 0.8$‰, respectively. This means that N_2O produced via nitrifier-denitrification was enriched in ^{18}O by 8.4‰ relative to the NO_2^-, and N_2O produced from NH_2OH was depleted in ^{18}O by 2.9‰ relative to O_2. The ^{18}O enrichment from nitrifier-denitrification is most likely the result of a combination of kinetic and branching isotope effects. There are few published estimates of these isotope effects that we can compare with our model results. Work on the heterotrophic denitrifier *Pseudomonas aureofaciens* indicates that the branching oxygen isotope effect of NO_2^- reduction is approximately 15‰ (Casciotti et al., 2007). However, it is not known whether the same isotope effect applies to nitrifier-denitrification or if there is also a kinetic isotope effect that influences the $\delta^{18}O$-N_2O. Recent work has also ad-

dressed the isotope effects for oxygen atom incorporation by C-113a (Casciotti et al., 2010), but was not able to separate fractionation during O_2 and H_2O incorporation.

Equations (5) and (6) assume that the oxygen atoms in N_2O produced by NH_2OH decomposition come only from O_2. If a fraction of this oxygen actually comes from H_2O, then the model value of $^{18}\varepsilon_{NH_2OH}$ reported in Table 3 could be too high for data from experiments in unlabeled H_2O ($\delta^{18}O$-$H_2O < \delta^{18}O$-O_2) and too low for data from labeled H_2O ($\delta^{18}O$-$H_2O > \delta^{18}O$-O_2). However, this structure was not apparent in the residuals of $^{18}\varepsilon_{NH_2OH}$ from labeled vs. unlabeled experiments. When a parameter for oxygen-exchange between H_2O and NH_2OH was included in Eq. (6), we were unable to resolve it with the present data set. However, if an exchange term is included in Eq. (6) so that 20% of the oxygen atoms in N_2O produced by NH_2OH decomposition are from H_2O, then using the values of SP_{NH_2OH}, SP_{ND}, and $^{18}\varepsilon_{ND}$ from Table 3 and values of SP_{total}, $\delta^{18}O$-N_2O_{total}, $\delta^{18}O$-NO_2^-, and $\delta^{18}O$-O_2 from Supplementary Tables 1 and 2, estimates of $^{18}\varepsilon_{NH_2OH}$ would decrease to -3.7‰ in unlabeled water and increase to 6.7‰ in labeled water if we assume that the oxygen atoms from water are incorporated without any isotope effect. However, 20% exchange is an extreme case and available evidence does not support significant exchange of oxygen atoms between NH_2OH and water during ammonia oxidation (Casciotti et al., 2010; Hollocher et al., 1981; Dua et al., 1979). Additional experiments in ^{18}O-labeled water could shed light on the issue of oxygen exchange.

The $\delta^{18}O$ and SP signatures of the N_2O in these experiments covaried (Fig. 5). The covariation depended on the $\delta^{18}O$ of the H_2O in the media: the slope of the linear regression of SP and $\delta^{18}O$-N_2O was negative (-0.904 ± 0.087) for experiments performed in ^{18}O-enriched H_2O ($+40$‰) and positive (0.152 ± 0.044) for experiments in unlabeled H_2O (-5‰) (Fig. 5). Our model provides an explanation for the covariation between SP and $\delta^{18}O$-N_2O because it describes mixing between two N_2O sources with distinct SP values and different proportions of oxygen from O_2 and H_2O. According to Eq. (6), the sign and magnitude of the regression slope will depend upon the difference between $\delta^{18}O$-O_2 and $\delta^{18}O$-H_2O.

32

Table 4. The fraction of N_2O produced by nitrifier-denitrification (F_{ND}) calculated using measured SP values, Eq. (4b), and the best fit values for SP_{ND} and SP_{NH_2OH} in Table 3.

density (cells/ml^{-1})	20% O_2	2% O_2	0.5% O_2
2×10^2	$0.26 \pm 0.06, n = 5$	$0.38 \pm 0.04, n = 5$	$0.43 \pm 0.09, n = 4$
2.1×10^4	$0.19 \pm 0.03, n = 5$	$0.18 \pm 0.04, n = 5$	$0.48 \pm 0.11, n = 5$
2×10^5	$0.11 \pm 0.03, n = 6$		$0.58 \pm 0.11, n = 6$
1.5×10^6			$0.87 \pm 0.09, n = 5$

Positive correlations between $\delta^{18}O$-N_2O and SP observed in environmental data have been interpreted as signs that N_2O consumption by denitrification is an important N_2O cycling process in the system under scrutiny (Koba et al., 2009; Yoshida and Toyoda, 2000; Popp et al., 2002; Toyoda et al., 2002; Schmidt et al., 2004). Indeed, there is experimental evidence demonstrating that progressive consumption of N_2O by denitrifier cultures results in a simultaneous increase in both SP and $\delta^{18}O$-N_2O (Ostrom et al., 2007). The theoretical basis for this behavior is the fact that the N-O bonds formed by the heavier nitrogen and oxygen isotopes have lower zero-point energies and are therefore more resistant to being broken than bonds between the lighter isotopes (Yung and Miller, 1997; Toyoda et al., 2002). As a result, decomposition of a symmetrical O-N-N-O intermediate during N_2O formation and also cleavage of the N-O bond during N_2O reduction to N_2 will produce N_2O with positively correlated $\delta^{18}O$ and SP values.

Our work demonstrates that SP and $\delta^{18}O$-N_2O can also covary as a result of N_2O production by nitrification, without invoking N_2O consumption by heterotrophic denitrifiers. The sign and magnitude of the correlation depends on the difference between the $\delta^{18}O$ of the O_2 and the H_2O that contribute oxygen atoms to the N_2O. In contrast to this study, where we manipulated $\delta^{18}O$-H_2O, there is little natural variation in $\delta^{18}O$-H_2O in the open ocean but much larger variation in $\delta^{18}O$-O_2 as a result of isotopic fractionation associated with respiratory O_2 consumption (Kroopnick and Craig, 1976; Bender, 1990; Levine et al., 2009). According to model Eq. (6), we would expect the slopes of the $\delta^{18}O$-N_2O:SP regressions (such as those in Fig. 5) to increase as $\delta^{18}O$-O_2 rises relative to $\delta^{18}O$-H_2O (or $\delta^{18}O$-NO_2^-). Nitrification may therefore influence the $\delta^{18}O$-N_2O:SP dynamics in the oxycline in two opposing ways : 1) a drop in O_2 concentration may promote nitrifier-denitrification and thus the incorporation of low-$\delta^{18}O$ oxygen atoms from H_2O into low-SP N_2O, and 2) respiratory O_2 consumption increases the $\delta^{18}O$ of the remaining O_2 pool, raising the $\delta^{18}O$ of the N_2O produced by NH_2OH decomposition as well as nitrifier-denitrification. In the future, the combined use of SP, $\delta^{18}O$-N_2O, and $\delta^{18}O$-O_2 may be used to resolve these effects. An important unknown that remains in the marine N_2O isotope

biogeochemistry is whether archaeal ammonia oxidizers also produce N_2O and if so, what their impact is on the N_2O budget and the isotopic signatures of N_2O in the ocean.

4 Conclusions

As shown previously, culturing conditions influence N_2O yields from ammonia-oxidizing bacteria. However, the yields observed in this study were much lower than those obtained in previous culture-based measurements, and they did not increase as dramatically at low oxygen concentrations except at high cell densities. These results are in line with modeling- and incubation-based oceanographic estimates of N_2O yields from nitrification and may be useful in future modeling of N_2O production and distributions in the ocean. Recent work interpreting isotopic signatures of biogenic N_2O has often relied on the assumption that a direct relationship between $\delta^{18}O$-N_2O and SP was indicative of N_2O consumption and production by denitrification. However, our work suggests that a direct relationship between these signatures may also occur as a result of nitrification, at least when the SP values vary between $-10‰$ and $36‰$. Nitrification produces this relationship through mixing between high-SP, ^{18}O-enriched N_2O produced by NH_2OH decomposition and low-SP, ^{18}O-depleted N_2O produced by nitrifier-denitrification.

Appendix A

Calculating the position-specific $^{15}N/^{14}N$ ratios of N_2O

Data collected during continuous flow isotopic analyses of N_2O included simultaneous signal intensities (in volt-seconds) of 30, 31, 44, 45, and 46 mass/charge detectors. The delta values and site preferences reported here were calculated using the raw peak area ratios of 31/30, 45/44, and 46/44 for a reference gas injection and the eluted sample peak. Isodat software reports these raw ratios as rR 31NO/30NO, etc. For each run, sample raw ratios were referenced to the standard ratios and these

"ratios of ratios" were multiplied by the appropriate standard ratios ($^{31}R_{standard} = 0.004054063$, $^{45}R_{standard} = 0.007743032$, $^{46}R_{standard} = 0.002103490$) to calculate $^{31}R_{sample}$, $^{45}R_{sample}$, and $^{46}R_{sample}$, respectively. For example,

$$^{31}R_{sample} = [rR\ 31NO/30NO_{sample}]/$$

$$[rR\ 31NO/30NO_{standard}] \times ^{31}R_{standard}$$

The $R_{standard}$ values are the calculated ratios that the Farraday cups in the Casciotti Delta^{PLUS} isotope ratio mass spectrometer (IRMS) should detect whenever the standard gas is analyzed under normal operating conditions. They depend on the actual isotopic/isotopomeric composition of the standard gas and also how that gas is fragmented in the IRMS. To calculate these three values we used 1) values of $\delta^{15}N^{\alpha}$, $\delta^{15}N^{\beta}$, and $\delta^{18}O$ for our standard gas as measured by Sakae Toyoda and 2) The relative yields of m/z 30 and 31 from $^{15}N^{14}NO$ and $^{14}N^{15}NO$ when these isotopomers are analyzed in the Casciotti IRMS (see Appendix B for details).

$^{31}R_{sample}$, $^{45}R_{sample}$, and $^{46}R_{sample}$ values are then entered into the following equations:

$$^{31}R = ((1-\gamma)\,^{15}R^{\alpha} + \kappa\,^{15}R^{\beta} + \,^{15}R^{\alpha}\,^{15}R^{\beta} + \,^{17}R(1 + \gamma\,^{15}R^{\alpha}$$

$$+ (1-\kappa)\,^{15}R^{\beta}))/\,(1 + \gamma\,^{15}R^{\alpha} + (1-\kappa)\,^{15}R^{\beta})$$

$$^{45}R = \,^{15}R^{\alpha} + \,^{15}R^{\beta} + \,^{17}R$$

$$^{46}R = (\,^{15}R^{\alpha} + \,^{15}R^{\beta})\,^{17}R + \,^{18}R + \,^{15}R^{\alpha}\,^{15}R^{\beta}$$

$$^{17}R/0.0003799 = (\,^{18}R/0.0020052)^{0.516}$$

where γ and κ are the yields of the scrambled fragment ions from $^{14}N^{15}NO$ ($^{30}NO^+$) and $^{15}N^{14}NO$ ($^{31}NO^+$), respectively (see Appendix B). The four equations above can be evaluated with a nonlinear equation solver to obtain values for $^{15}R^{\alpha}$, $^{15}R^{\beta}$, ^{17}R, and ^{18}R for each sample.

Appendix B

Calculating m/z 30 and 31 yield coefficients

When N_2O is introduced into the ion source of the mass spectrometer, NO^+ fragment ions are produced. While most of these ions contain N from the α position, a small amount of "scrambling" occurs, yielding NO^+ ions containing the β N. Accurate measurements of $^{15}R^{\alpha}$ and $^{15}R^{\beta}$ require quantification of the scrambling behavior for the mass spectrometer under standard operating conditions.

Westley et al. (2007) use six separate coefficients to describe the $^{30}NO^+$ and $^{31}NO^+$ fragmentation behaviors of the $^{14}N^{15}NO$, $^{15}N^{14}NO$, and $^{15}N^{15}NO$ molecules. We followed their recommendation and performed mixing analyses using purified $^{14}N^{15}NO$, $^{15}N^{14}NO$, and $^{15}N^{15}NO$ gases from ICON (Summit, N. J.) to investigate the fragmentation

behavior of individual isotopologues in our mass spectrometer (see supplementary material). We also compared this approach to the results of a simpler approach using two scrambling coefficients, γ and κ, to describe the relative production of $^{30}NO^+$ ions from $^{14}N^{15}NO$ and $^{31}NO^+$ ions from $^{15}N^{14}NO$, respectively. These coefficients were used in the system of equations that convert ^{31}R, ^{45}R, and ^{46}R to $^{15}R^{\alpha}$, $^{15}R^{\beta}$, ^{17}R, and ^{18}R for each sample (see Appendix A for the full set of equations).

We calculated γ and κ using a series of dual inlet measurements of two sample gases with known isotope and isotopomer ratios referenced to a standard gas that also has a known isotopic composition. In this case, the sample gases were from the laboratories of K. Koba (Tokyo University of Agriculture and Technology) and N. Ostrom (Michigan State University), and the standard gas was the reference gas from the Casciotti lab (WHOI). These three N_2O reference gases were all calibrated by S. Toyoda (Tokyo Institute of Technology).

For each sample gas the "measured" value of [rR 31NO/30NO$_{sample}$]/[rR 31NO/30NO$_{standard}$] was determined by averaging the results of a series of 10-cycle dual inlet analyses on the Casciotti IRMS. Then the "calculated" value of [rR 31NO/30NO$_{sample}$]/[rR 31NO/30NO$_{standard}$] (equivalent to $^{31}R_{sample}/^{31}R_{standard}$) was obtained by inserting Toyoda's calibrated values of $^{15}R^{\alpha}$, $^{15}R^{\beta}$, ^{17}R, and ^{18}R for the sample and standard gases into the equation below and guessing values of γ and κ:

$$^{31}R = ((1-\gamma)\,^{15}R^{\alpha} + \kappa\,^{15}R^{\beta} + \,^{15}R^{\alpha}\,^{15}R^{\beta} + \,^{17}R(1 + \gamma\,^{15}R^{\alpha} + (1-\kappa)\,^{15}R^{\beta}))/(1 + \gamma\,^{15}R^{\alpha} + (1-\kappa)\,^{15}R^{\beta})$$

The problem is one of optimization where the object is to vary γ and κ until the calculated values of $^{31}R_{sample}$ / $^{31}R_{standard}$ are as close as possible to the measured [rR 31NO/30NO$_{sample}$]/[rR 31NO/30NO$_{standard}$] for both sample gases. This two-coefficient model automatically obeys the constraint of Toyoda and Yoshida (1999) that $\delta^{15}N^{bulk} = (\,^{15}R^{\alpha} + \,^{15}R^{\beta})/2$. The optimized values obtained here are $\gamma = 0.1002$ and $\kappa = 0.0976$. These coefficients are consistent with reported values for fragment ion yields and scrambling coefficients (between 0.08–0.10) (Westley et al., 2007; Toyoda and Yoshida, 1999).

Following the alternative approach of Westley et al. (2007) we found that ionization of the $^{15}N^{14}NO$ ICON standard produced approximately one tenth as many $^{31}NO^+$ as the $^{14}N^{15}NO$ ICON standard (see supplementary material for data and calculations). This result is an independent confirmation of the scrambling coefficient approach described above (because $\kappa/(1-\gamma) = 0.108$) and it does not require a priori knowledge of the isotopomeric composition of the reference gas.

For the data presented in this paper, we opted to use two coefficients and assumed that the fragment ion yields of 30 and 31 sum to 1 for both $^{14}N^{15}NO$ and $^{15}N^{14}NO$. Using this approach we were able to reproduce the isotopomer ratio values of sample gases with a broad range of site preferences

(calibrated value for N. Ostrom tank = + 26.5‰ and the value measured using our approach = + 27.0‰; calibrated value of K. Koba tank = − 5.4‰ and measured = − 4.8‰).

Supplementary material related to this article is available online at:
http://www.biogeosciences.net/7/2695/2010/bg-7-2695-2010-supplement.pdf.

References

Alldredge, A. L. and Cohen, Y.: Can microscale chemical patches persist in the sea?, Microelectrode study of marine snow, fecal pellets, Science, 235, 689–691, 1987.

Andersson, K. K. and Hooper, A. B.: O_2 and H_2O are each sources of one O in NO_2^- produced from NH_3 by *Nitrosomonas*: ^{15}N-NMR evidence, FEBS Lett., 164, 236–240, 1983.

Andersson, K. K., Philson, S. B., and Hooper, A. B.: [18]O isotope shift in ^{15}N NMR analysis of biological N-oxidations: H_2O-NO_2^- exchange in the ammonia-oxidizing bacterium *Nitrosomonas*, P. Natl. Acad. Sci., 79, 5871–5875, 1982.

Arp, D. J., Chain, P. S. G., and Klotz, M. G.: The impact of genome analyses on our understanding of ammonia-oxidizing bacteria, Annu. Rev. Microbiol., 61, 503–528, 2007.

Bard, Y.: Nonlinear parameter estimation, Academic Press, New York, 1974.

Beaumont, H. J. E., Hommes, N. G., Sayavedra-Soto, L. A., Arp, D. J., Arciero, D. M., Hooper, A. B., Westerhoff, H. V., and van Spanning, R. J. M.: Nitrite reductase of *Nitrosomonas europaea* is not essential for production of gaseous nitrogen oxides and confers tolerance to nitrite, J. Bacteriol., 184, 2557–2560, 2002.

Beaumont, H. J. E., Lens, S., Reijnders, W. N. M., Westerhoff, H. V., and van Spanning, R. J. M.: Expression of nitrite reductase in *Nitrosomonas europaea* involves NsrR, a novel nitrite-sensitive transcription repressor, Mol. Microbiol., 54, 148–158, 2004.

Beman, M. J., Arrigo, K. R., and Matson, P. A.: Agricultural runoff fuels large phytoplankton blooms in vulnerable areas of the ocean, Nature, 434, 211–214, 2005.

Bender, M. L.: The $\delta^{18}O$ of dissoved O_2 in seawater: a unique tracer of circulation and respiration in the deep sea, J. Geophys. Res.-Oceans, 95, 22243–22252, 1990.

Buchwald, C. and Casciotti, K. L.: Oxygen isotopic fractionation and exchange during bacterial nitrite oxidation, Limnol. Oceanogr., 55, 1064–1074, 2010.

Cantera, J. J. and Stein, L. Y.: Molecular diversity of nitrite reductase genes (nirK) in nitrifying bacteria, Environmental Microbiology, 9, 765–776, 2007.

Carlucci, A. F. and McNally, P. M.: Nitrification by marine bacteria in low concentrations of substrate and oxygen, Limnol. Oceanogr., 14, 736–739, 1969.

Casciotti, K. L. and Ward, B. B.: Dissimilatory nitrite reductase genes from autotrophic ammonia-oxidizing bacteria, Appl. Environ. Microb., 67, 2213–2221, 2001.

Casciotti, K. L. and Ward, B. B.: Phylogenetic analysis of nitric oxide reductase gene homologues from aerobic ammonia-oxidizing bacteria, FEMS Microbiol. Ecol., 52, 197–205, 2005.

Casciotti, K. L., Sigman, D. M., Hastings, M. G., Bohlke, J. K., and Hilkert, A.: Measurements of the oxygen isotopic composition of nitrate in seawater and freshwater using the denitrifier method, Anal. Chem., 74, 4905–4912, 2002.

Casciotti, K. L., Bohlke, J. K., McIlvin, M., Mroczkowski, S. J., and Hannon, J. E.: Oxygen isotopes in nitrite: analysis, calibration, and equilibration, Anal. Chem., 79, 2427–2436, 2007.

Casciotti, K. L., McIlvin, M., and Buchwald, C.: Oxygen isotopic exchange and fractionation during bacterial ammonia oxidation, Limnol.Oceanogr., 55, 753–762, 2010.

Charpentier, J., Farias, L., Yoshida, N., Boontanon, N., and Raimbault, P.: Nitrous oxide distribution and its origin in the central and eastern South Pacific Subtropical Gyre, Biogeosciences, 4, 729–741, 2007, http://www.biogeosciences.net/4/729/2007/.

Cline, J. D., Wisegarver, D. P., and Kelly-Hansen, K.: Nitrous oxide and vertical mixing in the equatorial Pacific during the 1982–1983 El Niño, Deep-Sea Res., 34, 857–873, 1987.

Codispoti, L. A. and Christensen, J. P.: Nitrification, denitrification and nitrous oxide cycling in the eastern tropic south Pacific Ocean, Mar. Chem., 16, 277–300, 1985.

Codispoti, L. A., Brandes, J. A., Christensen, J. P., Devol, A. H., Naqvi, S. W. A., Paerl, H. W., and Yoshinari, T.: The oceanic fixed nitrogen and nitrous oxide budgets: moving targets as we enter the anthropocene?, Sci. Mar., 65, 85–105, 2001.

Cohen, Y. and Gordon, L. I.: Nitrous oxide in the oxygen minimum of the eastern tropical North Pacific: evidence for its consumption during denitrification and possible mechanisms for its production, Deep-Sea Res., 25, 509–524, 1978.

Cohen, Y. and Gordon, L. I.: Nitrous oxide production in the ocean, J. Geophys. Res., 84, 347–353, 1979.

Draper, N. R. and Smith, H.: Applied regression analysis, Wiley, New York, 2, 1981.

Dua, R. D., Bhandari, B., and Nicholas, D. J. D.: Stable isotope studies on the oxidation of ammonia to hydroxylamine by *Nitrosomonas europaea*, FEBS Lett., 106, 401–404, 1979.

Elkins, J. W., Wofsy, S., McElroy, M. B., Kolb, C. E., and Kaplan, W. A.: Aquatic sources and sinks for nitrous oxide, Nature, 275, 602–606, 1978.

Fuhrman, J. A. and Capone, D. G.: Possible biogeochemical consequences of ocean fertilization, Limnol. Oceanogr., 36, 1951–1959, 1991.

Fulweiler, R. W., Nixon, S. W., Buckley, B. A., and Granger, S. L.: Reversal of the net dinitrogen gas flux in coastal marine sed-

iments, Nature, 448, 180–181, 2007.

Galloway, J. N., Schlesinger, W. H., Levy II, H., Michaels, A., and Schnoor, J. L.: Nitrogen fixation: anthropogenic enhancement-environmental response, Global Biogeochem. Cy., 9, 235–252, 1995.

Goreau, T. J., Kaplan, W. A., Wofsy, S. C., McElroy, M. B., Valois, F. W., and Watson, S. W.: Production of NO_2^- and N_2O by nitrifying bacteria at reduced concentrations of oxygen, Appl. Environ. Microb., 40, 526–532, 1980.

Hallam, S. J., Mincer, T. J., Schleper, C., Preston, C. M., Roberts, K., Richardson, P. M., and DeLong, E. F.: Pathways of carbon assimilation and ammonia oxidation suggested by environmental genomic analyses of marine Crenarchaeota, PLoS Biol., 4, 521–536, 2006.

Hashimoto, L. K., Kaplan, W. A., Wofsy, S. C., and McElroy, M. B.: Transformations of fixed nitrogen and N_2O in the Cariaco Trench, Deep-Sea Res., 30, 575–590, 1983.

Helder, W. and de Vries, R. T. P.: Estuarine nitrite maxima and nitrifying bacteria (EMS-Dollard estuary), Neth J. Sea Res., 17, 1–18, 1983.

Hollocher, T. C., Tate, M. E., and Nicholas, D. J. D.: Oxidation of ammonia by Nitrosomonas europaea, J. Biol. Chem., 256, 10834–10836, 1981.

Hooper, A. B. and Terry, K. R.: Hydroxylamine oxidoreductase of Nitrosomonas production of nitric oxide from hydroxylamine, BBA.-Bioenergetics, 571, 12–20, 1979.

Ignarro, L. J., Fukuto, J. M., Griscavage, J. M., and Rogers, N. E.: Oxidation of nitric oxide in aqueous solution to nitrite but not nitrate: comparison with enzymatically formed nitric oxide from L-arginine, P. Natl. Acad. Sci., 90, 8103–8107, 1993.

IPCC: Climate Change 2007: The Physical Science Basis, Cambridge University Press, New York, NY, USA, 2007.

Jin, X. and Gruber, N.: Offsetting the radiative benefit of ocean iron fertilization by enhancing N_2O emissions, Geophys. Res. Lett., 30, 1–4, 2003.

Jorgensen, K. S., Jensen, H. B., and Sorensen, J.: Nitrous oxide production from nitrification and denitrification in marine sediment at low oxygen concentrations, Can. J. Microbiol., 30, 1073–1078, 1984.

Knowles, R., Lean, D. R. S., and Chan, Y. K.: Nitrous oxide concentrations in lakes: variations with depth and time, Limnol. Oceanogr., 26, 855–866, 1981.

Koba, K., Osaka, K., Tobari, Y., Toyoda, S., Ohte, N., Katsuyama, M., Suzuki, N., Itoh, M., Yamagishi, H., Kawasaki, M., Kim, S. J., Yoshida, N., and Nakajima, T.: Biogeochemistry of nitrous oxide in groundwater in a forested ecosystem elucidated by nitrous oxide isotopomer measurements, Geochim. Cosmochim. Ac., 73, 3115–3133, 2009.

Kool, D. M., Wrage, N., Oenema, O., Dolfing, J., and van Groenigen, J. W.: Oxygen exchange between (de)nitrification intermediates and H_2O and its implications for source determination of NO_3^- and N_2O: a review, Rapid Commun. Mass Sp., 21, 3569–3578, 2007.

Kroopnick, P. and Craig, H.: Oxygen isotope fractionation in dissolved oxygen in the deep sea, Earth Planet. Sc. Lett., 32, 375–388, 1976.

Law, C. S. and Ling, R. D.: Nitrous oxide flux and response to increased iron availability in the Antarctic Circumpolar Current, Deep-Sea Res. II, 48, 2509–2527, 2001.

Levine, N. M., Bender, M. L., and Doney, S. C.: The $\delta^{18}O$ of dissoved O_2 as a tracer of mixing and respiration in the mesopelagic ocean, Global Biogeochem. Cy., 23, GB1006, doi:10.1029/2007GB003162, 2009.

Lewis, R. S. and Deen, W. M.: Kinetics of the reaction of nitric oxide with oxygen in aqueous solutions, Chem. Res. Toxicol., 7, 568–574, 1994.

Lipschultz, F., Zafiriou, O. C., Wofsy, S. C., McElroy, M. B., Valois, F. W., and Watson, S. W.: Production of NO and N_2O by soil nitrifying bacteria, Nature, 294, 641–643, 1981.

Mariotti, A., Germon, J. C., Hubert, P., Kaiser, P., Letolle, R., Tardieux, A., and Tardieux, P.: Experimental determination of nitrogen kinetic isotope fractionation: some principles; illustration for the denitrification and nitrification processes, Plant Soil, 62, 413–430, 1981.

McIlvin, M. M. and Altabet, M.: Chemical conversion of nitrate and nitrite to nitrous oxide for nitrogen and oxygen isotopic analysis in freshwater and seawater, Anal. Chem., 77, 5589–5595, 2005.

McIlvin, M. M. and Casciotti, K. L.: Automated stable isotopic analysis of dissolved nitrous oxide at natural abundance levels, Limnol. Oceanogr.- Meth., 8, 54–66, 2010.

Naqvi, S. W. A., Jayakumar, D. A., Narvekar, P. V., Naik, H., Sarma, V. V. S. S., D'Souza, W., Joseph, S., and George, M. D.: Increased marine production of N_2O due to intensifying anoxia on the Indian continental shelf, Nature, 408, 346–349, 2000.

Nevison, C., Butler, J. H., and Elkins, J. W.: Global distribution of N_2O and the ⊠ N_2O-AOU yield in the subsurface ocean, Global Biogeochem. Cy., 17, GB1119, doi:10.1029/2003GB002068, 2003.

Norton, J. M., Klotz, M. G., Stein, L. Y., Arp, D. J., Bottomley, P. J., Chain, P. S. G., Hauser, L. J., Land, Miriam, L., Larimer, F. W., Shin, M. W., and Starkenburg, S. R.: Complete genome sequence of Nitrosospira multiformis, an ammonia-oxidizing bacterium from the soil environment, Appl. Environ. Microbiol., 74, 3559–3572, 2008.

Ostrom, N. E., Russ, M. E., Popp, B., Rust, T. M., and Karl, D. M.: Mechanisms of nitrous oxide production in the subtropical North Pacific based on determinations of the isotopic abundances of nitrous oxide and di-oxygen, Chemosphere-Global Change Science, 2, 281–290, 2000.

Ostrom, N. E., Pitt, A., Ostrom, P. H., Grandy, A. S., Huizinga, K. M., and Robertson, G. P.: Isotopologue effects during N_2O reduction in soils and in pure cultures of denitrifiers, J. Geophys. Res., 112, 1–12, 2007.

Pai, S.-C. and Yang, C.-C.: Formation kinetics of the pink azo dye in the determination of nitrite in natural waters, Anal. Chim. Acta, 232, 345–349, 1990.

Payne, W. J., Riley, P. S., and Cox, C. D. J.: Separate nitrite, nitric oxide, and nitrous oxide reducing fractions from Pseudomonas perfectomarinus, J. Bacteriol., 106, 356–361, 1971.

Popp, B. N., Westley, M. B., Toyoda, S., Miwa, T., Dore, J. E., Yoshida, N., Rust, T. M., Sansone, F. J., Russ, M. E., Ostrom, N. E., and Ostrom, P. H.: Nitrogen and oxygen isotopomeric constraints on the origins and sea-to-air flux of N_2O in the oligotrophic subtropical North Pacific gyre, Global Biogeochem. Cy., 16, GB1064, doi:10.1029/2001GB001806, 2002.

Poth, M. and Focht, D.: [15]N kinetic analysis of N_2O production by Nitrosomonas europaea: an examination of nitrifier denitrification, Appl. Environm. Microbr., 49, 1134–1141, 1985.

Remde, A. and Conrad, R.: Production of nitric oxide in *Nitrosomonas europaea* by reduction of nitrite, Arch. Microbiol., 154, 187–191, 1990.

Ritchie, G. A. F. and Nicholas, D. J. D.: Identification of the sources of nitrous oxide produced by oxidative and reductive processes in *Nitrosomonas europaea*, Biochemi. J., 126, 1181–1191, 1972.

Rodionov, D. A., Dubchak, I. L., Arkin, A. P., Alm, E. J., and Gelfand, M. S.: Dissimilatory metabolism of nitrogen oxides in bacteria: comparative reconstruction of transcriptional networks, PLoS Computational Biology, 1, 415–431, 2005.

Schmidt, H.-L., Werner, R. A., Yoshida, N., and Well, R.: Is the isotopic composition of nitrous oxide an indicator for its origin from nitrification or denitrification? A theoretical approach from referred data and microbiological and enzyme kinetic aspects, Rapid Commun. Mass Sp., 18, 2036–2040, 2004.

Shaw, L. J., Nicol, G. W., Smith, Z., Fear, J., Prosser, J., and Baggs, E. M.: *Nitrosospira* spp. can produce nitrous oxide via a nitrifier denitrification pathway, Environ. Microbiol., 8, 214–222, 2006.

Solorzano, L.: Determination of ammonia in natural waters by the phenolhypochlorite method, Limnol. Oceanogr., 14, 799–801, 1969.

Suntharalingam, P. and Sarmiento, J. L.: Factors governing the oceanic nitrous oxide distribution: simulations with an ocean general circulation model, Global Biogeochem. Cy., 14, 429–454, 2000.

Sutka, R. L., Ostrom, N. E., Ostrom, P. H., Gandhi, H., and Breznak, J. A.: Nitrogen isotopomer site preference of N_2O produced by *Nitrosomonas europaea* and *Methylococcus capsulatus* Bath, Rapid Commun. Mass Sp., 17, 738–745, 2003.

Sutka, R. L., Ostrom, N. E., Ostrom, P. H., Gandhi, H., and Breznak, J. A.: Nitrogen isotopomer site preference of N_2O produced by *Nitrosomonas europaea* and *Methylococcus capsulatus* Bath, Rapid Commun. Mass Sp., 18, 1411–1412, 2004.

Sutka, R. L., Ostrom, N. E., Ostrom, P. H., Breznak, J. A., Gandhi, H., Pitt, A. J., and Li, F.: Distinguishing nitrous oxide production from nitrification and denitrification on the basis of isotopomer abundances, Appl. Environ. Microbr., 72, 638–644, 2006.

Toyoda, S. and Yoshida, N.: Determination of nitrogen isotopomers of nitrous oxide on a modified isotope ratio mass spectrometer, Anal. Chem., 71, 4711–4718, 1999.

Toyoda, S., Yoshida, N., Miwa, T., Matsui, Y., Yamagishi, H., and Tsunogai, U.: Production mechanism and global budget of N_2O inferred from its isotopomers in the western North Pacific, Geophys. Res. Lett., 29(3), 1037, doi:10.1029/2001GL014311., 2002.

Toyoda, S., Mutobe, H., Yamagishi, H., Yoshida, N., and Tanji, Y.: Fractionation of N_2O isotopomers during production by denitrifier, Soil Biol. Biochem., 37, 1535–1545, 2005.

Treusch, A. H., Leininger, S., Kletzin, A., Schuster, S. C., Klenk, H.-P., and Schleper, C.: Novel genes for nitrite reductase and Amo-related proteins indicate a role of uncultivated mesophilic crenarchaeota in nitrogen cycling, Environ. Microbiol., 7, 1985–1995, 2005.

Walker, C. B., de la Torre, J. R., Klotz, M. G., Pinel, N., Arp, D. J., Brochier-Armanet, C., Chain, P. S. G., Chan, P. P., Gollabgir, A., and Hemp, J.: *Nitrosopumilus maritimus* genome reveals unique mechanisms for nitrification and autotrophy in globally distributed marine crenarchaea, Proceedings of the National Academy of Science, 107, 8818–8823, 2010.

Ward, B. B., Olson, R. J., and Perry, M. J.: Microbial nitrification rates in the primary nitrite maximum off southern California, Deep-Sea Res., 29, 247–255, 1982.

Watson, S. W.: Characteristics of a marine nitrifying bacterium, *Nitrosocystis oceanus* sp. nov., Limnol. Oceanogr., 10, R274–R289, 1965.

Westley, M. B., Popp, B. N., and Rust, T. M.: The calibration of the intramolecular nitrogen isotope distribution in nitrous oxide measured by isotope ratio mass spectrometry, Rapid Commun. Mass Sp., 21, 391–405, 2007.

Wrage, N., van Groenigen, J. W., Oenema, O., and Baggs, E. M.: A novel dual-isotope labelling method for distinguishing between soil sources of N_2O, Rapid Commun. Mass Sp., 19, 3298–3306, 2005.

Yoshida, N.: ^{15}N-depleted N_2O as a product of nitrification, Nature, 335, 528–529, 1988.

Yoshida, N. and Toyoda, S.: Constraining the atmospheric N_2O budget from intramolecular site preference in N_2O isotopomers, Nature, 405, 330–334, 2000.

Yoshida, N., Morimoto, H., Hirano, M., Koike, I., Matsuo, S., Wada, Eitaro adn Saino, T., and Hattori, A.: Nitrification rates and ^{15}N abundances of N_2O and NO_3^- in the western North Pacific, Nature, 342, 895–897, 1989.

Yoshinari, T.: Nitrous oxide in the sea, Mar. Chem., 4, 189–202, 1976.

Yung, Y. L. and Miller, C. E.: Isotopic fractionation of stratospheric nitrous oxide, Science, 278, 1778–1780, 1997.

Table A1: Cell abundances measured at the start and end of the cell density experiment. Averages are given for replicate treatments.

timepoint	density (cells/ml)	stdev (cells/ml)
20% O2 high cell density		
Tinitial	1539884	226511
Tfinal	1492285	56160
20% O2 medium cell density		
Tinitial	22992	3780
Tfinal	46755	4740
20% O2 low cell density		
Tinitial	250	-
Tfinal	17239	2099
2% O2 high cell density		
Tinitial	1527693	106827
Tfinal	1583817	46295
2% O2 medium cell density		
Tinitial	21031	1365
Tfinal	48062	45593
2% O2 low cell density		
Tinitial	103	-
Tfinal	16681	1545
0.5% O2 high cell density		
Tinitial	1399267	-
Tfinal	1376279	-
0.5% O2 medium cell density		
Tinitial	18054	3740
Tfinal	47720	-
0.5% O2, low cell density		
Tinitial	138	-
Tfinal	17495	3261

SUPPLEMENTARY MATERIAL

CAITLIN H FRAME, KAREN L CASCIOTTI

## 1. Calculating Isotopomer-Specific Ion Yields

Here we describe the results obtained from the calibration exercises recommended for calibration of isotopomer measurements using mixtures of pure isotopomer gases (ICON) and our N_2O reference gas (Westley et al., 2007). In this approach, the fragment ion yields from $^{15}N^{14}N^{16}O$ and $^{14}N^{15}N^{16}O$ are determined experimentally from analysis of these isotopomers mixed with our calibrated N_2O reference gas.

In dual inlet mode, we filled one bellows with a mixture of one of two isotopomers ($^{15}N^{14}N^{16}O$ or $^{14}N^{15}N^{16}O$) and variable proportions of our standard gas. The other bellows was filled with our standard gas. The ratios of the $\frac{^{31}NO^+}{^{30}NO^+}$ (^{31}R) and $\frac{^{45}N_2O^+}{^{44}N_2O^+}$ (^{45}R) measurements from the mixture and standard gases are graphed below as ratios ($\frac{^{31}R_{mixture}}{^{31}R_{standard}}$ and $\frac{^{45}R_{mixture}}{^{45}R_{standard}}$) in red and blue circles (Figure S.1). The raw data are given in the excel file included with the Supplementary Material.

Next, we developed a series of equations that relate $\frac{^{31}R_{mixture}}{^{31}R_{standard}}$ and $\frac{^{45}R_{mixture}}{^{45}R_{standard}}$ to the yields of $^{31}NO^+$, $^{30}NO^+$, $^{45}N_2O^+$, and $^{44}N_2O^+$ from the ICON isotopologues and our standard gas. The fractional yields of the fragment ions ($^{30}NO^+$, $^{31}NO^+$) and molecular ions ($^{44}N_2O^+$, $^{45}N_2O^+$) are assumed to be constants for each of the three gases under standard operating source conditions and are defined as follows:

$$31_{standard} = \frac{\text{yield } 31^+}{\text{mole standard}} \quad \text{and} \quad 31_{ICON} = \frac{\text{yield } 31^+}{\text{mole ICON}}$$

S.1: The ratios of the ^{31}R and ^{45}R measurements from the ICON mixture and standard gases.
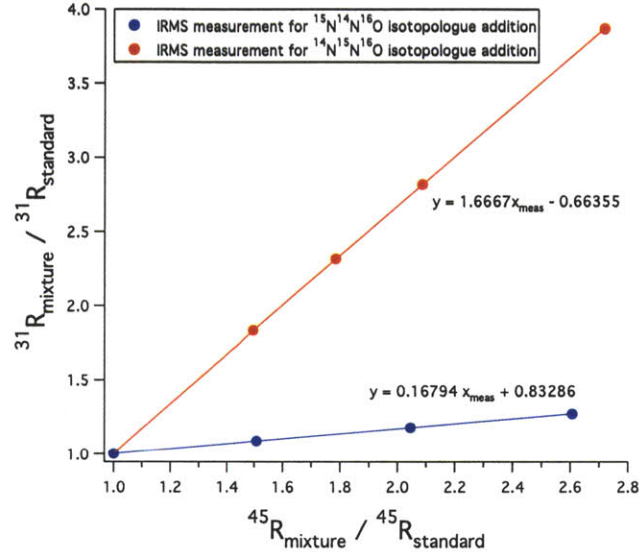
$$30_{\text{standard}} = \frac{\text{yield } 30^+}{\text{mole standard}} \quad \text{and} \quad 30_{\text{ICON}} = \frac{\text{yield } 30^+}{\text{mole ICON}}$$

$$45_{\text{standard}} = \frac{\text{yield } 45^+}{\text{mole standard}} \quad \text{and} \quad 45_{\text{ICON}} = \frac{\text{yield } 45^+}{\text{mole ICON}}$$

$$44_{\text{standard}} = \frac{\text{yield } 44^+}{\text{mole standard}} \quad \text{and} \quad 44_{\text{ICON}} = \frac{\text{yield } 44^+}{\text{mole ICON}}$$

Then, for any mixture of ICON gas and standard gas we have:

$$^{31}\text{R}_{\text{mixture}} = \frac{31_{\text{mixture}}}{30_{\text{mixture}}} = \frac{\text{F} \times \frac{\text{yield } 31^+}{\text{mole standard}} + (1-\text{F}) \times \frac{\text{yield } 31^+}{\text{mole ICON}}}{\text{F} \times \frac{\text{yield } 30^+}{\text{mole standard}} + (1-\text{F}) \times \frac{\text{yield } 30^+}{\text{mole ICON}}}$$

40

and

$$^{45}R_{\text{mixture}} = \frac{45_{\text{mixture}}}{44_{\text{mixture}}} = \frac{F \times \frac{\text{yield } 45^+}{\text{mole standard}} + (1-F) \times \frac{\text{yield } 45^+}{\text{mole ICON}}}{F \times \frac{\text{yield } 44^+}{\text{mole standard}} + (1-F) \times \frac{\text{yield } 44^+}{\text{mole ICON}}}$$

where the mixing fractions F and $1 - F$, are defined as follows:

$$F = \frac{\text{moles standard}}{\text{moles ICON+moles standard}}$$

$$1 - F = \frac{\text{moles ICON}}{\text{moles ICON+moles standard}}$$

Based on the above definitions of $^{31}R_{\text{mixture}}$ and $^{45}R_{\text{mixture}}$, if we divide $^{31}R_{\text{mixture}}$ by $^{31}R_{\text{standard}}$ or $^{45}R_{\text{mixture}}$ by $^{45}R_{\text{standard}}$ we get:

$$\frac{^{31}R_{\text{mixture}}}{^{31}R_{\text{standard}}} = \frac{F+(1-F)\times\frac{\text{yield } 31^+}{\text{mole ICON}} \div \frac{\text{yield } 31^+}{\text{mole standard}}}{F+(1-F)\times\frac{\text{yield } 30^+}{\text{mole ICON}} \div \frac{\text{yield } 30^+}{\text{mole standard}}}$$

$$\frac{^{45}R_{\text{mixture}}}{^{45}R_{\text{standard}}} = \frac{F+(1-F)\times\frac{\text{yield } 45^+}{\text{mole ICON}} \div \frac{\text{yield } 45^+}{\text{mole standard}}}{F+(1-F)\times\frac{\text{yield } 44^+}{\text{mole ICON}} \div \frac{\text{yield } 44^+}{\text{mole standard}}}$$

By making the following substitutions

$$A = \frac{\text{yield } 31^+}{\text{mole ICON}} \div \frac{\text{yield } 31^+}{\text{mole standard}}$$

$$B = \frac{\text{yield } 30^+}{\text{mole ICON}} \div \frac{\text{yield } 30^+}{\text{mole standard}}$$

$$C = \frac{\text{yield } 45^+}{\text{mole ICON}} \div \frac{\text{yield } 45^+}{\text{mole standard}}$$

$$D = \frac{\text{yield } 44^+}{\text{mole ICON}} \div \frac{\text{yield } 44^+}{\text{mole standard}}$$

we can simplify the expressions for $\frac{^{31}R_{\text{mixture}}}{^{31}R_{\text{standard}}}$ and $\frac{^{45}R_{\text{mixture}}}{^{45}R_{\text{standard}}}$:

$$\frac{^{31}R_{\text{mixture}}}{^{31}R_{\text{standard}}} = \frac{F + (1-F) \times A}{F + (1-F) \times B}$$

$$\frac{^{45}R_{\text{mixture}}}{^{45}R_{\text{standard}}} = \frac{F + (1-F) \times C}{F + (1-F) \times D}$$

Solving for F in terms of A, B, and $\frac{^{31}R_{\text{mixture}}}{^{31}R_{\text{standard}}}$ we have

$$F = \frac{A - \frac{^{31}R_{\text{mixture}}}{^{31}R_{\text{standard}}} \times B}{\frac{^{31}R_{\text{mixture}}}{^{31}R_{\text{standard}}} - 1 + A - \frac{^{31}R_{\text{mixture}}}{^{31}R_{\text{standard}}} \times B}$$

By substituting this expression of F into the equation for $\frac{^{45}R_{\text{mixture}}}{^{45}R_{\text{standard}}}$ (see the column labeled 'calc $^{45}R/^{45}R$std' in the supplementary spreadsheet), we now have an equation for $\frac{^{45}R_{\text{mixture}}}{^{45}R_{\text{standard}}}$ in terms of $\frac{^{31}R_{\text{mixture}}}{^{31}R_{\text{standard}}}$ with unknown parameters A, B, C, and D. This equation can be applied to both $^{14}N^{15}N^{16}O$ and $^{15}N^{14}N^{16}O$ ICON standard mixtures but they will have different sets of best fit values for A, B, C, and D which we call A, B, C, and D for the $^{15}N^{14}N^{16}O$ isotopomer and A', B', C', and D' for the $^{14}N^{15}N^{16}O$ isotopomer.

By definition, these parameters are all referenced to the appropriate ion yields from our reference gas, so it is possible to make direct comparisons between A and A', C and C', etc. The values of A and A' (the relative yields of $^{31}NO^+$) were fitted by varying A, B, C, and D until the calculated slopes and intercepts of the $\frac{^{45}R_{mixture}}{^{45}R_{standard}}$ vs. $\frac{^{31}R_{mixture}}{^{31}R_{standard}}$ lines aligned with those of the actual measurements from the ICON mixing analyses in Figure S.1. The ratios calculated for $\frac{^{45}R_{mixture}}{^{45}R_{standard}}$ using the fitted values of A, B, C, D, A', B', C', and D' and the measured values of $\frac{^{31}R_{mixture}}{^{31}R_{standard}}$ are graphed below (Figure S.2). The fitted

S.2: The values of $\frac{^{45}R_{mixture}}{^{45}R_{standard}}$ calculated using fitted values (A, B, C, D and A', B', C', D') for each ion yield.
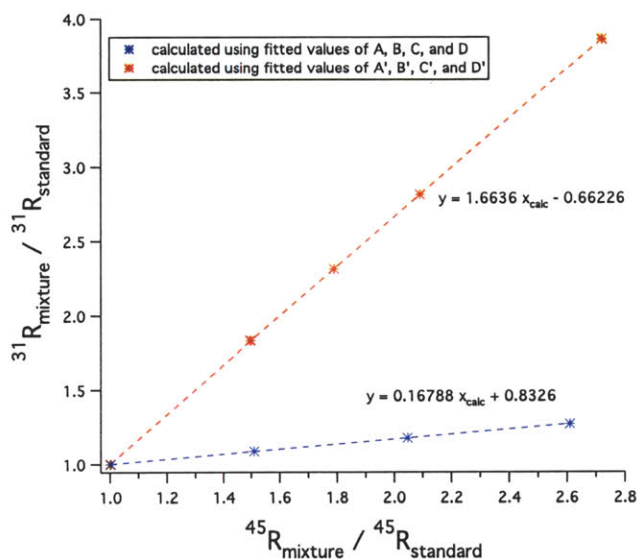
values are A = 22.65 and A' = 217. The numbers indicate that when the $^{15}N^{14}N^{16}O$ and $^{14}N^{15}N^{16}O$ isotopologues are ionized, they make 22.65 and 217 times as many $^{31}NO^+$ per mole of parent gas than the gas in our reference tank. Their ratio (= 0.104) indicates that in our ion source, the $^{14}N^{15}N^{16}O$ isotopologue yields about ten times as many $^{31}NO^+$ than the $^{15}N^{14}N^{16}O$ isotopologue.

Although the fitted values of B and B' could be used to produce a similar estimate of the $^{30}NO^+$ yields of the ICON standards referenced to our standard tank, the slopes of

the calibration lines are not very sensitive to changes in B and B' because the gas in our standard tank also produces a large yield of $^{30}NO^+$.

We note that in this model of the $\frac{^{45}R_{mixture}}{^{45}R_{standard}}$ vs. $\frac{^{31}R_{mixture}}{^{31}R_{standard}}$ line, the best fit values of A and A' are dependent on the relative ion yields of $^{45}N_2O^+$ from each isotopomer (the values of the C and C' parameters). We used values of C and C' that are essentially equal to each other and very close to values that we estimated by analyzing individual ICON standard gases using a single Faraday cup and peak jumping as discussed in Westley et al (2007).

2. N_2O AND NO_2^- ACCUMULATION DURING NH_3 OXIDATION

The N_2O data presented in the main text were from end-point experiments. Here we present the results of a time-course experiment used to monitor the N_2O yields over the course of an incubation. The experiment was set up and initiated in the same way as the other experiments. The initial cell density was approximately 5×10^4 cells ml^{-1}. Replicate bottles were sacrificed by adding 1 ml of 6M NaOH at different timepoints along the course of the oxidation of 50 μM NH_4^+. Total N_2O was measured for each bottle by analyzing it on the mass spectrometer with the same purge and trap system described in the main text. Yields were consistently 3×10^{-4} for bottles containing 20% O_2 and dropped from 8×10^{-4} at the 6 hour timepoint down to 4×10^{-4} at the 72 hour timepoint for bottles containing 0.5% O_2.

S.3: Growth of C-113a on 50 μM NH_4^+. N_2O accumulates steadily as NH_3 is oxidized and NO_2^- accumulates. N_2O production drops off when NH_3 is completely oxidized.
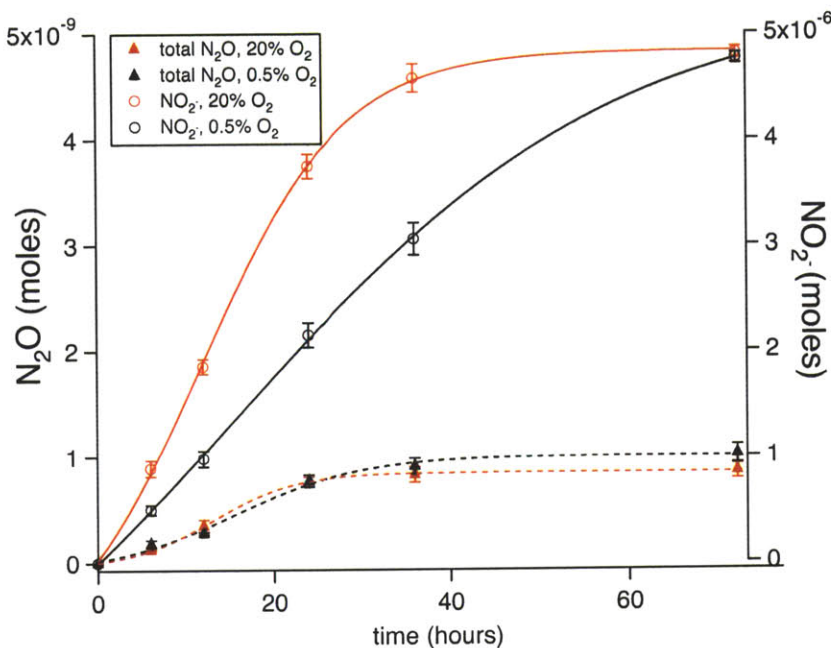
3. Sensitivity Analyses of Site Preference End-member values, SP_{ND} and SP_{NH2OH}, to $^{18}\epsilon_{ND}$ and $^{18}\epsilon_{NH2OH}$

We were able to manipulate the $\delta^{18}O$ of the NO_2^- and N_2O produced during ammonia oxidation by carrying parallel experiments out in ^{18}O-enriched and unenriched water. In equation (6) (see the main text), the sensitivity of SP_{ND} and SP_{NH2OH} to the values of the isotope effects $^{18}\epsilon_{ND}$ and $^{18}\epsilon_{NH2OH}$ depends on the values of $\delta^{18}O\text{-}NO_2^-$, $\delta^{18}O\text{-}N_2O_{total}$, and SP_{total}. Here we demonstrate that the value of the SP_{ND} end-member may be less sensitive to $^{18}\epsilon_{ND}$ and $^{18}\epsilon_{NH2OH}$ in ^{18}O-labeled H_2O.

To test the sensitivity of SP_{ND} to $^{18}\epsilon_{ND}$, $^{18}\epsilon_{NH2OH}$, and SP_{NH2OH}, values were substituted into equation (6) as follows: $SP_{total} = 17‰$, $\delta^{18}O\text{-}N_2O_{total} = 19‰$ in unlabeled water and $35‰$ in labeled water, $\delta^{18}O\text{-}NO_2^- = 6‰$ in unlabeled water and $44‰$ in labeled water, and $\delta^{18}O\text{-}O_2 = 25.3‰$ in all experiments. We note that these values fall within the ranges of the values of SP, $\delta^{18}O\text{-}N_2O$ (see Figure 5 in the main text), and $\delta^{18}O\text{-}NO_2^-$ that were

45

actually observed but they are not representative of all datapoints that were included as model inputs for the non-linear regression analysis discussed in the main text. In Figures S.4A and S.4B, the best fit value of SP_{NH_2OH} (36.3‰) was used to calculate SP_{ND} and $^{18}\epsilon_{NH_2OH}$ for different $^{18}\epsilon_{ND}$. In Figures S.4C and S.4D, the best fit value of $^{18}\epsilon_{ND}$ (-8.4‰) was used to calculate SP_{ND} and $^{18}\epsilon_{NH_2OH}$ for different SP_{NH_2OH}.

Using the parameter values discussed above, SP_{ND} is more sensitive to $^{18}\epsilon_{ND}$ in unlabeled water (Figure S.4A) than in labeled water (Figure S.4B), as indicated by the larger vertical distance between contours (lines of constant $^{18}\epsilon_{ND}$) in S.4A than in S.4B. SP_{ND} is also more sensitive to $^{18}\epsilon_{NH_2OH}$ in unlabeled water (Figures S.4A and S.4C) than labeled water (Figures S.4B and S.4D). This is evident in that the lines of constant $^{18}\epsilon_{ND}$ or SP_{NH_2OH} are more horizontal in S.4B and S.4D than they are in S.4A or S.4C.

We also see this in Supplementary Tables 1 and 2, where we have recalculated SP_{ND} using values of $^{18}\epsilon_{NH_2OH}$, $^{18}\epsilon_{ND}$, and SP_{NH_2OH} that are one standard deviation higher or lower than the best fit values. For the same set of best fit values and standard deviations, the calculated range of SP_{ND} values is larger in unlabeled water (Supplementary Table 1) than in labeled water (Supplementary Table 2).

This data set had a larger range of $\delta^{18}O$-N_2O values than it would have had if we had only included data from cultures in unlabeled water. The larger range of $\delta^{18}O$-N_2O in labeled water helps explain the reduced sensitivity of the model parameters to each other in labeled water. Future experiments may expand this range even further by increasing the difference between the substrate $\delta^{18}O$-O_2 and $\delta^{18}O$-H_2O values.
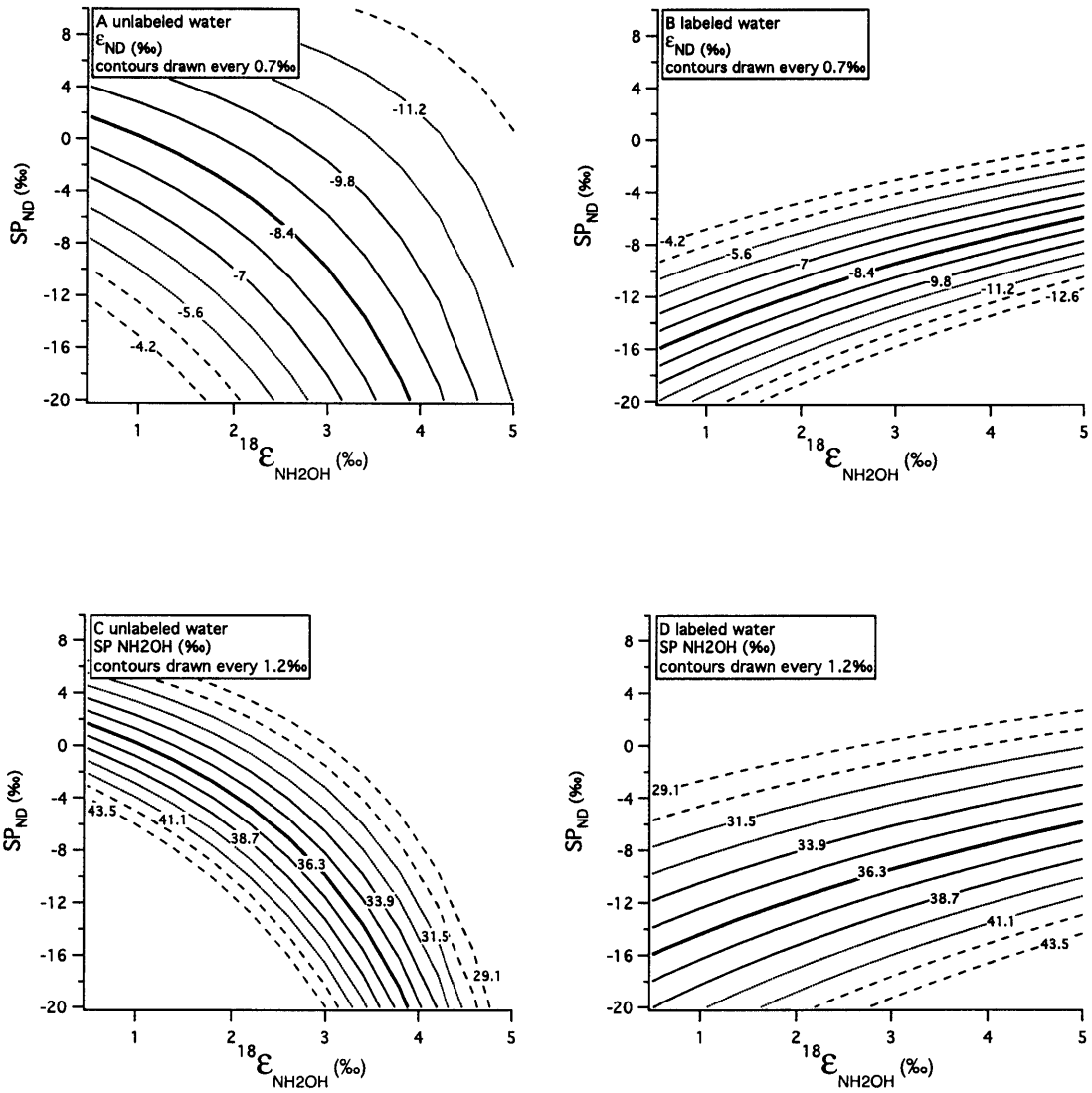
S.4: Sensitivity of SP_{ND} estimates from the end-member mixing model to variations in $^{18}\epsilon_{NH_2OH}$ for different values of $^{18}\epsilon_{ND}$ (contours in panels A and B) or SP_{NH_2OH} (contours in panels C and D), in water labeled with ^{18}O (panels B and D) and in unlabeled water (panels A and C). In all plots, lines were drawn every $\sigma/2$ (based on the estimated standard

deviations in Table 1 of the main text) for the contoured variable.

TABLE 1. The effect of uncertainty in $^{18}\epsilon_{NH_2OH}$, $^{18}\epsilon_{ND}$, and SP_{NH_2OH} on the calculated value of SP_{ND} in unlabeled water ($\delta^{18}O \simeq$ -5‰). All entries are in ‰. Bold entries in the first three columns have been changed ± one standard deviation above and below the best fit values.

$^{18}\epsilon_{NH_2OH}$	$^{18}\epsilon_{ND}$	SP_{NH_2OH}	SP_{ND}	SP_{total}	$\delta^{18}O\text{-}N_2O_{total}$	$\delta^{18}O\text{-}NO_2-$	$\delta^{18}O\text{-}O_2$
2.1	-8.4	36.3	**-4.1**	17	19	6	25.3
2.9	-8.4	36.3	**-9.1**	17	19	6	25.3
3.7	-8.4	36.3	**-17.2**	17	19	6	25.3
2.9	**-9.8**	36.3	**-1.2**	17	19	6	25.3
2.9	**-8.4**	36.3	**-9.1**	17	19	6	25.3
2.9	**-7.0**	36.3	**-17.1**	17	19	6	25.3
2.9	-8.4	**33.9**	**-5.9**	17	19	6	25.3
2.9	-8.4	**36.3**	**-9.1**	17	19	6	25.3
2.9	-8.4	**38.7**	**-12.4**	17	19	6	25.3

TABLE 2. The effect of uncertainty in $^{18}\epsilon_{NH_2OH}$, $^{18}\epsilon_{ND}$, and SP_{NH_2OH} on the calculated value of SP_{ND} in ^{18}O-labeled water ($\delta^{18}O \simeq$ 40‰). All entries are in ‰. Bold entries in the first three columns have been changed ± one standard deviation above and below the best fit values.

$^{18}\epsilon_{NH_2OH}$	$^{18}\epsilon_{ND}$	SP_{NH_2OH}	SP_{ND}	SP_{total}	$\delta^{18}O\text{-}N_2O_{total}$	$\delta^{18}O\text{-}NO_2-$	$\delta^{18}O\text{-}O_2$
2.1	-8.4	36.3	**-11.5**	17	35	44	25.3
2.9	-8.4	36.3	**-9.7**	17	35	44	25.3
3.7	-8.4	36.3	**-8.1**	17	35	44	25.3
2.9	**-9.8**	36.3	**-11.8**	17	35	44	25.3
2.9	**-8.4**	36.3	**-9.7**	17	35	44	25.3
2.9	**-7**	36.3	**-7.5**	17	35	44	25.3
2.9	-8.4	**33.9**	**-6.3**	17	35	44	25.3
2.9	-8.4	**36.3**	**-9.7**	17	35	44	25.3
2.9	-8.4	**38.7**	**-13.0**	17	35	44	25.3

3: NITROUS OXIDE PRODUCTION BY NITRIFICATION DURING A COASTAL PHYTOPLANKTON BLOOM

1. ABSTRACT

Coastal nitrogen cycling contributes significantly to marine nitrous oxide (N_2O) emissions. Nitrification is a part of this cycle that produces N_2O. However, the factors that control the N_2O yield of nitrification in coastal microbial communities are not well understood. Potential nitrification rates and N_2O production rates were measured over four consecutive weeks during a spring bloom of the cyanobacteria *Synechococcus* in Woods Hole Harbor off Cape Cod, Massachusetts using ^{15}N tracer techniques. The transformation of 99.8% ^{15}N ammonium (NH_4^+) into nitrite (NO_2^-) and nitrate (NO_3^-) was measured during a 24 hour incubation consisting of a 12 hour dark period followed by a 12 hour light period. The isotopic composition of the NH_4^+ was also measured and used to correct nitrification and N_2O production rates for significant regenerative dilution of the ^{15}N-NH_4^+ over time (20-40% of the initial enrichment). Nitrification rates were low and nearly constant over the course of the bloom (0.2-0.4 $\frac{nmole}{l \times day}$) and the rates during the dark and light periods were similar. In contrast, N_2O production increased steadily as the *Synechococcus* bloom expanded, starting at 0.7 $\frac{fmole}{l \times day}$ and peaking at 3.8 $\frac{fmole}{l \times day}$ along with the *Synechococcus* abundance. N_2O yields from nitrification were high, ranging from 4×10^{-3} to 33×10^{-3} with the yield peaking at the same time as the *Synechococcus* abundance peaked. NO_2^- and oxygen (O_2) concentrations, which are known to affect N_2O yields in nitrifier cultures, remained constant over the course of each incubation ($\sim$65nM and 20%, respectively), suggesting that (an)other factor(s), such as a different microbial community composition or rising organic and particulate concentrations was driving the change in yield.

2. INTRODUCTION

Nitrous oxide (N_2O) is a long-lived greenhouse gas whose atmospheric concentration has risen since the industrial revolution, along with carbon dioxide (CO_2) (Weiss et al., 1981; Prinn et al., 1990). Unlike CO_2, the increase in N_2O is not directly driven by fossil fuel combustion. Rather, it is mainly due to increasing use of nitrogen-rich fertilizers and other agricultural activities (Seitzinger and Kroeze, 1998; Prinn et al., 1990). River nitrogen fluxes are directly correlated with population density (Howarth et al., 1996) so that

human impacted coastal regions that would otherwise be nutrient limited are particularly susceptible to phytoplankton blooms (Beman et al., 2005). Large N_2O fluxes observed in these coastal areas have been linked to elevated organic carbon, nitrogen, and oxygen (O_2) concentrations during phytoplankton blooms (Harrison and Matson, 2003).

Nitrification and denitrification both produce N_2O in coastal environments, but their relative importance is not well known. Large fluxes of organic matter from surface waters stimulate sedimentary denitrification by supplying organic carbon and causing anaerobic conditions. Nitrification is stimulated by direct inputs of anthropogenic ammonium (NH_4^+) as well as NH_4^+ regenerated from organic nitrogen by zooplankton and heterotrophic bacteria. NH_4^+ is also taken up by phytoplankton and other microorganisms to fill their nutritional nitrogen requirements, and is often the preferred nitrogen source over other dissolved inorganic nitrogen (DIN) compounds (McCarthy et al., 1977; Levasseur et al., 1993). In shallow estuary sediments, when demand for NH_4^+ is greater than the NH_4^+ regeneration rate, competition between phytoplankton and nitrifiers can limit sedimentary nitrification rates (An and Joye, 2001). Light and turbidity may also influence nitrification rates because phytoplankton require light and some nitrifier strains can be inhibited by it (Guerrero and Jones, 1996a,b). In highly productive systems, nitrifiers may also use O_2 produced during rapid daytime photosynthesis (An and Joye, 2001).

Given the potentially complex ecological relationships among nitrification, primary production, and NH_4^+ regeneration, it is not necessarily clear if or how phytoplankton blooms influence nitrification rates in coastal surface waters. Furthermore, changes in the chemical and biological environment that accompany a phytoplankton bloom may also influence the yield of N_2O during nitrification. As discussed in the previous chapter, the N_2O yield of nitrification is defined as the fraction of NH_4^+ nitrogen atoms that wind up in N_2O as ammonia oxidizers convert ammonia (NH_3) to nitrite (NO_2^-). In chapter 2 we showed that the N_2O yield of pure cultures of ammonia-oxidizing bacteria depends on the O_2 and NO_2^- concentrations as well as the abundance of ammonia oxidizer cells in the cultures.

Coastal environments are a small fraction of the total ocean area but they account for 15-61% of oceanic N_2O emissions (Bange et al., 1996a,b). The uncertainty of this estimate

is large because coastal N_2O production is spatially and temporally patchy and the physical variables that influence air-sea gas exchange, such as wind and temperature, change rapidly. The contribution of surface nitrification to the N_2O flux out of the ocean is also not well constrained because fluxes are generally small compared to atmospheric background concentrations (Bange, 2006). ^{15}N tracer methods are highly sensitive to low-rate processes, making them better suited to measuring surface nitrification and N_2O production than concentration-based rate measurements. These rates are calculated by adding $^{15}NH_4^+$ to seawater and tracking ^{15}N as it is converted from NH_4^+ to NO_2^-, nitrate (NO_3^-), and N_2O. However, regeneration of NH_4^+ during these experiments can interfere with rate measurements by diluting the initial $^{15}NH_4^+$ with $^{14}NH_4^+$.

Here we use $^{15}NH_4^+$ and a combination of NH_4^+, NO_2^-, NO_3^-, and N_2O isotopic measurements to investigate whether nitrification rates and N_2O production rates change during a spring phytoplankton bloom in Woods Hole Harbor (Cape Cod, Massachusetts). The bloom is a highly predictable expansion of the number of picocyanobacteria of the genus *Synechococcus* that is driven by seasonal increases in water temperature and insolation (Waterbury et al., 1986). The bloom begins in late March or early April as *Synechococcus* abundances increase exponentially from a winter density of 100-1000 cells ml^{-1}, peaking at 10^5 cells ml^{-1} in mid June.

3. Materials and Methods

3.1. **Incubation Setup.** Incubations were set up once a week for four consecutive weeks between May 9 and June 2, 2010. During each experiment, 2 4L polycarbonate bottle incubations were used to measure rates of NH_4^+ and $NO_3^- + NO_2^-$ transformation and uptake, as well as *Synechococcus* abundance. Subincubations in headspace bottles (165ml) that contained 100ml seawater and were sealed with teflon-lined butyl rubber septa were set up simultaneously to measure N_2O production over the course of the experiment.

Water was collected after sun-down at high tide off Dyers Dock in Woods Hole Harbor and strained through a sieve with 0.5mm holes into an acid-washed, seawater-rinsed 20L carboy and two 4L polycarbonate bottles. ^{15}N-NH_4^+ (99.8%) was added to the carboy to

bring the concentration of added NH_4^+ to $1\mu M$. Water from the carboy was dispensed into two 4L polycarbonate bottles and six 165 ml serum bottles. For filtered controls, the water in the two independently collected 4L bottles was pumped through a $0.2\mu m$ pore-size filter into two clean 4L carboys, $1\mu M$ tracer was added, and a set of two 165 ml serum bottles was also filled with 100ml of the same filtered water. Bottles were incubated at $13°$ C for 12 hours in the dark followed by 12 hours under artificial light ($\sim$20 μEm^{-2} s^{-1})

Two 45ml samples were collected from large bottles for chemical and isotopic analyses after 0, 12, and 24 hours. At each timepoint, two experimental 165ml bottles were poisoned with $500\mu l$ of saturated mercuric chloride ($HgCl_2$). At t = 24 hours, a pair of filtered-control 165ml bottles was also poisoned.

3.2. *Synechococcus* cell counts.
Samples for cell counts were collected at T = 0 and T = 24 hours. One 45ml sample was frozen immediately and one was preserved with 0.25% glutaraldehyde before freezing. Initial (T0) counts were made by gently filtering 5 to 10ml of each sample through white polycarbonate filters with 0.2 μm pores. Duplicate mounted filters were examined using a Zeiss microscope with an epifluorescence illumination system.

3.3. NH_4^+ Concentration.
NH_4^+ concentrations were measured in triplicate on unfiltered water immediately after collection using the orthophthaldialdehyde-fluorescence method described by Holmes et al. (1999) and a Turner field fluorometer with filters for NH_4^+ concentration measurements. Standards were prepared in both freshly deionized water and in the same seawater used in each set of incubations. Matrix effects were taken into account using the seawater standard curves and corrections for background NH_4^+ and background fluorescence in the seawater standards were made using the deionized water standard curves. Details of the standard calibration are included in the Appendix.

3.4. NO_3^- + NO_2^- Concentrations.
Each NO_3^- + NO_2^- concentration was measured in duplicate using standard solutions prepared in deionized water. NO_3^- + NO_2^- was reduced to NO by injection into a hot Vanadium (III) bath in line with a chemiluminescence detector (Braman and Hendrix 1989). Concentrations were low so large sample volumes (5 to 10ml) were used to increase the signal to noise ratio.

3.5. NO_2^- Concentrations. NO_2^- was measured in duplicate using the Griess-Ilosvay colorimetric method (Pai and Yang, 1990) and standards prepared in deionized water. A spectrophotometer was used to measure 543 nm light absorbance through a 10cm path-length cell. Turbidity corrections, calculated as the difference in absorbance between filtered and unfiltered incubation water before the addition of reagents, were 27-37% of the total absorbance signal with the addition of reagents.

3.6. O_2 Concentrations. Headspace O_2 concentrations were determined with a gas chromatograph with a ^{63}Ni electron capture detector (Shimadzu GC-8A). The O_2 peaks from $20\mu l$ injections of sample headspace were recorded and integrated using Shimadzu EZStart software (v. 7.2.1) and calibrations were made with standard injections of air.

3.7. NH_4^+ Isotopic Composition. NH_4^+ isotopic measurements were made in triplicate. Unfiltered samples for NH_4^+ isotope analyses were treated immediately after collection by converting NH_4^+ to NO_2^- by the hypobromite oxidation method described by Zhang et al. (2007) and modified as follows. All samples were placed in 20ml headspace vials rinsed with deionized water and stoppered with rinsed rubber septa. Vial + reagent blanks were measured at each timepoint by standard addition (1-5 nmole) of isotopically quantified NH_4^+ standards USGS-25 (-30.41‰) and USGS-26 (53.75‰). Blanks were typically about 5 nmoles. Working reagents and sodium hydroxide solutions were prepared freshly before each measurement to avoid ambient NO_2^- and NH_3 accumulation. Background NO_2^- was removed by adding 20 μl sulfanilic acid working reagent (1.75ml deionized water, 2 ml of sulfanilic acid stock (125 μM) stored refrigerated, and 6.25ml of 40% HCl) to 3.7095 ml of sample, stoppering the vials with butyl rubber septa, shaking, incubating at room temperature for 30 min, loosening the septa, and heating samples to just below their boiling temperature for 15 min. While the samples were still warm 13.65 nmole of carrier NH_4^+ (USGS-26) was added as $136.5\mu l$ of 100 μM carrier solution, bringing the total NH_4^+ to 15-17 nmoles. The hypobromite reagent was added as 384.6 μl of working solution (20 ml deionized water + 1.2 ml 6M HCl + 2ml Br stock prepared according Zhang et al. (2007) incubated for one hour in the dark before addition of 20 ml 10M sodium hydroxide

(NaOH)). Stoppered samples were incubated for 30min at room temperature and then 384.6 μl of sodium arsenite stock solution (2.55g NaAsO$_3$ in 50 ml of deionized water) was added. Samples were acidified with 384.6μl of glacial acetic acid, stoppered, and closed with aluminum crimps immediately before reduction to N$_2$O by the azide method (McIlvin and Altabet, 2005). Samples were analyzed with an isotope ratio mass spectrometer at the University of California, Davis stable isotope facility.

3.8. NO_3^-+NO_2^- and NO_2^- Isotopic Composition. NO_3^-+NO_2^- was reduced to N$_2$O by the denitrifier method (Sigman et al., 2001; Casciotti et al., 2002) immediately after adding 10 or 20 nmoles of carrier NO_3^- to 8.8ml sample, bringing the moles of sample NO_3^- + NO_2^- to 7.5-15% of the moles carrier NO_3^- + NO_2^-. The lower carrier to sample ratio was for all samples except those from the first incubation. Each set of measurements was made along with two sets of the NO_3^- isotopic standards USGS-32, USGS-34, and USGS-35 (Bohlke et al., 2007). For NO_2^--only measurements, NO_2^- in 8.8ml of sample was reduced to N$_2$O using the azide method (McIlvin and Altabet, 2005) immediately after adding 5nmole of carrier NO_2^- and 1μmole of diluting NH_4^+. The samples were measured with two sets of the NO_2^- isotopic standards, N-23, N-7373, and N-10219 (Casciotti et al., 2007). Limited sample volumes allowed only a single measurement of the NO_2^--only isotopic composition. N$_2$O isotopic composition was measured with a Finnigan DeltaPLUS XP IRMS.

3.9. N$_2$O Concentration and Isotopic Composition. Isotopic analysis of N$_2$O in the 165ml serum bottles was made on a Finnigan DeltaPLUS XP IRMS with the automated purge and trap system described by McIlvin and Casciotti (2010). Before the samples were analyzed, 500 μl of 0.33 M natural abundance isotope ratio NH_4^+, NO_2^-, and NO_3^- were added to each sample to dilute any ^{15}N tracer. The total N$_2$O in each 165ml incubation bottle was purged with helium on-line with the mass spectrometer. N$_2$O concentration measurements were made using a linear conversion between m/z peak area 44 and total moles of N$_2$O. The reported precision for these measurements is 0.13‰ for δ^{15}N-N$_2$O and 0.18‰ for δ^{18}O-N$_2$O (McIlvin and Casciotti, 2010).

Where indicated, $\delta^{15}N$ values were converted to isotopic mass fractions (^{15}F) with the following equations:

$$^{15}R_{sample} = (\frac{\delta^{15}N_{sample}}{1000} + 1) \times {}^{15}R_{standard}$$

$$^{15}F = \frac{1}{1 + \frac{1}{^{15}R}}$$

3.10. **Assessment of Uncertainty.** The propagated errors of the ^{15}F-NH_4^+ measurements were dominated by the uncertainty in the size of the blank. An uncertainty of ± 2 nmole was assumed, however occasional fliers with higher blanks appeared during standard additions.

Although the NH_4^+ concentration measurement is precise (Figure 1) and has a low detection limit, its accuracy depends on the correction for background fluorescence in the seawater used for the standard additions. A geometric correction was used here but there is some debate about how to make this correction (see Taylor et al. (2007) and the Appendix).

For ^{15}F-NO_3^-+NO_2^- measurements, a $50\mu l$ pipetting error was assumed for each 8.8ml sample addition. A $1\mu l$ pipetting error was assumed for $100\mu l$ carrier additions and a $1\mu M$ error was assumed for the carrier NO_3^- concentration.

4. RESULTS

Synechococcus abundances increased from 4.8×10^4 cells ml^{-1} on May 9 to 15.4×10^4 cells ml^{-1} on May 23 and then decreased to 8.2×10^4 cells ml^{-1} on June 2 (Table 1). During the first three incubations, NH_4^+ concentrations decreased rapidly (15-30 nM hour^{-1}) during the dark period and remained relatively constant during the light period (Figure 1). In the last incubation, the NH_4^+ concentration increased during the dark period and then dropped during the light period. ^{15}F-NH_4^+ values decreased between 15 and 43% by the end of every incubation (Figure 2), indicating that NH_4^+ regeneration balanced a significant proportion of NH_4^+ uptake. In the fourth incubation, regeneration outpaced uptake during the dark period so that at T12, NH_4^+ concentrations were higher than the T0 values.

Initial NO_3^- + NO_2^- (N+N) concentrations were low (0.1 to 0.2 μM). They decreased slightly over time during the May 15, May 23, and June 2 incubations and remained constant during the May 9 incubation (Figure 3). NO_2^- concentrations remained low (60-70 nM) and

composed 30-50% of the total N+N, with no clear concentration trend over time (Figure 4). However, nitrification resulted in detectable accumulation of ^{15}N tracer in the N+N (Figure 5) and the NO_2^- (Figure 6) pools. Tracer did not appear in the N+N of incubations with filtered sea water, indicating that the $>0.2\mu$m particulate fraction was responsible for NH_4^+ oxidation. $^{15}F_{N+N}$ increased fastest during the May 15 and June 2 incubations (Figure 5). NO_2^- enrichment (Figure 6) increased more than the N+N enrichment, as expected for a species with a smaller reservoir size and a similar flux magnitude to the NO_3^- pool.

The conceptual nitrogen cycle used to model inorganic nitrogen transformations in this system is represented in Figure 7. Nitrification rates were modeled two different ways: in model 1 a constant nitrification rate, R_{nit} (moles N * time^{-1}) and first order N+N uptake with rate constant k (time^{-1}) were used, and in model 2 a constant nitrification rate and a constant [N+N] were used to make a simpler check on the general magnitude of the results from model 1. The following differential equations were the basis of model 1:

(1) $\frac{d^{15}[N+N]}{dt} = R_{nit} * {}^{15}F_{NH_4^+}(t) + k * {}^{15}F_{N+N} * [N+N]$

(2) $\frac{d^{14}[N+N]}{dt} = R_{nit} * {}^{14}F_{NH_4^+}(t) + k * {}^{14}F_{N+N} * [N+N]$

where the isotopic fraction of NH_4^+ ($^{15}F_{NH_4^+}(t)$) is assumed to change linearly over time with a slope of ^{15}m and a y-intercept ($^{15}F_{NH_4^+0}$) equal to the starting isotopic fraction of NH_4^+:

$$^{15}F_{NH_4^+}(t) = {}^{15}F_{NH_4^+0} + {}^{15}m * t$$

and

$$^{14}F_{NH_4^+}(t) = 1 - {}^{15}F_{NH_4^+}(t) = {}^{14}F_{NH_4^+0} + {}^{14}m * t$$

The solutions to (1) and (2) are

$$^{15}[N+N](t) = {}^{15}[N+N]_0 * e^{-kt} + \frac{R_{nit}*^{15}F_{NH_4^+0}}{k} * (1 - e^{-kt}) + \frac{^{15}m*R_{nit}}{k} * (t - \frac{1}{k} + \frac{e^{-kt}}{k})$$

$$^{14}[N+N](t) = {}^{14}[N+N]_0 * e^{-kt} + \frac{R_{nit}*^{14}F_{NH_4^+0}}{k} * (1 - e^{-kt}) + \frac{^{14}m*R_{nit}}{k} * (t - \frac{1}{k} + \frac{e^{-kt}}{k}).$$

Input values included t (time), $^{15}F_{N+N}(t)$ (the isotopic fraction of N+N over time), and the appropriate values of ^{15}m and ^{14}m. The parameter values in Table 1 were determined using least squares minimization.

The basis for model 2 was equation 3:

(3) $\overline{^{15}F_{NH_4^+}} \times R_{nit} * \Delta t = \Delta(^{15}F_{N+N} * [N + N]_{const})$,

where the average enrichment of NH_4^+, $\overline{^{15}F_{NH_4^+}} = \dfrac{^{15}F_{NH_4^+}(t_i) + {}^{15}F_{NH_4^+}(t_{i+1})}{2}$ and [N+N] is assumed to be constant over time. This assumption introduces error that depends on the importance of the N+N uptake rate. When N+N uptake is important, the estimated nitrification rate from model 2 overestimates the actual rate because a greater change in ^{15}F can be made for a given amount of nitrification in a smaller N+N pool. Since uptake caused a measurable decrease in [N+N] over time (Figure 3), the nitrification rates of model 2 should be considered a back-of-the-envelope check on the ranges estimated using model 1. Nitrification rates from model 2 will be higher than those that allow N+N uptake that is significantly faster than nitrification. Using model 1, the dark and light rate constants for N+N uptake were relatively high ($\sim$ 0.2-0.3 hr^{-1}), making the uptake rates about two orders of magnitude higher than the nitrification rates.

Using model 1, potential nitrification rates during the dark incubation period were similar to rates during the light period for all four sets of incubations (0.2-0.3 $\frac{nmole}{l \times day}$, Table 1) and all rates were lower than those calculated with model 2 (1.1-2.8 $\frac{nmole}{l \times day}$). The dark and light potential nitrification rates calculated with model 2 were similar for individual incubation dates, ranging between 1.1 and 2.2 $\frac{nmole}{l \times day}$ during the dark incubation periods and between 1.3 and 2.8 $\frac{nmole}{l \times day}$ during the light periods (Table 2). In both models, the calculated nitrification rates were higher than they would have been if the $^{15}F_{NH_4^+}$ values were assumed to be 1 throughout each incubation. The $^{15}F_{NH_4^+}$ measurements had a particularly large impact on the May 9 and May 23 nitrification rate calculations, when the $^{15}F_{NH_4^+}$ at T0 was much lower than 1 (Figure 2).

Tracer also appeared in N_2O present in the serum bottle incubations. $\delta^{15}N$-N_2O values increased steadily from T0 values of 6 to 12‰ to 16 to 40‰ at T24 (Figures 8-9). $\delta^{18}O$-N_2O values increased over time as well in the May 15 and May 23 experiments (Figure 10). Production rates were calculated using similar approaches to the ones described for nitrification, with values from sacrificial bottles taking the place of time point measurements:

(4) $\frac{d^{15}[N2O]}{dt} = R_{N_2O} * {}^{15}F_{NH_4^+}(t)$ (model 3, Table 3)

Integrating this function and substituting the linear $^{15}F_{NH_4^+}$ equation,

$$^{15}F_{NH_4^+}(t) = {}^{15}F_{NH_4^+0} + {}^{15}m * t$$

produces:

$$^{15}F_{N_2O}(t) = R_{N_2O} * {}^{15}m * t^2 + R_{N_2O} * {}^{15}F_{NH_4^+0} * t + {}^{15}F_{N_2O0}$$

Model 3 is the analogous N_2O model to nitrification model 1, except that there is no consumption/uptake term for N_2O, only a production flux, R_{N_2O} (where R_{N_2O}*24 hours*2nmol headspace N_2O*1L/(0.1 L incubation volume) = mole $l^{-1} *$ day^{-1} in Table 3).

Model 4 is analogous to nitrification model 2 and is presented here as another back-of-the-envelope check on the results of model 3:

$$(5) \quad \overline{^{15}F_{NH_4^+}} \times R_{N_2O} * \Delta t = \Delta(^{15}F_{N_2O} * [N_2O]_{const}) \quad (\text{model 4, Table 4})$$

The analogous $^{14}F_{N_2O}$ equations were not used in these rate calculations because they were insensitive to the N_2O production term. This is true because the N_2O produced during the incubations was a very small fraction of the total headspace N_2O and headspace N_2O concentrations did not change significantly over the course of the incubation.

Since there is no uptake flux for N_2O, the two models should be (and are) in better agreement with each other than the analogous nitrification models. Production rates modeled for the entire incubation (dark + light period) with model 3 ranged between 0.6 and 3.8 $\frac{fmole}{lxday}$ (Table 3). Split dark and light production rates calculated with model 4 ranged between 0.6 and 3.0 $\frac{fmole}{lxday}$ in the dark and 0.4 to 3.1 $\frac{fmole}{lxday}$ in the light (Table 4). Unlike the nitrification rates, the N_2O production rates followed the same trend as the *Synechococcus* cell abundances, increasing between May 9 and May 23 and then dropping on June 2. The N_2O yield calculation (fractional N_2O yield = $\frac{2 \times RateN_2O}{RateNitrification}$) based on these rates and the nitrification rates estimated with model 1 increased from 4.9×10^{-3} on May 9 to 9.9×10^{-3} on May 15 and 32.5×10^{-3} on May 23, and then dropped to their lowest value, 3.9×10^{-3} on June 2. The O_2 concentrations in the headspaces of the serum bottle incubations remained at atmospheric equilibrium (20% O_2) for each timepoint during the May 23 and June 2 incubations (Figure 11).

5. Discussion

Water temperature controls the onset of the springtime *Synechococcus* bloom (Waterbury et al 1986) and experiments were initiated when the temperature reached 13 °C and should have corresponded with the exponential phase of the bloom. The doubling time of *Synechococcus* is 4.3 days during this phase (Waterbury et al., 1986), although short-term events such as storms can reduce growth rates. *Synechococcus* abundances measured here did not increase exponentially, suggesting that the bloom was either already in its senescent stage or that sampling captured the effects of short term disturbances in the harbor. Precipitation and runoff should not have had an effect as there was no precipitation in the two days prior to the start of each incubation. *Synechococcus* accounts for 5-10% of primary production in this environment (Waterbury et al., 1986). Additional work characterizing the rest of the microbial community may be necessary in order to understand what is driving the larger nitrogen cycle dynamics in this system.

Potential nitrification rates were low compared to estuarine and some open ocean estimates (2-7$\frac{\text{nmole}}{\text{l} \times \text{day}}$, (Olson, 1981b)) but were comparable to surface rates measured by Ward et al (1984) off the coast of Washington state (0.2-0.7$\frac{\text{nmole}}{\text{l} \times \text{day}}$). Rates were substantially slower than estimated N+N uptake rates (Table 1). This is expected for an ecosystem supported by steady influxes of new NO_3^- from terrestrial, atmospheric, or other coastal sources. The dark and light periods of each incubation were modeled separately because both the nitrification rates and the uptake rates were expected to change with the light regime. For example, in high-nutrient waters, NO_3^- uptake by phytoplankton is highest during the day (Goering et al., 1964; Eppley et al., 1971; Cochlan et al., 1991) and there is evidence that nitrification is photo-inhibited in the surface of the open ocean (Olson, 1981a). However, dark and light nitrification rates estimated with both model 1 and model 2 were similar, as were the N+N uptake rates estimated with model 1 (Table 1 and Table 2). Rates of N+N disappearance during the dark and light periods were approximately equal (Figure 3 and Figure 4). Since nitrification rates were low relative to uptake, the net N+N uptake in these two figures is probably close to the gross N+N uptake. Uptake rates were much

higher than nitrification rates (Table 1), so that turnover of N+N in this system must be determined almost entirely by uptake and physical transport. For simplicity, model 1 does not include an isotope effect for N+N uptake. This effect probably had little impact on the observed $^{15}F_{N+N}$: the isotope effects of uptake are typically small in phytoplankton and bacterial cultures, (between 1 and 8‰, Granger et al. (2010)) as well as in the euphotic zone (Altabet et al., 1999). Furthermore, the fraction of starting N+N consumed over the course of the incubations was small (< 0.3).

The 1 μM tracer NH_4^+ added to these incubations was a large perturbation of ambient concentrations (30-180nM) but was necessary to track isotopic dilution of the ^{15}N-NH_4^+ and to trace ^{15}N into N_2O. Therefore, the rates measured here must be qualified as potential rates, not *in situ* rates. Phytoplankton respond to increased NH_4^+ concentrations by increasing their uptake rates (MacIsaac and Dugdale, 1969). Previous work has measured a 300 nM saturating concentration for NH_4^+ uptake in Vineyard Sound, Massachusetts (Glibert et al., 27). Few studies have tested the kinetics of NH_4^+ oxidation in marine environments, but they indicate that the half-saturation concentration for NH_4^+ oxidation is 150nM (Hashimoto et al., 1983). In cultured NH_3 oxidizing bacteria the half-saturation concentrations are much higher (100s of μM) (Jiang and Bakken, 1999). However, the archaeal ammonia oxidizer, *Nitrosopumilus maritimus* has a much lower half-saturation constant (135 nM) that is closer to marine NH_4^+ concentrations (Martens-Habbena et al., 2009). If NH_4^+ oxidation in Vineyard Sound behaves according to archaeal and measured marine kinetics, then the nitrification rate measurements could be at least twice as high as the unperturbed rates.

N_2O production rates and yields increased in sync with the *Synechococcus* cell abundances (Table 3, Table 4, and Figures 8-9) but not in direct proportion to them. These results are intriguing and their possible biological significance will be discussed, but there are reasons to suspect that the N_2O sample preservation method may have influenced the measured $\delta^{15}N$-N_2O values. The serum bottles poisoned at T0 were expected to have $\delta^{15}N$-N_2O values close to the atmospheric value of 6‰. However, the May 9, May 23 and June 2 incubations all had higher values (Figure 8), suggesting either that there was

post-preservation N_2O production from one of the ^{15}N-labeled pools of nitrogen or that the seawater was not in isotopic equilibrium with the atmosphere at the time of collection. Poisoning seawater with $HgCl_2$ is a standard preservation method for N_2O isotopic and concentration measurements (e.g. Yoshida et al. (1989); Dore and Karl (1996); Popp et al. (2002); Westley et al. (2006); Yamagishi et al. (2007)). The ratio of saturated $HgCl_2$ solution to seawater used here was 0.5 ml : 100 ml. Although this ratio is higher than that used to preserve samples in chapter 3 (0.06 ml : 100 ml), similar ratios have been reported in the literature (e.g., 0.4 ml : 100 ml (Dore et al., 1998)).

The bottles from all four incubations were analyzed at the same time, one week after the last incubation, and five weeks after the first incubation so that samples from later incubations were analyzed after shorter amounts of time than samples from earlier incubations. The disappearance of NO_2^- over time in $HgCl_2$-preserved samples has been reported before (Aminot and Kerouel, 1996; Kattner, 1999) but the mechanism of disappearance is not known. A Hg°-dependent NO_2^- reduction mechanism producing N_2O is thermodynamically favorable (C. Lamborg, personal communication), but overnight tests on fresh seawater containing NH_4^+, NO_2^-, or NO_3^- preserved with $HgCl_2$ showed no immediate reaction (unreported data).

The increases in the apparent $\delta^{18}O$-N_2O values observed in Figure 10 may shed some light on which of the ^{15}N-labeled nitrogen pools gave rise to the $^{15}N_2O$ produced during the incubation. The $\delta^{18}O$-N_2O values increased over time in the May 9, May 15, and May 23 incubations. The isotopic compositions of O_2 and H_2O in the incubations were both near natural abundance, and very little N_2O was actually produced during the incubation. The apparent increase was probably not due to an actual increase in the abundance of $N_2^{18}O$. For reference, each of the serum bottle incubations represented in Figures 8, 9, and 10 contained ~ 2.1 nmole of N_2O and individual bottles were within 0.05 nmole of each other across all experiments. However, large inputs of doubly labeled $^{15}N^{15}NO$ may have caused an increase in m/z 46 ions that would have been interpreted as $N_2^{18}O$ by our analytical software. Based on the results of the large bottle incubations and assuming a binomial distribution of ^{15}N and ^{14}N in the N_2O, the NO_2^- and N+N pools never reached

^{15}N enrichments high enough to form detectable concentrations of ^{15}N^{15}NO without also forming much larger quantities of ^{15}N^{14}NO and ^{14}N^{15}NO than were actually observed in Figures 8 and 9. That is, the observed production of ^{15}N^{14}NO and ^{14}N^{15}NO was lower than expected if ^{14}N and ^{15}N in the N+N pool were reacting to form N$_2$O with probabilities proportional to their respective concentrations. This suggests that the N$_2$O produced in these incubation bottles was actually formed with nitrogen atoms from the NH$_4^+$ pool, which contained a much higher fraction of ^{15}N than either of the N+N pools.

If nitrification produced N$_2$O during these incubations, the yields are similar to those observed by Goreau et al. (1980) at 20% O$_2$ in *Nitrosomonas* cultures but they are about 10 times higher than other observations made on cultured ammonia oxidizers (Frame and Casciotti, 2010) (Table 5). Some of the observed yields are actually lower than those calculated by Dore and Karl (1996) for the euphotic zone at station ALOHA using ^{15}N tracer measurements of NH$_4^+$ oxidation and surface flux mass balances to model N$_2$O production (yield $= 27 \times 10^{-3}$). Considering the large uncertainties associated with the eddy-diffusion coefficients used to calculate 1-D surface fluxes, the agreement between studies is good. Based on a Redfield O$_2$: NO$_3^-$ stoichiometry of 9.3-10.7, our results also agree with local atmospheric anomalies in N$_2$O and O$_2$ concentrations that coincided with a coastal upwelling event off the coast of California (ΔN$_2$O/Δatmospheric potential O$_2$ $= -1.2 \times 10^{-4}$ (Lueker et al., 2003)). Using the same O$_2$: NO$_3^-$ stoichiometry, the yields here are also in agreement with values measured in the South Atlantic in the following chapter. Dissolved O$_2$ concentrations were never low enough to stimulate nitrifier-denitrification and ambient NO$_2^-$ concentrations changed very little over the course of each incubation (Figure 4). However, aggregation of NH$_3$-oxidizer cells into particles with higher cell densities, higher NO$_2^-$ concentrations, or lower O$_2$ concentrations than the surrounding water may create localized conditions conducive to nitrifier-denitrification. There are a number of findings that suggest that nitrifiers prefer living near each other. For example, Ward et al. (1984) observed clustering of *Nitrosococcus* cells in shallow coastal waters. Growth of cultures of the archaeal ammonia oxidizers *N. maritimus* are inhibited when culture conditions are not static. Finally, the bacterial ammonia oxidizer *Nitrosomonas europaea* forms biofilms in

liquid culture media (Laanbroek and Gerards, 1993). A seasonal increase in productivity could enhance N_2O yields by providing ammonia oxidizers with substrate to aggregate on.

6. CONCLUSIONS

Paired measurements of nitrification and N_2O production allow ground truthing of N_2O yields measured in cultures of ammonia oxidizers as well as yield estimates made with oceanographic N_2O, O_2, and N+N concentration data. Possible methodological issues with sample preservation may have influenced potential yields measured here. Nevertheless, the experimental results indicate that N_2O yields do not increase linearly in proportion to nitrification rates, and that a variable other than ambient O_2 or NO_2^- concentration causes the increase in yield.

7. ACKNOWLEDGMENTS

We thank John Waterbury for generously making his lab space available for most of the experimental work in this study as well as Freddy Valois who contributed her microscopy and *Synechococcus* expertise. Thanks also to Joe Hannon for providing the derivation of the model rate equations found in Appendix C.

8. APPENDIX A: STANDARDIZATION FOR NH_4^+ CONCENTRATIONS MEASURED WITH THE OPA-FLUORESCENCE METHOD OF HOLMES ET AL. (1999)

Immediately before each set of NH_4^+ concentration measurements, a set of standards was prepared with the same seawater used for each tracer incubation and another set was prepared with freshly-drawn deionized water (Figure 12). In between incubation time points, the seawater used for standards was refrigerated in a closed polycarbonate bottle. The equation of the final calibration curve was obtained by using the slope of the seawater standard curve and a y-intercept that was corrected for total background fluorescence. According to Taylor et al. (2007) this background fluorescence has 3 sources: the fluorescence of the reagents themselves, the background NH_4^+ present in the seawater, and other naturally occurring compounds that fluoresce in the presence of the OPA reagent. The correction for

reagent fluorescence was made by shifting the y-intercept of the seawater standard curve down by the same number of fluorescence units as the y-intercept of the deionized water standard curve. In Figure 12, this was done by moving the seawater y-intercept at point B down to point C, where B - C = A and A is the y-intercept of the deionized water standard curve. The next two components of the fluorescence correction are not fully resolvable without knowing the background NH_4^+ concentration. In an effort to systematically apportion this unresolved fluorescence between actual NH_4^+ in the seawater and other sources of fluorescence in the seawater, the base of the seawater standard curve was moved along a perpendicular line drawn between it and the deionized water standard curve. This was accomplished by moving point C to point F, where the line $\overline{CF}$ is perpendicular to the deionized water standard curve. The length of line $\overline{CD}$ was assumed to be the background NH_4^+ concentration, $\overline{AE}$ was the fluorescence due to the background NH_4^+, and the length of line $\overline{CE}$ was assumed to be the background fluorescence of seawater. In these experiments, the average unresolved fluorescence signal (= B - A) was 73 fluorescence units, or about 9% of the total signal.

9. APPENDIX B: STANDARDIZATION FOR NH_4^+ ISOTOPIC MEASUREMENTS MADE USING THE METHOD OF ZHANG ET AL. (2007)

Standards were analyzed for every set of NH_4^+ measurements made at every time point for each incubation. Six standard additions were made for each of two USGS NH_4^+ isotope standards (USGS-26 and USGS-25). The isotopic composition and mass of the blanks was calculated by fitting the standard addition data using the reported isotopic compositions and known masses of added standard (Figure 13). The $\delta^{15}N$-NH_4^+ values of the blanks were usually less than 0‰. Each batch of vials and butyl rubber stoppers was treated similarly by rinsing thoroughly with freshly deionized water and then air drying. The size of the blank was found to increase if acid or soap were introduced into the washing procedure.

10. Appendix C: Derivation of the solution to the differential equation used to model simultaneous ammonia oxidation and nitrate uptake

For an inhomogeneous ordinary differential equation of the form

$y' + Ay - B(Cx+D) = 0$

where

$y' = \frac{d[^{15}N]}{dt}$ or $\frac{d[^{14}N]}{dt}$

$y = [^{15}N]$ or $[^{14}N]$

$x = $ time

$A = k$, rate constant of uptake

$B = Rnit$

$C = $ slope of the $^{15}F_{NH_4^+}$ vs. time equation

$D = $ intercept of the $^{15}F_{NH_4^+}$ vs. time equation

Multiply through by the integrating factor, the exponential of the integral of the zeroth order term, A, which is e^{Ax}:

$e^{Ax} y' + A e^{Ax} y = B e^{Ax} (Cx + D)$

This turns the left-hand side into a product-rule derivative:

$(e^{Ax} y)' = e^{Ax} y' + A e^{Ax} y$

$(e^{Ax} y)' = Be^{Ax}(Cx + D)$

Integrate

$e^{Ax} y = \int Be^{Ax}(Cx + D)dx + K$

$= BC \int xe^{Ax}dx + BD \int e^{Ax}dx + K$

The integration of the second term follows from the differentiation of exponentials (ie, $(e^{Ax})' = Ae^{Ax}$):

$\int e^{Ax}dx = (e^{Ax})/A$

To integrate the first term $\int xe^{Ax}\,dx$, use integration by parts. Set $u = x$, $dv = e^{Ax}\,dx$. The identity for integration by parts is $\int udv = uv - \int vdu$. Then $du = dx$ and $v = \int e^{A}x\,dx = (e^{Ax})/A$. So:

$\int xe^{Ax}\,dx = \int u\,dv = uv - \int v\,du = x(e^{Ax})/A - \int (e^{Ax})/A\,dx$

$= x(e^{Ax})/A - (e^{Ax})/A^2$

Take

$ye^{Ax} = BC \int xe^{Ax}dx + BD \int e^{Ax}dx + K$

and substitute the two integrals on the right-hand side:

$ye^{Ax} = BC(x(e^{Ax})/A - (e^{Ax})/A^2) + BD((e^{Ax})/A) + K$

Then multiply through by e^{-Ax}:

$y = BC[x/A - 1/A^2] + BD[1/A] + Ke^{-Ax}$

The constant of integration K is determined by the initial conditions.

REFERENCES

Altabet, M. A., Pilskaln, C., Thunell, R., Pride, C., Sigman, D., Chavez, F., and Francois, R. (1999). The nitrogen isotope biogeochemistry of sinking particles from the margin of the eastern north pacific. *Deep-Sea Research I*, 46:655–679.

Aminot, A. and Kerouel, R. (1996). Stability and preservation of primary calibration solutions of nutrients. *Marine Chemistry*, 52:173–181.

An, S. and Joye, S. B. (2001). Enhancement of coupled nitrification-denitrification by benthic photosynthesis in shallow estuarine sediments. *Limnology and Oceanography*, 46(1):62–74.

Bange, H. W. (2006). Nitrous oxide and methane in european coastal waters. *Estuarine Coastal and Shelf Science*, 70:361–374.

Bange, H. W., Rapsomanikis, S., and Andreae, M. O. (1996a). The aegean sea as a source of atmospheric nitrous oxide and methane. *Marine Chemistry*, 53:41–49.

Bange, H. W., Rapsomanikis, S., and Andreae, M. O. (1996b). Nitrous oxide in coastal waters. *Global Biogeochemical Cycles*, 10(1):197–207.

Beman, M. J., Arrigo, K. R., and Matson, P. A. (2005). Agricultural runoff fuels large phytoplankton blooms in vulnerable areas of the ocean. *Nature*, 434:211–214.

Bohlke, J. K., Smith, R. L., and Hannon, J. E. (2007). Isotopic analysis of n and o in nitrite and nitrate by sequential selective bacterial reduction to N_2O. *Analytical Chemistry*, 79:5888–5895.

Casciotti, K. L., Bohlke, J. K., McIlvin, M., Mroczkowski, S. J., and Hannon, J. E. (2007). Oxygen isotopes in nitrite: analysis, calibration, and equilibration. *Analytical Chemistry*, 79:2427–2436.

Casciotti, K. L., Sigman, D. M., Hastings, M. G., Bohlke, J. K., and Hilkert, A. (2002). Measurements of the oxygen isotopic composition of nitrate in seawater and freshwater using the denitrifier method. *Analytical Chemistry*, 74:4905–4912.

Cochlan, W. P., Harrison, P. J., and Denman, K. L. (1991). Diel periodicity of nitrogen uptake by marine phytoplankton in nitrate-rich environments. *Limnology and Oceanography*, 36(8):1689–1700.

Dore, J. E. and Karl, D. M. (1996). Nitrification in the euphotic zone as a source of nitrite, nitrate, and nitrous oxide at station ALOHA. *Limnology and Oceanography*, 41(8):1619–1628.

Dore, J. E., Popp, B. N., Karl, D. M., and Sansone, F. J. (1998). A large source of atmospheric nitrous oxide from subtropical north pacific surface waters. *Nature*, 396:63–66.

Eppley, R. W., Carlucci, A. F., Holm-Hansen, O., Kiefer, D., McCarth, J. J., Venrick, E., and Williams, P. M. (1971). Phytoplankton growth and composition in shipboard cultures supplied with nitrate, ammonium, or urea as the nitrogen sources. *American Society of Limnology and Oceanography*, 16(5):741–751.

Frame, C. H. and Casciotti, K. L. (2010). Biogeochemical controls and isotopic signatures of nitrous oxide production by a marine ammonia-oxidizing bacterium. *Biogeosciences*, 7:2695–2709.

Glibert, P. M., Lipschultz, F., McCarthy, J. J., and Altabet, M. A. (27). Isotope dilution models of uptake and remineralization of ammonium by marine plankton. *Limnology and Oceanography*, 4:639–650.

Goering, J. J., Dugdale, R. C., and Menzel, D. W. (1964). Cyclic diurnal variations in the uptake of ammonia and nitrate by photosynthetic organisms in the sargasso sea. *Limnology and Oceanography*, 9(3):448–451.

Goreau, T. J., Kaplan, W. A., Wofsy, S. C., McElroy, M. B., Valois, F. W., and Watson, S. W. (1980). Production of NO_2^- and N_2O by nitrifying bacteria at reduced concentrations of oxygen. *Applied and Environmental Microbiology*, 40(3):526–532.

Granger, J., Sigman, D. M., Rohde, M. M., Maldonado, M. T., and Tortell, P. D. (2010). N and o isotope effects during nitrate assimilation by unicellular prokaryotic and eukaryotic plankton cultures. *Geochimica et Cosmochimica Acta*, 74:1030–1040.

Guerrero, M. A. and Jones, R. D. (1996a). Photoinhibition of marine nitrifying bacteria. i. wavelength-dependent response. *Marine Ecology Progress Series*, 141:183–192.

Guerrero, M. A. and Jones, R. D. (1996b). Photoinhibition of marine nitrifying bacteria. ii dark recovery after monochromatic or polychromatic irradiation. *Marine Ecology Progress Series*, 141:193–198.

Harrison, J. and Matson, P. (2003). Patterns and controls of nitrous oxide emissions from waters draining a subtropical agricultural valley. *Global Biogeochemical Cycles*, 17(3):doi:10.10292002GB001991.

Hashimoto, L. K., Kaplan, W. A., Wofsy, S. C., and McElroy, M. B. (1983). Transformations of fixed nitrogen and N_2O in the cariaco trench. *Deep-Sea Research*, 30(6A):575–590.

Holmes, R. M., Aminot, A., and Kerouel, R. (1999). A simple and precise method for measuring ammonium in marine and freshwater ecosystems. *Canadian Journal of Fisheries and Aquatic Sciences*, 56:1801–1808.

Howarth, R. W., Billen, G., Swaney, D., Townsend, A., Jaworski, N., Lajtha, K., Downing, J. A., Elmgren, R., Caraco, N., Jordan, T., Berendse, F., Freney, J., Kudeyarov, V., Murdoch, P., and Zhao-Liang, Z. (1996). Regional nitrogen budgets and riverine n and p fluxes for the drainages to the north atlantic ocean: Natural and human influences. *Biogeochemistry*, 35:75–139.

Jiang, Q.-Q. and Bakken, L. R. (1999). Nitrous oxide production and methane oxidation by different ammonia-oxidizing bacteria. *Applied and Environmental Microbiology*, 65(6):2679–2684.

Kattner, G. (1999). Storage of dissolved inorganic nutrients in seawater: poisoning with mercuric chloride. *Marine Chemistry*, 67:61–66.

Laanbroek, H. J. and Gerards, S. (1993). Competition for limiting amounts of oxygen between *Nitrosomonas europaea* and *Nitrobacter winogradskyi* grown in mixed continuous cultures. *Archives of Microbiology*, 159:453–459.

Levasseur, M., Thompson, P. A., and Harrison, P. J. (1993). Physiological acclimation of marine-phytoplankton to different nitrogen-sources. *Journal of Phycology*, 29(5):587–595.

Lueker, T. J., Walker, S. J., Vollmer, M. K., Keeling, R. K., Nevison, C. D., and Weiss, R. F. (2003). Coastal upwelling air-sea fluxes revealed in atmospheric observations of O_2/N_2, CO_2 and N_2O. *Geophysical Research Letters*, 30(6):doi:10.1029/2002GL016615.

MacIsaac, J. J. and Dugdale, R. C. (1969). Kinetics of nitrate and ammonia uptake by natural populations of marine phytoplankton. *Deep-Sea Research*, 16(1):45–57.

Martens-Habbena, W., Berube, P. M., Urakawa, H., de la Torre, J. R., and Stahl, D. A. (2009). Ammonia oxidation kinetics determine niche separation of nitrifying archaea and bacteria. *Nature*, 461:976–981.

McCarthy, J. J., Taylor, W. R., and Taft, J. L. (1977). Nitrogenous nutrition of the plankton in the chesapeake bay. 1. nutrient availability and phytoplankton preferences. *Limnology and Oceanography*, 22:996–1011.

McIlvin, M. M. and Altabet, M. (2005). Chemical conversion of nitrate and nitrite to nitrous oxide for nitrogen and oxygen isotopic analysis in freshwater and seawater. *Analytical Chemistry*, 77:5589–5595.

McIlvin, M. M. and Casciotti, K. L. (2010). Automated stable isotopic analysis of dissolved nitrous oxide at natural abundance levels. *Limnology and Oceanography Methods*.

Olson, R. J. (1981a). Differential photoinhibition of marine nitrifying bacteria-a possible mechanism for the formation of the primary nitrite maximum. *Journal of Marine Research*, 39(2):227–238.

Olson, R. J. (1981b). N-15 tracer studies of the primary nitrite maximum. *Journal of Marine Research*, 39(2):203–226.

Pai, S.-C. and Yang, C.-C. (1990). Formation kinetics of the pink azo dye in the determination of nitrite in natural waters. *Analytica Chimica Acta*, 232:345–349.

Popp, B. N., Westley, M. B., Toyoda, S., Miwa, T., Dore, J. E., Yoshida, N., Rust, T. M., Sansone, F. J., Russ, M. E., Ostrom, N. E., and Ostrom, P. H. (2002). Nitrogen and oxygen isotopomeric constraints on the origins and sea-to-air flux of N_2O in the oligotrophic subtropical north pacific gyre. *Global Biogeochemical Cycles*, 16(4):12–1–10.

Prinn, R., Cunnold, D., Rasmussen, R., Simmonds, P., Alyea, F., Crawford, A., Fraser, P., and Rosen, R. (1990). Atmospheric emissions and trends of nitrous oxide deduced from 10 years of ALE − GAGE data. *Journal of Geophysical Research*, 95(D11):18369–18385.

Seitzinger, S. P. and Kroeze, C. (1998). Global distribution of nitrous oxide production and n inputs in freshwater and coastal marine ecosystems. *Global Biogeochemical Cycles*, 12(1):93–113.

Sigman, D. M., Casciotti, K. L., Andreani, M., Barford, C., Galanter, M., and Bohlke, J. K. (2001). A bacterial method for the nitrogen isotopic analysis of nitrate in seawater and freshwater. *Analytical Chemistry*, 73:4145–4153.

Taylor, B. W., Keep, C. F., Hall Jr, R. O., Koch, B. J., and Tronstad, L. M. (2007). Improving the fluorometric ammonium method: matrix effects, background fluorescence, and standard additions. *Journal of the North American Benthological Society*, 26(2):167–166.

Ward, B. B., Talbot, M. C., and Perry, M. J. (1984). Contributions of phytoplankton and nitrifying bacteria to ammonium and nitrite dynamics in coastal waters. *Continental Shelf Research*, 3(4):383–398.

Waterbury, J. B., Watson, S. W., Valois, F. W., and Franks, D. G. (1986). Biological and ecological characterization of the marine unicellular cyanobacterium *Synechococcus*. *Canadian Bulletin of Fisheries and Aquatic Sciences*, 214:71–120.

Weiss, R. F., Keeling, C. D., and Craig, H. (1981). The determination of tropospheric nitrous oxide. *Journal of Geophysical Research*, 86(C8):7197–7202.

Westley, M. B., Yamagishi, H., Popp, B. N., and Yoshida, N. (2006). Nitrous oxide cycling in the black sea inferred from stable isotope and isotopomer distributions. *Deep-Sea Research-II*, 53:1802–1816.

Yamagishi, H., Westley, M. B., Popp, B., Toyoda, S., Yoshida, N., Watanabe, S., and Koba, K. (2007). Role of nitrification and denitrification on the nitrous oxide cycle in the eastern tropical north pacific and gulf of california. *Journal of Geophysical Research*, 112(G02015):doi:10.1029/2006JG000227.

Yoshida, N., Morimoto, H., Hirano, M., Koike, I., Matsuo, S., Wada, E., Saino, T., and Hattori, A. (1989). Nitrification rates and ^{15}N abundances of N_2O and NO_3^- in the western north pacific. *Nature*, 342:895–897.

Zhang, L., Altabet, M. A., Wu, T., and Hadas, O. (2007). Sensitive measurement of NH_4^+ $^{15}N/^{14}N(\delta^{15}NH_4^+)$ at natural abundance levels in fresh and saltwaters. *Analytical Chemistry*, 79(14):5297–5303.

FIGURE 1. NH_4^+ concentrations over time in experimental incubations. The solid and dashed lines of a single color represent experimental replicates. Error bars indicate the standard deviation among triplicate concentration measurements.

FIGURE 2. The ^{15}F of NH_4^+ over time in experimental incubations. The solid and dashed lines of a single color represent experimental replicates. Measurements were made in triplicate. Propagated error from the blank and carrier subtractions are indicated.
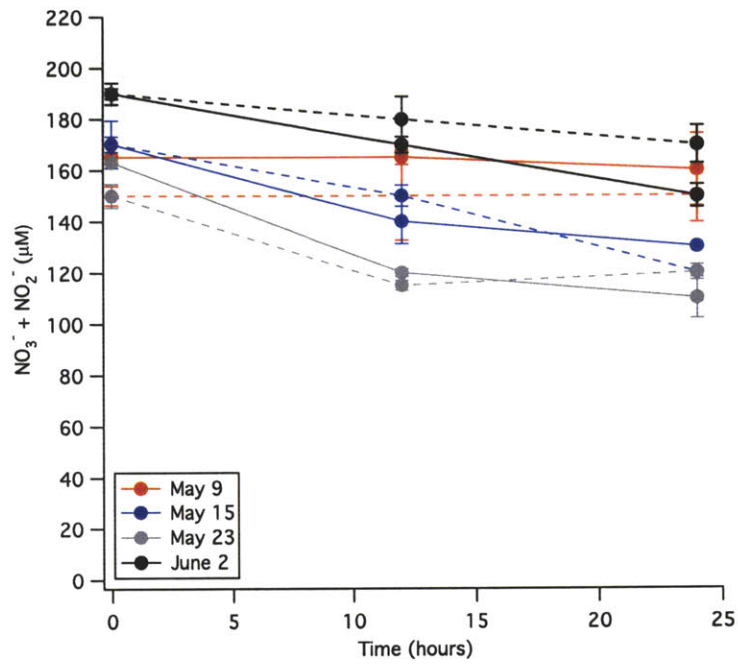
FIGURE 3. NO_3^- concentrations over time in experimental incubations. The solid and dashed lines of a single color represent experimental replicates. Error bars indicate the standard deviation between duplicate measurements.
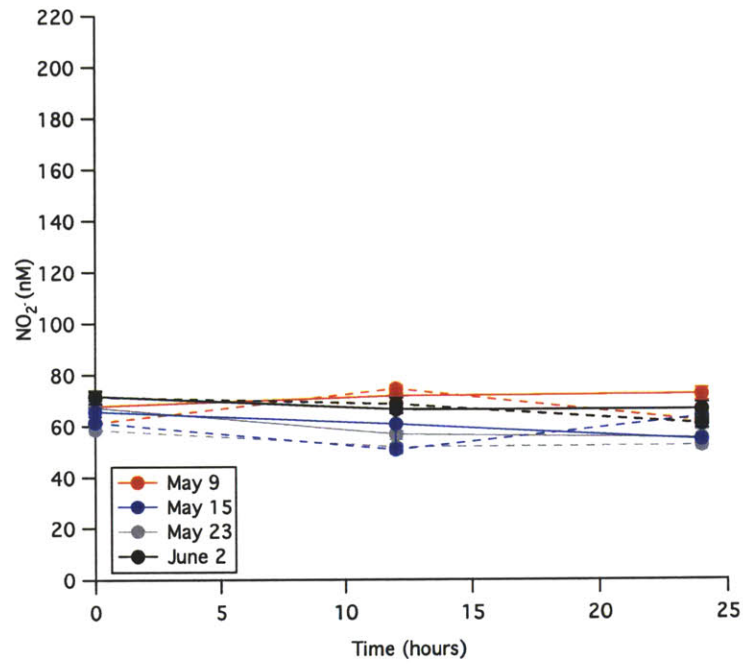
FIGURE 4. NO_2^- concentrations over time in experimental incubations. The solid and dashed lines of a single color represent experimental replicates. Error bars indicate the standard deviation between duplicate measurements.
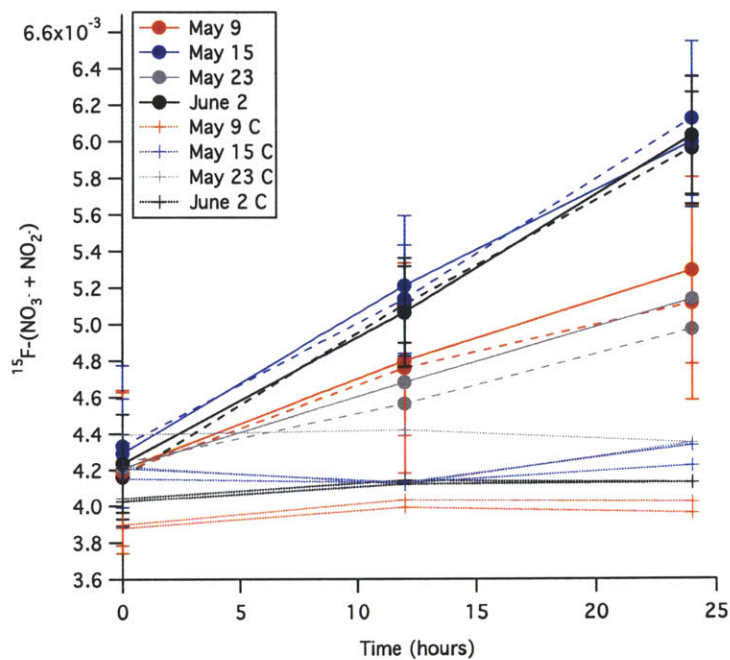
FIGURE 5. The ^{15}F of $NO_3^- + NO_2^-$ over time in experimental and filtered control incubations. The solid and dashed lines of a single color represent experimental replicates. Circles represent experimental incubations and pluses represent filtered controls. Error bars indicate the error propagated through the carrier NO_3^- correction.

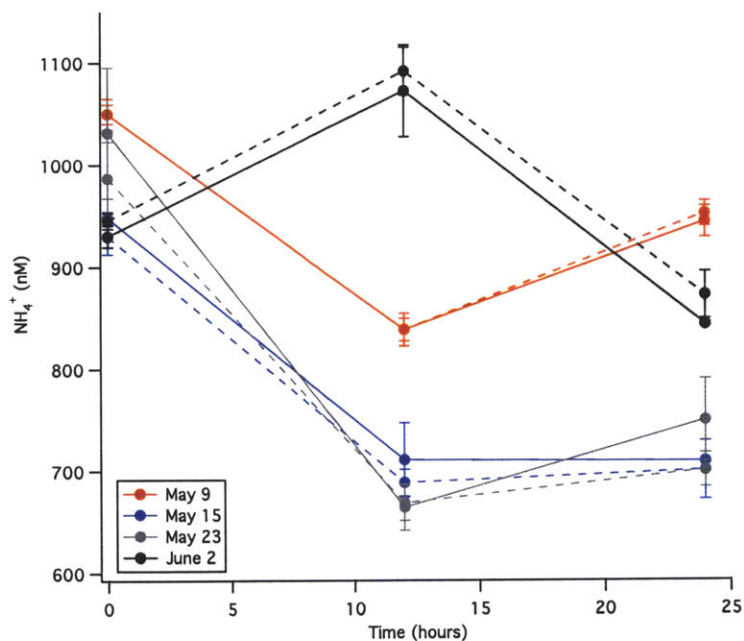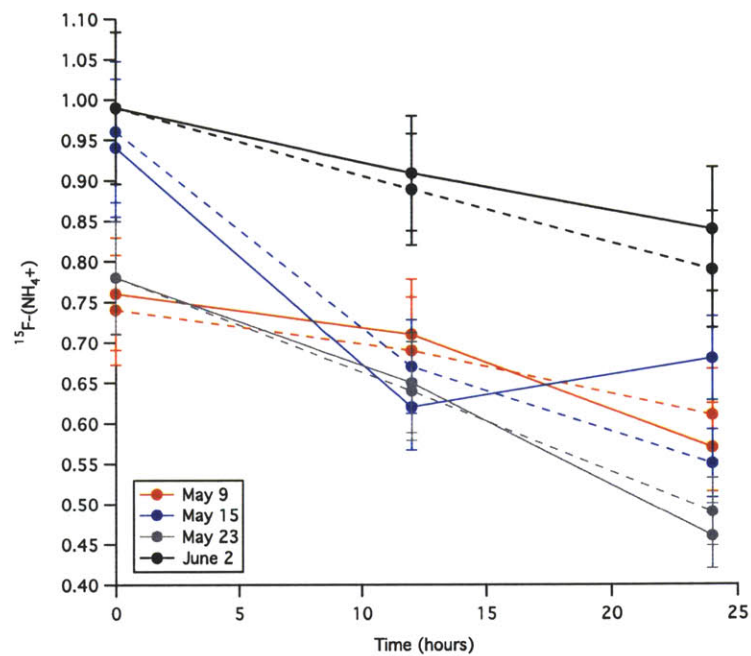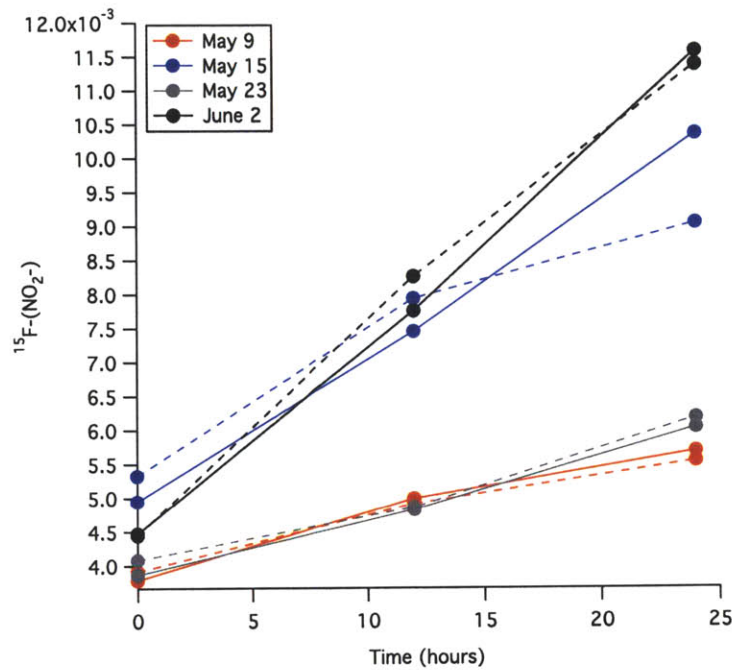FIGURE 6. The ^{15}F of NO_2^- over time in experimental incubations. The solid and dashed lines of a single color represent experimental replicates. Errors on this measurement may be larger than the signal itself and are not included because a single isotopic measurement was made.
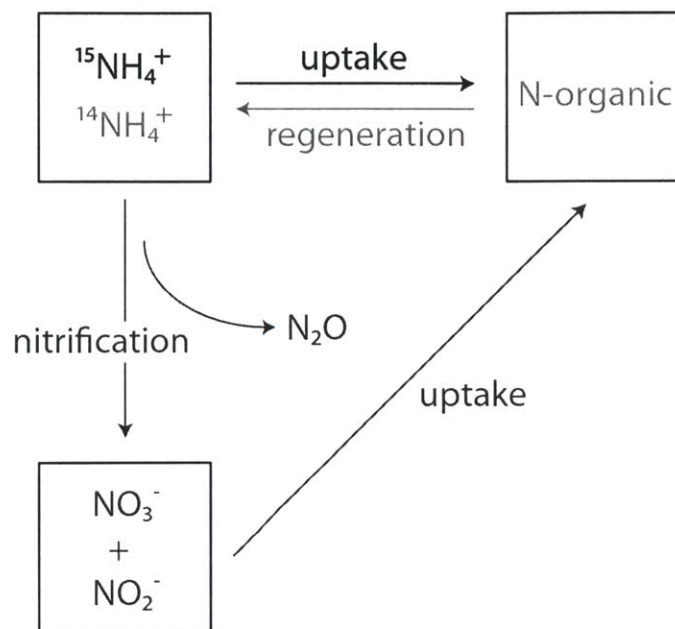
FIGURE 7. The transfer of ^{15}N in this system from $^{15}NH_4^+$ into $^{15}NO_2^-$ and $^{15}NO_3^-$ tracks nitrification. The dilution of the initial $^{15}NH_4^+$ tracer over time indicates that NH_4^+ regeneration is also significant. Darker text and arrows indicate greater ^{15}N enrichment.
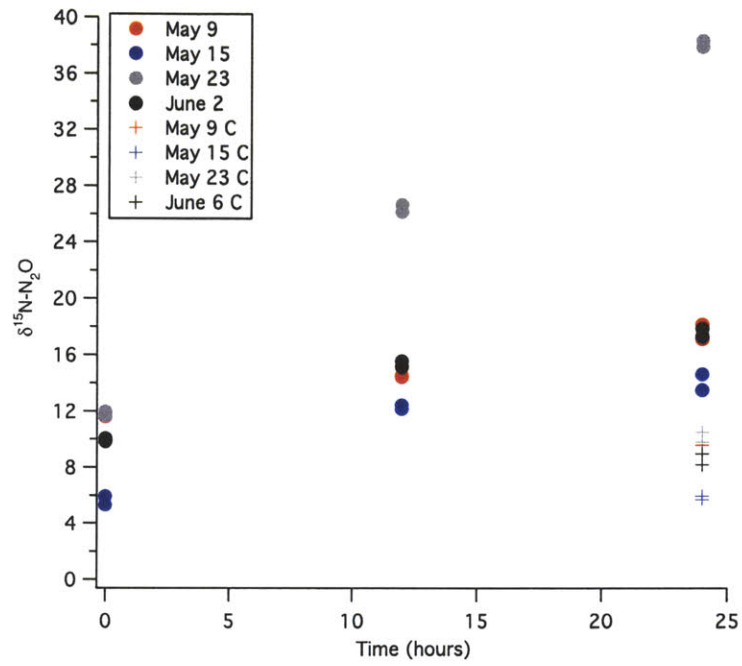
FIGURE 8. The δ^{15}N-N$_2$O values measured in the sacrificial serum bottle incubations. Circles represent experimental incubations and pluses represent filtered control incubations.
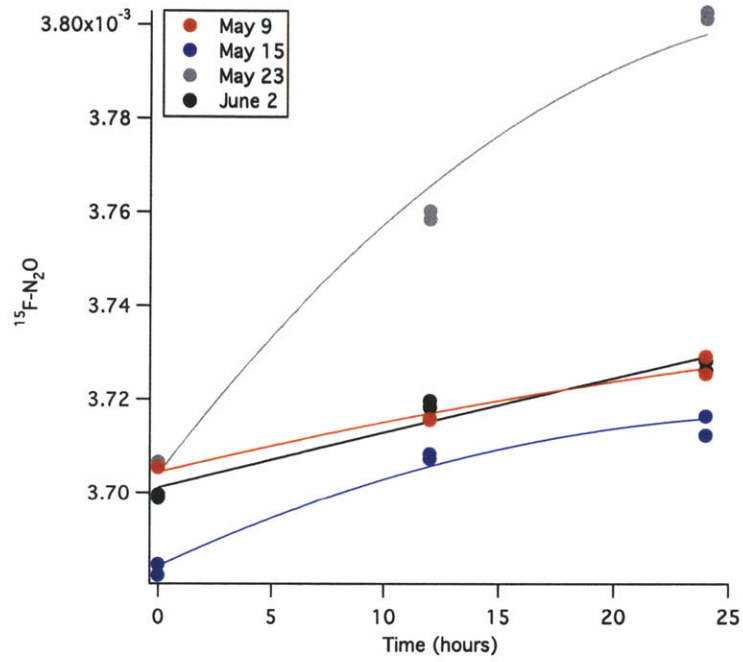
FIGURE 9. The ^{15}F of N_2O over time in sacrificial serum bottle incubations. Lines indicate the best fit parameters estimated using the integrated equation used in model 3 described in the text. The best fit parameters are given in Table 3.
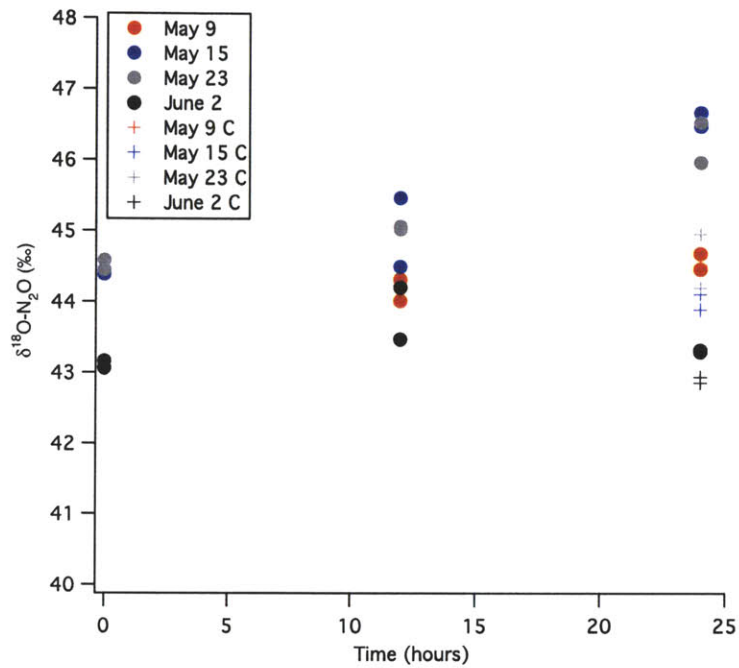
FIGURE 10. The δ^{18}O-N$_2$O values measured in sacrificial serum bottle incubations. Circles represent experimental incubations and pluses represent filtered control incubations.
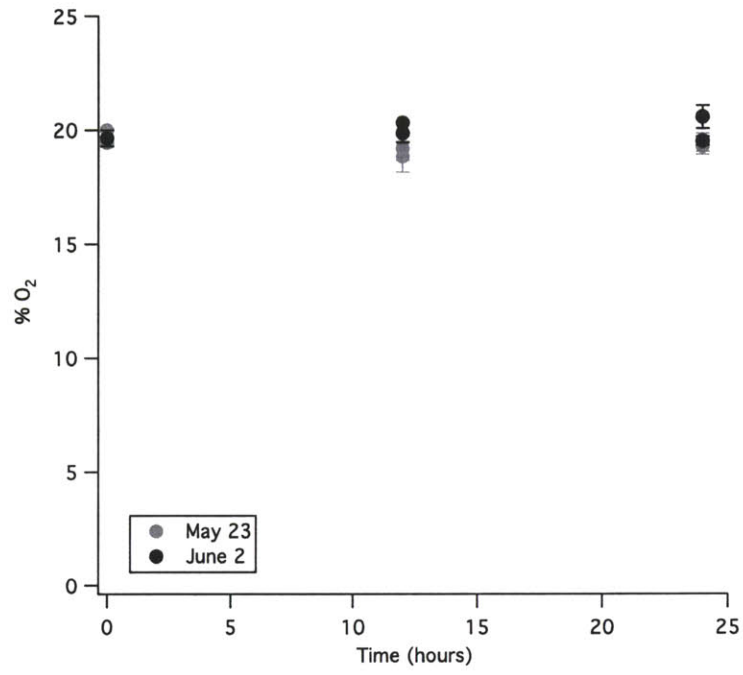
FIGURE 11. The % O_2 in the headspaces of the serum bottle incubations from May 23 and June 2.
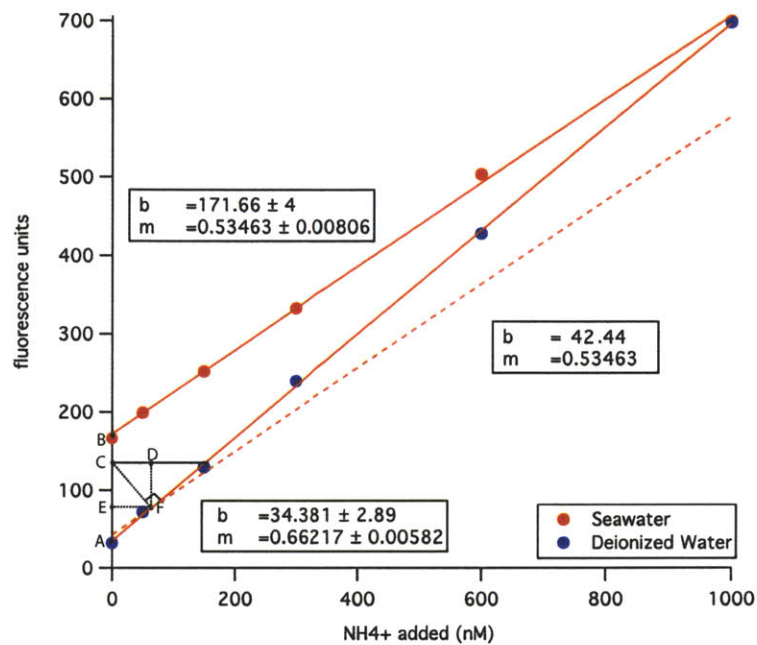
FIGURE 12. A set of NH_4^+ concentration standard curves in seawater and deionized water. The final calibration curve is given by the red dashed line, with a slope of 0.53463 and an intercept of 42.44.
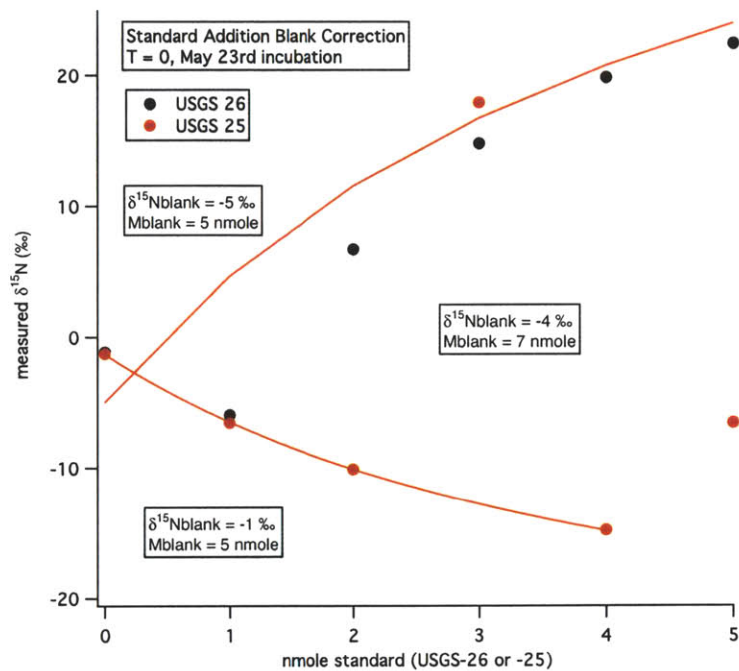
FIGURE 13. A representative standard addition of USGS-26 (black dots) and USGS-25 (red dots) NH_4^+. The data shown are from the T0 NH_4^+ isotopic measurements made for the May 23rd incubation. The red lines indicate the fitted blank values of -5‰ and 5 nmole for the USGS-26 standard addition and -1‰ and 5 nmole for the USGS-25 standard addition. When data from both standards were analyzed together, fitted values of -4‰ and 7 nmole were obtained. The values obtained when both standards were analyzed together were used to make the blank corrections to the experimental measurements. The data points for 3 nmole and 5 nmole USGS-25 were assumed to be fliers and were not included in the fitting analysis.

TABLE 1. *Synechococcus* cell counts, nitrification rates, and rate constants (k) for N+N uptake calculated with model 1 (see text).

Date	*Syn* cells ml^{-1}	Rate$_{dark}$ ($\frac{nmole}{l \times day}$)	Rate$_{light}$ ($\frac{nmole}{l \times day}$)	k$_{dark}$ (hr^{-1})	k$_{light}$ (hr^{-1})
May 9	4800 ± 1130	0.29±0.12	0.19±0.10	0.022	0.022
May 15	9350 ± 2900	0.26±0.06	0.37±0.19	0.022	0.026
May 23	15400 ± 2550	0.23±0.15	0.16±0.10	0.023	0.027
June 2	8200 ± 990	0.31±0.06	0.32±0.07	0.025	0.025

TABLE 2. Nitrification rates calculated with model 2 (no net N+N uptake).

Date	Rate$_{dark}$ ($\frac{nmole}{l \times day}$)	Rate$_{light}$ ($\frac{nmole}{l \times day}$)
May 9	1.6	1.3
May 15	2.2	2.8
May 23	1.1	1.5
June 2	1.9	2.1

TABLE 3. N$_2$O production rates calculated with model 3

Date	R$_{N_2O}$ ×10^6 (hour^{-1})	N$_2$O production rate ($\frac{fmole}{l \times day}$)
May 9	1.4 ± 0.14	0.7 ± 0.1
May 15	2.78 ± 0.22	1.3 ± 0.1
May 23	7.97 ± 0.46	3.8 ± 0.2
June 2	1.20 ± 0.15	0.6 ± 0.1

TABLE 4. N_2O production rates calculated with model 4

Date	Rate N_2O_{dark} ($\frac{fmole}{l \times day}$)	Rate N_2O_{light} ($\frac{fmole}{l \times day}$)
May 9	0.6	0.7
May 15	1.2	0.4
May 23	3.0	3.1
June 2	0.8	0.4

TABLE 5. N_2O yields calculated with model 1 and model 3. Yields were calculated using dark nitrification rates.

Date	average yield ($\frac{mole-N}{mole-N}$)
May 9	4.9×10^{-3}
May 15	9.9×10^{-3}
May 23	32.5×10^{-3}
June 2	3.9×10^{-3}

4. NITROUS OXIDE PRODUCTION AND TRANSPORT IN THE SOUTH ATLANTIC OCEAN

1. Abstract

Marine nitrous oxide (N_2O) production is a significant source of this greenhouse gas to the atmosphere. The flux of N_2O to the atmosphere is a combination of soil, marine, and anthropogenic sources that has expanded steadily over the past hundred years. Stable isotopic characterization of marine N_2O is valuable because it provides a way of constraining the ocean's contribution to this flux. It also provides a means of identifying which microbial nitrogen cycle processes contribute to the distribution of N_2O in the ocean. Here, N_2O concentration and isotopic data are reported from a 2007 cruise across the South Atlantic during the austral spring. The cruise track spanned four distinct provinces, the oligotrophic subtropical gyre, the upwelling of the subequatorial gyre, the intensified upwelling of the Angola Gyre (AG), and the wind-driven coastal upwelling of the Benguela Current off southwestern Africa. It revealed subsurface N_2O concentrations as high as 49.4 nM and surface supersaturations that increased in the more productive upwelling zones. Using the $\delta^{18}O$-N_2O, $\delta^{15}N^{bulk}$-N_2O, and the position-specific nitrogen signatures $\delta^{15}N^{\alpha}$-N_2O and $\delta^{15}N^{\beta}$-N_2O, three potential sources of N_2O to the atmosphere were identified, a shallow isotopically depleted source associated with the thermocline and the primary nitrite maximum, a larger mid-depth source fueled by nitrification during remineralization of organic matter exported out of the surface, and a deep source exported from the subsurface waters of the Southern Ocean.

The mid-depth N_2O source created a concentration maximum at 300-400 m depth whose concentration increased as O_2 consumption inside the AG increased. This, combined with its isotopic composition ($\delta^{18}O$-N_2O = 42.0 ± 0.5‰, $\delta^{15}N^{bulk}$-N_2O = 6.4 ± 0.2‰, $\delta^{15}N^{\alpha}$-N_2O = 12.2 ± 0.6‰, $\delta^{15}N^{\beta}$-N_2O = 0.6 ± 0.2‰), and particularly its relative enrichment in $^{15}N^{\alpha}$ over $^{15}N^{\beta}$ or Site Preference (SP = 11.7‰) and low $\delta^{18}O$-N_2O signature, indicates that nitrification contributed significantly to the N_2O. A lighter source at 50-200 m was produced by nitrification with a 50-60% contribution from nitrifier-denitrification ($\delta^{18}O$-N_2O = 38.8 ± 0.5‰, $\delta^{15}N^{bulk}$-N_2O = 5.2 ± 0.2‰, $\delta^{15}N^{\alpha}$-N_2O = 9.2 ± 0.7‰, $\delta^{15}N^{\beta}$-N_2O = 1.3 ± 0.4‰). This source intensified inside the AG ($\delta^{18}O$-N_2O = 38.2 ± 0.4‰, $\delta^{15}N^{bulk}$-N_2O = 4.4 ± 0.1‰,

91

$\delta^{15}N^{\alpha}$-N_2O = 7.6 ± 0.4‰, $\delta^{15}N^{\beta}$-N_2O = 1.1 ± 0.1‰) with the shoaling of the thermocline and the expansion of the primary nitrite maximum. The deep source was a mixture of N_2O from the atmosphere, N_2O from global stable oxygen deficient zones transferred via the Southern Ocean, and the shallower nitrification and nitrifier-denitrification sources. The isotopic signatures of this N_2O were near those of modern atmospheric N_2O ($\delta^{18}O$-N_2O = 45.8 ± 0.8‰, $\delta^{15}N^{bulk}$-N_2O = 7.9 ± 0.3‰, $\delta^{15}N^{\alpha}$-N_2O = 15.7 ± 0.6‰, $\delta^{15}N^{\beta}$-N_2O = 0.2 ± 0.2‰). Thus, although individual sources of marine N_2O are isotopically distinct from the atmosphere, their mixture produces an oceanic source signature that is close to that of the atmosphere, creating a buffer of atmospheric N_2O against changes driven by terrestrial N_2O production.

2. INTRODUCTION

Nitrous oxide (N_2O) is a climatically important greenhouse gas that is also involved in stratospheric ozone destruction (Yung and Miller, 1997). Atmospheric N_2O concentrations have steadily risen over the past 100-150 years (Sowers et al., 2002), further forcing the global greenhouse effect. The main sources of N_2O are probably microbial, releasing an estimated 12 Tg of nitrogen per year from terrestrial soils and 3 Tg per year from the ocean (Solomon et al., 2007). The major sink of tropospheric (N_2O) is a combination of ultraviolet photolysis and photo-oxidation in the stratosphere (Cantrell et al., 1994; Hanisco and Kummel, 1993; Preston and Barr, 1971). However, these sources and sinks are variable in both space and time and predicting future environmental fluxes requires a clearer mechanistic understanding of the sources and sinks of atmospheric N_2O. The stable isotopic composition of N_2O can be used to identify and constrain different sources.

A number of studies have investigated the nitrogen and oxygen isotopic signatures of N_2O produced by nitrification and denitrification, the two main biological processes that generate N_2O in the oceans and in soils (Kool et al., 2007; Toyoda et al., 2005; Ostrom et al., 2007; Sutka et al., 2003, 2004; Yoshida, 1988) and several oceanographic studies have used these signatures to characterize localized production and consumption mechanisms (Ostrom et al., 2000; Popp et al., 2002; Westley et al., 2006; Yamagishi et al., 2007; Yoshida et al.,

1989). However, closure of the global N_2O isotope budget using this "bottom up" approach (Solomon et al., 2007) has been elusive thus far, in part because different regions of the ocean contain N_2O with different stable isotopic signatures, making it difficult to identify a single set of signatures for the net marine N_2O source. Unlike the troposphere, which is well-mixed with respect to N_2O, the mixing time of the ocean is long relative to *in situ* rates of N_2O production, consumption, and air-sea gas exchange.

To date, isotopic measurements made on marine N_2O have focused heavily on the Pacific Ocean, particularly the tropical and subtropical gyres (Kim and Craig, 1990; Ostrom et al., 2000; Popp et al., 2002) and the stable oxygen deficient zones (ODZs) of the eastern boundary waters off of North America (Yoshinari et al., 1997; Yamagishi et al., 2007) and South America (Charpentier et al., 2007). Measurements have also been made in the stable ODZs of the Arabian Sea (Yoshinari et al., 1997; Naqvi et al., 1998; McIlvin and Casciotti, 2010) and the Black Sea (Westley et al., 2006). Stable ODZs are known hot spots of N_2O production, yet they account for a small fraction of the total ocean volume and surface area. The major sources and sinks of marine N_2O are likely to be different between ODZs and the well-oxygenated regions.

Nitrification and specifically, ammonia oxidation, occurs in and above the nutricline of oxic waters (Yool et al 2007) where it is probably the major source of N_2O in the open ocean. This N_2O enters the atmosphere on timescales determined by surface mixing and much slower rates of exchange across the nutricline. In contrast, both denitrification and nitrification may contribute N_2O to the waters immediately above and below stable ODZs, and denitrification consumes N_2O in the anoxic ODZ cores. These stable ODZs are characterized by limited direct exchange with the atmosphere (Naqvi et al., 2006; Stramma et al., 2008) and weak lateral transport (Nevison et al., 2003), and so may build up significant excesses of N_2O.

These processes affect both the concentrations and the isotopic composition of dissolved N_2O. The signatures trace the distribution patterns of a particular N_2O source as the N_2O mixes out of its formation region. They also provide us with information on the

biological processes that produced it. The relevant isotope systems are the bulk ^{15}N signature (δ^{15}N^{bulk}-N$_2$O), the Site Preference or relative enrichment of the internal nitrogen atom (N$^{\alpha}$) over the external nitrogen atom (N$^{\beta}$) in the asymmetric N$_2$O molecule (SP = δ^{15}N$^{\alpha}$-N$_2$O − δ^{15}N$^{\beta}$-N$_2$O), and the ^{18}O signature (δ^{18}O-N$_2$O).

Ammonia-oxidizers carry out the conversion of ammonia (NH$_3$) to nitrite (NO$_2^-$), the first step in the nitrification process. They produce N$_2$O in two ways: as a side-product during the NH$_3$ oxidation reaction (Hooper and Terry, 1979; Ritchie and Nicholas, 1972; Poth and Focht, 1985) and during nitrifier-denitrification, a NO$_2^-$ reduction pathway that is enzymatically similar to denitrification (Shaw et al., 2006; Casciotti and Ward, 2001; Walker et al., 2010). Pure cultures of ammonia oxidizing bacteria produce N$_2$O with a range of δ^{15}N^{bulk} and SP signatures that varies depending upon which of these two pathways is more important (Sutka et al., 2003, 2004; Frame and Casciotti, 2010). The δ^{18}O signature of this N$_2$O also depends on the O$_2$ concentration, following that of O$_2$ in oxic environments and dropping closer to that of seawater in low-O$_2$ environments (Ostrom et al., 2000; Frame and Casciotti, 2010).

Denitrifying bacteria produce N$_2$O during incomplete nitrate (NO$_3^-$) reduction (Firestone and Tiedje, 1979). This N$_2$O is depleted in ^{15}N and enriched in ^{18}O relative to the substrate NO$_3^-$ (Casciotti et al 2007), with a SP that is near 0‰ (Toyoda et al., 2005). In the absence of O$_2$, denitrification may also consume N$_2$O, converting it to N$_2$. This process is fractionating, enriching the residual N$_2$O in ^{15}N and ^{18}O (Yoshinari et al., 1997; Naqvi et al., 1998), and preferentially increasing the ^{15}N enrichment of the internal nitrogen atom over the external nitrogen atom. As a result, the SP of the residual N$_2$O increases in parallel with the δ^{18}O in a ratio of 1:2.2‰ as N$_2$O is progressively consumed (Ostrom et al., 2007).

In the ocean, these biological processes leave their mark against a N$_2$O distribution that is set by physical processes, particularly gas exchange with the atmosphere. The atmosphere is a significant and well-mixed N$_2$O source and air-sea gas exchange drives N$_2$O in surface waters towards the equilibrium concentration and isotopic composition of the atmosphere (δ^{15}N^{bulk} = 6‰, δ^{18}O = 45‰, SP = 18.7‰, and δ^{15}N$^{\alpha}$ $\doteq$ 17‰ δ^{15}N$^{\beta}$ $\doteq$ -2‰ (Yoshida and Toyoda, 2000; Griffith et al., 2009; Croteau et al., 2010)). Anthropogenic

activity has increased atmospheric N_2O concentrations over the past 100-150 years so that the current concentration (322 ppb) is 17% higher than the preindustrial concentration (275 ppb). As a result, water masses that equilibrated with the atmosphere and subducted more than 150 years ago contain a proportionately smaller amount of atmospheric N_2O than younger water masses (Walter et al., 2006; Freing et al., 2009). Other factors, such as thermal disequilibrium, advection, and upwelling are also important drivers of marine N_2O distributions and exchange with the atmosphere. For example, N_2O is more soluble in colder water, so that water that outcrops in colder regions can dissolve more atmospheric N_2O than warmer water. In addition water that subducts before fully equilibrating will not be reset to the atmospheric equilibrium concentration and isotopic composition.

Coastal upwelling regions are recognized hot spots of N_2O release to the atmosphere (e.g, the northwest Indian Ocean (Law and Owens, 1990), California coast (Lueker et al., 2003; Nevison et al., 2004)). These regions may be particularly strong sources of N_2O to the atmosphere for two reasons. First, intense vertical mixing draws to the surface deep water that has accumulated N_2O while submerged (Nevison et al., 1995; Lueker et al., 2003; Charpentier et al., 2010). Second, high nutrient deep water stimulates phytoplankton blooms as it enters the euphotic zone (Lueker et al., 2003). Marine nitrification rates are tied to rates of surface primary production because organic nitrogen from the surface decomposes to NH_4^+ in the nutricline, stimulating nitrification, and thus N_2O production.

The Benguela upwelling system along southwestern Africa supports high levels of primary production, particularly during the austral spring and summer. It is predicted to be a large N_2O source (Nevison et al., 2004) and intensifying O_2 depletion observed there over the past 50 years (Stramma et al., 2008) suggests that the source may be growing larger. Here we present N_2O concentration and isotopic data from the oligotrophic waters of the subtropical gyre to the eutrophic waters of the subequatorial gyre and the coastal upwelling of the Benguela Current. We collected this data during the 2007 CoFeMUG cruise across the South Atlantic. The spatial resolution of sampling was high, both laterally along the cruise track and vertically from surface to deep. This allowed us to observe the distribution of N_2O as well as its probable circulation along South Atlantic currents. Here we present

concentration and isotopic measurements from 23 of the 28 stations occupied during the CoFeMUG cruise (Figure 1). To our knowledge, this is the first report of such measurements in the Atlantic.

3. MATERIALS AND METHODS

The CoFeMUG cruise crossed the South Atlantic between mid November and mid December 2007 (Noble et al., 2011). It consisted of three transects: a West to East transect from the coast of Brazil to the Angolan coast ($330\,^{\circ}$W, $11\,^{\circ}$S - $12.2\,^{\circ}$E, $14.75\,^{\circ}$S), a coastal transect along Angola and Namibia ($12.2\,^{\circ}$E, $14.75\,^{\circ}$S - $14.5\,^{\circ}$E, $25\,^{\circ}$S), and a southern East to West transect leaving the coast of Namibia ($14.5\,^{\circ}$E, $25\,^{\circ}$S - $10\,^{\circ}$E, $25\,^{\circ}$S) (Figure 1).

Salinity, potential temperature, and oxygen data were recorded by the ship's CTD. Oxygen sensor data were calibrated with Winkler titrations at the beginning and end of the cruise. Nutrient concentration measurements (phosphate, nitrate, and silicate) and NO_3^- isotopic measurements were made on filtered samples that were kept frozen until analysis. Nutrient concentration measurements were made for all depths and all stations by a nutrient facility (see Noble et al. (2011) for details).

NO_3^- isotopic measurements were made on samples collected at stations 5-17 between 0 and 1000m. NO_3^- samples were converted to N_2O for nitrogen and oxygen isotope analyses using the denitrifier method (Sigman et al., 2001; Casciotti et al., 2002) and measured along with USGS isotopic standards (Bohlke et al., 2007) on the same IRMS

Single water samples for N_2O analyses were collected from about ten depths between 20 and 1000m at stations 5 though 27. Immediately after rosette recovery, water samples were collected by twice overfilling glass 165 ml serum bottles (Wheaton prod. no. 223748) from the bottom up using tygon tubing attached to each niskin bottle. They were poisoned with 100 μl of saturated $HgCl_2$ solution and then sealed with butyl stoppers (MicroLiter Analytics prod. no. 20-0025) and aluminum crimps. Poisoned samples were stored for at least 2 months in the dark at room temperature before analysis.

Isotopic analyses of N_2O were made using a Finnigan Delta[PLUS] XP IRMS calibrated for isotopomer-specific measurements (see Frame and Casciotti (2010) for details). Bottles

were purged with He and N_2O was trapped on-line with a custom-built purge and trap system (McIlvin and Casciotti, 2010). The total moles of N_2O were determined from each bottle using a constant linear relationship between N_2O mass and m/z 44 peak area.

All data were plotted in Igor Pro, v. 6.03. Contour plots were made in Igor Pro using linear interpolation.

4. Results and Discussion

4.1. Overview. The following approach was used in the analysis below: the descriptive physical oceanography of the South Atlantic was used to identify the water masses that were sampled during the cruise. The N_2O samples that were collected during the cruise were classified into types based on the similarity of their isotopic signatures and the overall variability of the entire isotopic data set. The water masses from which the samples came were identified using the conservative and semi-conservative tracers salinity, potential temperature, and silicate concentration. The biological processes that gave rise to each type of N_2O were evaluated based on the sample's location and by comparing its isotopic signatures with those measured in pure cultures of ammonia oxidizing bacteria and denitrifying bacteria. Finally, an assessment was made of the importance of each type of N_2O to the overall isotopic budget of marine N_2O.

4.2. Surface Currents. The northernmost cruise transect extended from the Brazilian coast, through the northern part the subtropical gyre, across the Angola Gyre (AG), and ended at the Angolan coast (Figure 1). The most oligotrophic conditions occurred between stations 1 and 8, where downwelling in the subtropical gyre caused the deepest thermoclines and haloclines observed during the cruise (150-200m) (Figures 2a and 2b). In this zone, surface O_2 concentrations were at atmospheric equilibrium, the subsurface O_2 minimum was small (Figure 3a), and $NO_3^- + NO_2^-$ concentrations at the top of the thermocline were low (Figure 3b). Surface N_2O concentrations (Figure 3c) were at equilibrium with the atmosphere at these stations.

In the subequatorial gyre (stations 9-19), cyclonic upwelling caused the thermocline to shoal. The shallowest thermoclines occurred inside the AG (stations 13-19), where

intensified upwelling caused significant upward doming of the isotherms (Figure 2a) and isohalines (Figure 2b) in the surface 300m. Nutrients drawn to the surface in this region (Figure 3b) stimulated primary production, causing subsurface O_2 concentrations to drop (Figure 3a). To the north, organic-rich discharge from the Congo River may have also contributed additional surface nutrients (van Bennekom and Berger, 1984). Inside the AG, surface N_2O concentrations were above equilibrium with the atmosphere (up to 3 times higher).

In the coastal transect, the shallow southward flow of the coastal Angola Current converged with the northward flow of the deeper coastal arm of the Benguela Current (Gordon and Bosley, 1991). At the convergence zone, deeper water surfaced, causing the isohalines to become nearly vertical (Figure 2b) and allowing N_2O that accumulated in this water during its circuit around the AG to be released to the atmosphere (Figure 3c). In the southern transect, southeast trade winds drew the coastal branch of the Benguela Current offshore (Figure 1), fueling ekman pumping and drawing colder, oxygenated water up from depth along the coast (Figures 2a and 3a).

4.3. **Subsurface Watermasses.** The potential temperature (T) and salinity (S) data fall along a mixing line that intersects the T-S values of the major subsurface watermasses in the South Atlantic (Figure 4). Data were collected between 0 and 1000m, a range in which the deepest (densest) samples are also the least saline (Figure 4). The deepest water sampled was closest in T and S to the Antarctic Intermediate Water (AAIW1 and AAIW2) with a colder, more saline contribution from the Circumpolar Deep Water (CDW, Figure 4). Most of the T-S data lie on a conservative mixing line between this water and South Atlantic Central Water (SACW, Figure 4). In the literature, the SACW is commonly split into the shallower SACW1, which is warmer $(16 - 18\,^\circ C)$ and more saline, and SACW2, whose T is between $12 - 13\,^\circ C$. SACW1 and SACW2 are also split into equatorial (SACWE) and tropical (SACWT) branches, with younger/more recently ventilated water present in the tropical branches. The most saline (up to 36.9 psu) samples were collected at the surface

in the far western part of the northern transect, a high surface-salinity field off southern Brazil (Stramma and Schott, 1999).

The highest N_2O concentrations (up to 49.4nM) were observed in the eastern part of the northern transect between 300 and 400m (Figure 3c), which falls between the SACW2 and AAIW on the T-S mixing line (Figure 4). The N_2O concentration maximum was coincident with the O_2 concentration minimum, (19.8 μM, Figure 3a) and slightly shallower than the $NO_3^- + NO_2^-$ concentration maximum (Figure 3b). The plume of high-N_2O, low-O_2 water extended westward along the northern transect, gradually decreasing in intensity but remaining well above the contemporary and historical atmospheric saturation concentrations (10-13 nM). The core of high-N_2O water also extended down the coast to station 21 (20 °S, 12 °E). In the off-shore waters of the southern transect, a smaller N_2O maximum ($\sim$27 nM) was also present at 300m. High benthic N_2O concentrations were observed in the near-shore stations (stations 23 and 24) of the southern transect (Figure 3c).

A shallow plume of N_2O between stations 13 and 19 was depleted in ^{15}N and ^{18}O relative to both the atmospheric N_2O above it as well as the N_2O concentration maximum below it (Figure 5a-d). The plume was centered between 40 and 200m and its minimum observed signatures were $\delta^{18}O$-N_2O = 37.4‰ (150m, station 19), $\delta^{15}N^{bulk}$ = 3.2‰ (54m, station 18), and SP = 4.2‰ (70m, station 18). We infer that dissolved atmospheric N_2O has a $\delta^{18}O$-N_2O = 45.0‰, $\delta^{15}N^{bulk}$ = 6.4‰, and SP = 18.4‰, based on the isotopic signatures of the N_2O present in the shallow surface water of the western half of the northern transect. The deep concentration maximum contained N_2O with a $\delta^{18}O$-N_2O = 42.0‰, $\delta^{15}N^{bulk}$ = 6.4‰, and SP = 11.7‰. Below the concentration maximum (600-1000m), the N_2O was slightly more enriched than modern atmospheric N_2O but had a lower SP, where $\delta^{18}O$-N_2O = 45-46‰, $\delta^{15}N^{bulk}$ = 7-8‰, and SP = 15-16‰.

4.4. **Cluster analysis of N_2O isotopic composition.** Physical processes can be as important as biological processes in determining the distributions of dissolved N_2O (Nevison et al., 2003, 2004; Suntharalingam and Sarmiento, 2000). Since physical dynamics are particularly influential in the Benguela upwelling region, we used a classification scheme based

on the isotopic composition of the dissolved N_2O to identify and organize the different types of N_2O that were observed. The goal of the analysis was to identify which water masses and/or biogeochemical conditions were associated with the different N_2O types. Different N_2O types tended to correspond to specific locations along the cruise track. For this analysis, the mathematical boundaries that separate one type of N_2O from another depend on the amount of variation in the entire data set and therefore, they are not entirely independent of the sampling scheme. Because samples within each type are co-located and isotopically homogeneous, they may have formed either through thorough mixing of N_2O from multiple biological sources or through an individual biological process producing N_2O with a single set of isotopic signatures. The values of the three atom-specific isotopic signatures ($\delta^{18}O$-N_2O, $\delta^{15}N^\alpha$, and $\delta^{15}N^\beta$) were standardized by subtracting each signature's mean value and then dividing by the signature's standard deviation. A dendrogram was assembled by hierarchically pairing samples based on their covariances (Figure 6) in Matlab (v. 2009b) using the pdist, linkage, and dendrogram functions in the statistics tool box. The branches of clusters with above-average linkage values were colored. The ability of the dendrogram to accurately represent the original covariances between data pairs was assessed by calculating the cophenetic correlation coefficient between the leaves of the dendrogram and their original covariances (value $= 0.7358$). For reference, the metadata for each sample (station, depth, $\delta^{15}N^\alpha$, and $\delta^{15}N^\beta$, $\delta^{18}O$-N_2O, potential temperature, salinity, N_2O concentration, O_2 concentration, and $NO_3^- + NO_2^-$ concentration) were included to the right of the dendrogram. The metadata for samples in the larger clusters were colored according to their general location along the cruise track (northern transect outside the AG, northern transect inside the AG, coastal transect, southern transect).

The data fell into a number of clusters, the largest of which are labeled in Figure 6 as A (n = 38), H (n = 15), and I (n = 29). These clusters corresponded to shallow (169 $\pm$ 56m), intermediate (370 $\pm$ 49m), and deep (765 $\pm$ 298 m) samples. Samples in cluster A, the shallowest cluster, were almost entirely from the northern transect, both inside and outside the AG. These samples were isotopically light ($\delta^{18}O$-$N_2O = 38.8 \pm 0.5‰$, $\delta^{15}N^{bulk} = 5.2 \pm 0.2$, and SP= $7.9 \pm 1.0‰$) and were taken from water with a range of

O_2 concentrations (19 to $150\mu M$, average = $61 \pm 39\mu M$). The mean N_2O concentration in this cluster was $36 \pm 7nM$. Samples in cluster H, at intermediate depths, came from both the northern transect (inside and outside the AG) and the southern transect. They were isotopically heavier than the cluster A samples, but also depleted relative to atmospheric N_2O ($\delta^{18}O$-N_2O = 42.0 ± 0.5‰, $\delta^{15}N^{bulk}$ = 6.4 ± 0.2, and SP= 11.7 ± 0.5‰). The O_2 and N_2O concentrations of these samples were similar to those in Cluster A ($[O_2]$ = 30 to $160\mu M$, average = $75 \pm 45\mu M$ and $[N_2O]$ = $35 \pm 8nM$). Cluster I samples were from higher O_2 water (60 to $180\mu M$, average = $118 \pm 33\mu M$) but also above-equilibrium N_2O concentrations ($29 \pm 4nM$). The average isotopic composition of these samples was slightly heavier than atmospheric N_2O ($\delta^{18}O$-N_2O = 45.8 ± 0.8‰, $\delta^{15}N^{bulk}$ = 7.9 ± 0.3, and SP= 15.7 ± 0.6‰).

Besides these larger clusters, we also identified a group of samples that only came from inside the AG, from within the top 100m (Cluster B). This was the lightest N_2O observed during the entire cruise ($\delta^{18}O$-N_2O = 38.2 ± 0.4‰, $\delta^{15}N^{bulk}$ = 4.4 ± 0.1, and SP= 6.5 ± 0.5‰). The N_2O concentrations in these samples were high ($30 \pm 3nM$) and as was the range of O_2 concentrations (60 to $180\mu M$, average = $103 \pm 52\mu M$). Few of the coastal transect samples fell into larger clusters with samples from the northern and southern transects. Those that did tended to fall out in or near the shallower clusters, A and B. We have not tested the statistical robustness of the dendrogram's topology. However, the underrepresentation of the coastal data in the larger clusters suggests that a different set of processes produced these N_2O signatures, perhaps through intensified or multiple-endmember mixing as well as a unique set of in situ biological processes including sedimentary and terrestrial processes. The smaller number of samples collected in the coastal transect could have also contributed to their underrepresentation in any larger clusters.

4.5. N_2O **Concentration versus Conservative Tracers.** Previous studies in the South Atlantic (Brea et al., 2004; Poole and Tomczak, 1999) have identified the salinities, potential temperatures, and silicate concentrations that are characteristic of each of the major parent water masses flowing through this basin (i.e., the SACW1, SACW2, AAIW, and CDW).

By plotting N_2O concentration against these conservative and semi-conservative tracers, we were able to identify which water masses contained specific isotopic types of N_2O. Although salinity (Figure 7a-d) and potential temperature (Figure 8a) are used most often to identify water masses, a silicate concentration plot was also included (Figures 8b) because it was better at representing the contributions of the silicate-rich AAIW and CDW to the deeper water (Brea et al., 2004).

Subsurface N_2O concentrations were significantly higher than atmospheric equilibrium concentrations. The N_2O concentration maximum (samples from cluster H) was mainly located in the SACW2 based on temperature, salinity, and depth, but also included smaller AAIW and CDW components (Figures 7a and 8a-b). N_2O from cluster I was associated with the deepest water masses, AAIW and CDW. This N_2O was significantly oversaturated with respect to atmospheric equilibrium ($\sim$75% higher) but occupied a region in isotope space that was most similar to the signatures of modern atmospheric N_2O. The shallowest subsurface water was a mixture of the SACW1 and SACW2 that was oversaturated by 100-260% (Figures 7a and 8a-b). The lowest N_2O concentrations (7-8nM) were observed in well-mixed surface waters that were at or very close to atmospheric equilibrium concentrations.

The same water masses circulate through the AG and the outer subequatorial gyre. However, subsurface N_2O concentrations were consistently higher inside the AG (Figures 7a-d and 8a-b) than anywhere else along the cruise track. The largest increase in N_2O concentration occurred in the concentration maximum (400m, S = 34.7-35 psu), where O_2 concentrations dropped to the lowest observed values (Figure 7d). A second zone of N_2O production occurred at the top of the thermocline (50-100m, S = 35.4-36.0 psu). In the next section, we use these concentration differences to quantify the amount of N_2O production linked to enhanced productivity in the AG.

4.6. N_2O and nutrient remineralization stoichiometry ($\Delta N_2O/\Delta O_2$, N*). Stoichiometric relationships between subsurface N_2O production and O_2 consumption or $NO_3^- + NO_2^-$ remineralization relate N_2O to organic matter remineralization rates. Ideally, they can be

used to estimate what fraction of the nitrogen that supports surface production will be converted to N_2O. However, N_2O:O_2 stoichiometries ($\Delta N_2O/\Delta O_2$) estimated by regressing N_2O supersaturation (ΔN_2O) against Apparent Oxygen Utilization (AOU) have produced a number of different values depending on the regions and depths included (Nevison et al., 1995). The variations are caused by mixing between water masses with different N_2O and O_2 concentrations and biological changes that increase the yield of N_2O as O_2 concentrations change (Nevison et al., 2003).

N_2O and O_2 concentrations are inversely related (Figure 9a-b). Based on the slopes of N_2O:O_2 regression lines, the magnitude of $\Delta N_2O/\Delta O_2$ is significantly higher in the northern transect (-0.19 nM/μM) than the coastal or southern transects (-0.14 nM/μM). In the northern transect, the N_2O and O_2 distributions are dominated by four extrema: (1) the surface water, where dissolved O_2 and N_2O are near equilibrium with the atmosphere ($N_2O = \sim 7$ μM, $O_2 = \sim 220$ μM), (2) the deep N_2O source ($N_2O = \sim 28$nM, $O_2 = \sim 150\mu$M), (3) the N_2O concentration maximum ($N_2O = \sim 47$nM, $O_2 = \sim 20\mu$M), and (4) the shallow, secondary N_2O maximum found inside the AG ($N_2O = \sim 33$nM, $O_2 = \sim 50\mu$M). The distribution of data points between these extrema make it difficult to distinguish the effects of production from simple mixing between end-members.

Comparing data taken from inside and outside the AG is like resampling the same water masses before and after they have been through the AG upwelling regime. This approach reduces the influence of mixing and preformed N_2O on $\Delta N_2O/\Delta O_2$ calculations. In Table 1, the average N_2O, O_2, and $NO_3^- + NO_2^-$ concentrations from inside and outside the AG are compared for samples from within the three major N_2O types (clusters A, H, and I in Figure 6). The average N_2O concentration increased 3.7nM in all three clusters. The thermocline waters of the subequatorial gyre have an estimated 9 year residence time (Bosley, 1991), making the average N_2O production rate in the gyre 0.4 nM yr^{-1}. This rate falls in the middle of the range of values calculated by Freing et al. (2009) for the top 1000m of the North Atlantic. The magnitude of the $\Delta N_2O/\Delta O_2$ ratios decreased from -0.25×10^{-3} in the shallow cluster to -0.17×10^{-3} in the concentration maximum and -0.11×10^{-3} in the deep cluster, with $\sim 25\%$ uncertainty based on the standard deviations among samples.

Nevison et al. (2003) calculated a very similar deep water ratio of -0.12×10^{-3} based on data from $\sigma_{26.9}$ in the northwestern South Atlantic (this would correspond to samples from Cluster H here). The ratio in the concentration maximum is the same as that calculated by Naqvi and Noronha (1991) for the oxygenated waters above the deep ODZ in the Arabian Sea. The higher yields observed in shallower water imply a change in the mechanism of N_2O production. Nitrifier-denitrification has been shown to enhance the overall yield of N_2O from ammonia-oxidizers (Frame and Casciotti, 2010) but denitrification can also increase N_2O concentrations without consuming O_2 (Naqvi et al., 2000).

N*, the excess or depletion of NO_3^- relative to PO_4^{3-} based on Redfield stoichiometry is a tracer whose value increases in regions where N_2 fixation is important and decreases when denitrification occurs (Gruber and Sarmiento, 1997). High N* values were observed in the subequatorial gyre between 100 and 600m, particularly within the AG (Figure 10b). N_2O concentrations were also slightly positively correlated with N* ($r^2 = 0.31$, Figure 10a), suggesting that nitrification enhanced by surface N_2 fixation produced the N_2O (Nevison et al., 2003). The water in the AG tended to have higher N_2O concentrations than the stations in the outer gyre and the coastal and southern transects (Figure 9). The water in the AG is the most aged, suggesting that the accumulation of N_2O is related to remineralization processes.

4.7. Linking N_2O isotopic composition and production mechanisms: oceanographic observations.

Previous oceanographic studies have reported stable isotopic signatures for N_2O from three different types of environments: the surface and shallow subsurface waters of the oligotrophic subtropical gyres, seasonal high productivity coastal upwelling zones, and stable ODZs that lie under certain highly productive surface waters. Data from all three environments are relevant to the signatures found in the South Atlantic.

In the North Pacific subtropical gyre (station ALOHA), a shallow (200m) isotopic minimum ($\delta^{18}O = 40.8‰$, $\delta^{15}N = 5.8‰$) was attributed to nitrification by Dore et al. (1998). At the same site, Ostrom et al. (2000) supported this conclusion based on the covariation

of $\delta^{18}O$-O_2 and $\delta^{18}O$-N_2O. They reasoned that nitrifier-denitrification made an important contribution to this N_2O because the $\delta^{18}O$-N_2O observed at this depth was closer to the $\delta^{18}O$-H_2O than at any other depth. Finally, a low site preference (SP minimum = 8‰) was observed at this depth by Popp et al. (2002), supporting the hypothesis that nitrifier-denitrification contributed to the N_2O at the top of the thermocline. In the Chilean upwelling zone, Charpentier et al (2007) also observed a SP minimum of N_2O at the top of the thermocline (50m, SP = 12‰ and $\delta^{18}O$ = 52‰). The dynamics in that system were similar to the Benguela system: oligotrophic South Pacific central gyre water mixed with high nutrient, low O_2 upwelled water near the Chilean coast. In this area, the concentration maximum (400m) was more enriched in ^{18}O and had a higher SP ($\delta^{18}O$-N_2O = 54‰, SP = 24‰) than the concentration maximum observed in the South Atlantic, possibly contributing to the higher SP and $\delta^{18}O$ values that they observed in the shallow isotopic minimum.

The shallow thermocline signatures noted by Dore et al. (1998), Ostrom et al. (2000), and Popp et al. (2002) are close to those of Cluster A in the northern transect, but are slightly more enriched in ^{18}O. Cluster B, the shallower N_2O from the thermocline of the AG, is both isotopically depleted and lower in SP than the ALOHA data and the Chilean upwelling data. However, like both of these types of N_2O, the N_2O in Clusters A and B is lighter and lower in SP than the atmospheric N_2O above it and the N_2O of the concentration maximum below it. These past studies have concluded that this N_2O is the product of nitrification and nitrifier-denitrification. The SP signatures measured for cultures of ammonia oxidizing bacteria support the conclusion, but the $\delta^{15}N^{bulk}$ signatures and $\delta^{18}O$ signatures are both significantly higher than those measured in culture ($\delta^{15}N^{bulk}$ = 40-50‰ higher, $\delta^{18}O$ = 22‰ higher).

Upwelling and nutrient injection in the coastal transect produced redox gradients in the water column that did not exist in the northern or southern transects. Some of the lowest and highest O_2 concentrations were observed here (Figure 3a) and this was the only region where low values of N* were observed (Figure 10b). Most of the N_2O here failed to cluster with any data from the rest of the cruise, suggesting a unique source or combination of

sources. The $\delta^{18}O$ of the N_2O observed here was particularly high (Figure 11b) given its low SP and $\delta^{15}N$ signatures ($\delta^{15}N^{bulk}$-N_2O = 4‰, $\delta^{18}O$-N_2O = 46-47‰, SP = 6‰). This could be the result of nitrification in water with an extremely high $\delta^{18}O$-O_2, or production by denitrification. However, in the same region, Kuypers et al. (2005) attributed large fixed N losses in the region to anammox bacteria. No data has been published on the isotope effects associated with anammox, but they could influence the $\delta^{15}N$ and $\delta^{18}O$ values of the N_2O precursors NO_2^- and NO_3^-. A similar mismatch between N and O signatures was observed by Naqvi et al. (1998, 2006) in the coastal surface waters of the monsoonal upwelling region in the Arabian Sea. A large surface source of N_2O there was highly depleted in ^{15}N but not ^{18}O ($\delta^{15}N$-N_2O = 0.8‰, $\delta^{18}O$-N_2O = 46‰). In the oxycline of the Black Sea, Westley et al (2003) attributed ^{15}N-depleted, ^{18}O-enriched ($\delta^{15}N$ = -10.8‰ and $\delta^{18}O$ = 60 to 70‰) N_2O to a combination of production by nitrification and consumption by denitrification on the basis of its high SP (25-30‰).

Although there are no stable ODZs in the Atlantic, the ODZs of the Eastern Tropical North Pacific (ETNP), Eastern Tropical South Pacific (ETSP), and the Arabian Sea all produce and export large amounts of N_2O (Nevison et al., 2003). These ODZs have an impact on South Atlantic N_2O through the circulation of the Southern Ocean, which receives water from each of the major ocean basins. The isotopic composition of the 500m concentration maximum in the Southern Ocean is very similar to that of the deep N_2O Cluster I ($\delta^{18}O$-N_2O = 46‰, $\delta^{15}N^{bulk}$-N_2O = 7.5‰, SP = 16‰) (Figure 12) (Boontanon et al., 2010). The AAIW and CDW both contributed to this deep water and may have brought N_2O from the polar region with them. The N_2O exported from the 800m concentration maximum in the ETNP was observed to have an isotopic composition that was enriched in ^{18}O and had a high SP ($\delta^{18}O$-N_2O = 54‰, $\delta^{15}N^{bulk}$-N_2O = 9‰, SP = 23‰) (Dore et al., 1998; Popp et al., 2002; Kim and Craig, 1990; Yamagishi et al., 2007). Charpentier et al. (2007) observed similar signatures in the N_2O concentration maximum (400m) just south of the ETSP ($\delta^{18}O$-N_2O = 54‰, $\delta^{15}N^{bulk}$-N_2O = 7.5‰, SP = 24‰). In the Arabian Sea, ^{18}O and SP were similarly enriched in the concentration maximum ($\delta^{18}O$-N_2O = 64‰ and

SP = 24‰, $\delta^{15}N^{bulk}$-N_2O = 12.5‰) (McIlvin and Casciotti, 2010). In the eastern boundary upwelling zone of the Arabian Sea, Naqvi et al. (1998) also noted the impact of N_2O consumption at depth as $\delta^{18}O$-N_2O and $\delta^{15}N$-N_2O increased into the deep O_2 minimum ($\delta^{18}O$-N_2O= 58‰, $\delta^{15}N$-N_2O = 20‰).

The SP and $\delta^{18}O$-N_2O of the Southern Ocean lie very nearly on a mixing line between the N_2O exported from the ETNP and ETSP and the shallow subsurface N_2O (cluster A) in the South Atlantic (Figure 12). If this is a true mixing line, then the N_2O of the Southern Ocean appears to be split nearly evenly between a nitrification/Cluster A-like contribution and a contribution from the major ODZs. The Southern Ocean may provide the closest available approximation of an integrated marine isotopic signature because of its role in global ocean circulation.

4.8. Linking N_2O isotopic composition and production mechanisms: culture signatures.
So far, transport from the Southern Ocean has been identified as the source of deep N_2O in the South Atlantic (cluster I) based on the similarity of isotopic signatures and concentrations. We assumed that the two shallower sources were the result of localized biological processes based on the increase in N_2O concentration fueled by surface production. Do the isotopes support this conclusion? The isotope effects associated with measurements made in pure bacterial cultures of nitrifiers and denitrifiers are evaluated below.

The biological sources of N_2O are nitrification, nitrifier-denitrification, and denitrification. The isotopic composition of N_2O from each of these sources depends on the isotopic composition of its substrate molecules and the enzymatic mechanisms that produce the N_2O. Since the $\delta^{15}N$ of NH_4^+ was not measured on the cruise, we have to approximate the substrate $\delta^{15}N$ signature with the $\delta^{15}N$ of the $NO_3^- + NO_2^-$ at the top of the thermocline. In the northern transect, this value ranged between 5 and 6.5‰, decreasing near the African coast (Figure 13b). The shoreward depletion in ^{15}N is probably the result of increased expression of the isotope effect of $NO_3^- + NO_2^-$ uptake by phytoplankton (Altabet et al., 1999) as surface $NO_3^- + NO_2^-$ concentrations increased or it is the result of input of isotopically light nitrogen from N_2 fixing organisms (Bourbonnais et al., 2009) (Figure 13a). The

only measurements of the isotope effects of N_2O production during ammonia oxidation indicate that the $\delta^{15}N^{bulk}$ isotope effect is large (57‰) and normal for nitrifier-denitrification and much smaller for nitrification ($\leq$ 2‰) (Frame and Casciotti, 2010). The $\delta^{15}N$ of the shallow thermocline N_2O was 4-5‰, which is too high to have been produced by bacterial nitrifier-denitrification. N_2O is a by product of nitrification, not the major product, so that the completeness of substrate NH_4^+ consumption should not affect the expression of the isotope effects associated with N_2O production.

As discussed above, the $\delta^{18}O$ of the shallow thermocline N_2O is about 22‰ higher than any values observed for ammonia oxidizing bacteria cultures. The $\delta^{18}O$ of N_2O produced by nitrification should track the $\delta^{18}O$ of O_2 (Ostrom et al., 2000). However, in productive waters the $\delta^{18}O$ signature of N_2O is altered by photosynthesis in the euphotic zone and respiratory O_2 consumption during respiration and remineralization. The $\delta^{18}O$ of atmospheric O_2 is 23.5‰ but photosynthesis drives the value towards that of water (0‰) (Quay et al., 1993; Luz and Barkan, 2005) and respiratory fractionation can drive the value higher by up to 20-30‰.

Even if the N_2O formation mechanism does not have its own isotope effect, the $\delta^{18}O$ of N_2O produced in a system that is closed to both O_2 and N_2O should lag behind the $\delta^{18}O$-O_2 observed in the same water parcel. This is because the $\delta^{18}O$-N_2O behaves the same way as that of a major product accumulating in a rayleigh system, i.e. it is integrating over all the N_2O formed during the reaction's progress (Mariotti et al., 1981). In contrast, the O_2 that is being respired is the major reactant and its $\delta^{18}O$ increases rapidly as consumption progresses to completion. To test the impact of closed-system respiratory O_2 consumption on the $\delta^{18}O$-N_2O, the $\delta^{18}O$-O_2 was modeled as a rayleigh function of O_2 concentration (Equation 1), where the degree of discrimination against $^{18}O_2$ is set by the kinetic fractionation factor α ($\alpha = k_{18O_2}/k_{16O_2}$):

(1) $\delta^{18}O\text{-}O_2 = 1000‰ \times [(\frac{[O_2]\text{measured}}{[O_2]\text{eq}})^{\alpha-1} - 1]$

Two values of α have been proposed, a more fractionating value (0.981) observed during respiration by heterotrophic bacteria (Kiddon et al., 1993; Quay et al., 1993) and a higher (less fractionating) value (0.990) calculated by Levine et al. (2009) using $\delta^{18}O$-O_2 and O_2

concentration data from the South Atlantic. The assumptions used are that N_2O production is a linear function of O_2 consumption (constant $\Delta N_2O/\Delta O_2$) and the $\delta^{18}O$-N_2O is entirely set by the $\delta^{18}O$-O_2 (no O from H_2O is incorporated). Integrating Equation 1 as O_2 is completely consumed (atmospheric equilibrium concentration to 0) produces $\delta^{18}O$-N_2O values that fall within the range of observed values when $\alpha = 0.981$ (Table 2) and agree with the average $\delta^{18}O$-N_2O observed in the N_2O concentration maximum/O_2 minimum ($42.0 \pm 0.5\textperthousand$). When the degree of respiratory fractionation is reduced ($\alpha = 0.990$), maximum $\delta^{18}O$-N_2O values also drop, as expected (Table 3).

One possible inconsistency in this calculation is that it predicts $\delta^{18}O$-O_2 values that are higher than the corresponding $\delta^{18}O$-N_2O values, which was not observed by Ostrom et al. (2000) when paired $\delta^{18}O$-O_2 $\delta^{18}O$-N_2O measurements were made at station ALOHA. If some fractionation occurs during incorporation of O into N_2O so that ^{18}O-N_2O formation is favored over the lighter isotopologue, the $\delta^{18}O$-N_2O would be pushed higher than the $\delta^{18}O$-O_2. Preliminary work characterizing this net isotope effect in bacterial ammonia-oxidizers indicates that O_2-dependent N_2O formation does not heavily fractionate O isotopes found in the N_2O (Frame and Casciotti, 2010) but more work needs to be done to test this. Another consideration is that at very low O_2 concentrations, the $\delta^{18}O$-O_2 will be sensitive to small amounts of recharge with high-O_2 water. N_2O concentrations should be high in this type of water and the range of $\delta^{18}O$-N_2O values is smaller than it is for $\delta^{18}O$-O_2, so that observed $\delta^{18}O$-N_2O values will be less sensitive to similar amounts of recharge with atmosphere-equilibrated water.

While the high end of the nitrifier $\delta^{18}O$-N_2O range is set by the O_2-dependent pathway, nitrifier-denitrification produces ^{18}O depleted N_2O. Nitrifier-denitrification by bacterial ammonia-oxidizers produces N_2O enriched by about $8\textperthousand$ relative to the $\delta^{18}O$ of the substrate NO_2^- (Frame and Casciotti, 2010). The $\delta^{18}O$-NO_2^- was not measured during the cruise, but data from the Arabian Sea show a $\delta^{18}O$-NO_2- of 9 to $10\textperthousand$ in the primary NO_2^- maximum and 13-$15\textperthousand$ in the secondary NO_2- maximum (Casciotti, unpublished). If similar values hold for the primary NO_2- maximum in this dataset, bacterial nitrifier-denitrification

should produce N_2O with a $\delta^{18}O$ between 17 and 23‰. This is significantly lower than any of the signatures observed in the South Atlantic.

SP is probably the clearest proxy for the different N_2O production processes because it is the only signature that is thought to be independent of the isotopic composition of the substrate molecules (Toyoda et al., 2002). The SP signatures produced by bacterial ammonia-oxidizers (-10.7‰ for nitrifier-denitrification to +36.3‰ for nitrification (Sutka et al., 2004; Frame and Casciotti, 2010)) bracket the SP values observed in the deep concentration maximum and the shallow isotopic minimum. If a similar range applies to the marine N_2O sources, then nitrifier-denitrification produces 60% of the Cluster A source, 52% of the Cluster H source, and 63% of the Cluster B source. The SP signatures are currently the only isotopic basis for attributing these N_2O sources to ammonia-oxidizers. However, nothing is known about the isotope effects of archaeal ammonia-oxidizers. If archaeal NH_3 oxidation proceeds via some intermediate other than NH_2OH, any N_2O produced during this reaction may have significantly different N, O, and SP signatures.

Denitrifying bacteria can switch rapidly from O_2 to NO_3^--based respiration when O_2 concentrations drop below a certain threshold ($\sim$5 μM). Although N_2O is an intermediate formed during complete NO_3^- reduction to N_2, after the switch to NO_3^- respiration, the activity of nitrous oxide reductase lags behind the other enzymes in the respiratory NO_3^- reduction chain, releasing N_2O into the environment without further reduction (Firestone and Tiedje, 1979). Suboxic and hypoxic regions that experience sporadic O_2 injections are particularly favorable for this type of N_2O production (Naqvi et al., 2000). Moreover, it has been hypothesized that rapid decay of organic matter in low-O_2 environments can provide anoxic microenvironments that support denitrification even when ambient O_2 concentrations are too high for water-column denitrification to occur (Yoshida et al., 1989).

Three mechanisms set the range of $\delta^{18}O$-N_2O values produced by denitrification (summarized in Table 4). The first, normal kinetic isotope effects, have been reported for oxygen and nitrogen by Granger et al (2006) and Barford et al (1999) during NO_3^- consumption by denitrification (for *Paracoccus aureofaciens* $^{18}\epsilon_{NO_3^-} = 22$‰ and $^{15}\epsilon_{NO_3^-} = 23.5$‰, for

Paracoccus denitrificans $^{15}\epsilon_{NO_3^-} = 28.6‰$). This results in production of N_2O that is isotopically lighter than the substrate NO_3^- (Casciotti et al., 2002). The second is a large "branching" isotope effect ($^{18}\epsilon_{NO_2^-} = 40‰$) that produces N_2O that is ^{18}O-enriched relative to the substrate NO_3^-. A branching isotope effect also applies during NO_2^- reduction to N_2O, but it is significantly lower ($^{18}\epsilon_{NO_2^-} = 10‰$ Casciotti et al. (2007)). The branching effect occurs when light oxygen atoms are preferentially removed from the substrate NO_3^- or NO_2^- and transferred to H_2O (Casciotti and McIlvin, 2007). In an open system, the net effect of the branching isotope effect and the fully expressed kinetic isotope effect should be $+18‰$. At the other extreme, in a closed system, only the branching isotope effect will be expressed ($+40‰$). The $\delta^{18}O$ of thermocline NO_3^- was between 2 and 3‰, so that the $\delta^{18}O$ of N_2O produced by denitrification of this NO_3^- would have fallen between 20‰ and 43‰, depending on the system's degree of closure with respect to NO_3^-. There is no branching isotope effect for the nitrogen atoms of NO_3^- because they are bonded together rather than removed during the reduction process. Therefore, the $\delta^{15}N$-N_2O produced by NO_3^- reduction will always be at least as light as the substrate NO_3^- and depleted up to 23.5‰ in an open, steady-state system. The highest observed $\delta^{15}N$-NO_3^- values in the thermocline of the northern transect were about 5 to 7‰ in (Figure 13b), so that N_2O produced by NO_3- reduction would have a $\delta^{15}N$ of $+5$- $-16.5‰$. The values of $\delta^{15}N^{bulk}$-N_2O and $\delta^{18}O$-N_2O in Clusters A, B, and H are both consistent with closed system denitrification (a $+40‰$ O isotope effect and a 0‰ N isotope effect). Coastal sediments and large particles could provide closed systems for denitrification. However, denitrifiers produce N_2O with much lower SP signatures than those observed (SP denitrification = -5‰ (Toyoda et al., 2005)).

Denitrifiers can also consume N_2O, reducing it to N_2 and completing the NO_3^- reduction pathway. N_2O consumption is highly fractionating, raising the $\delta^{15}N^{bulk}$-N_2O, $\delta^{18}O$-N_2O, and SP values of the residual N_2O. During consumption, the ratio of isotope effects for SP and $\delta^{18}O$-N_2O is 1:2.2 (Ostrom et al., 2007). The South Atlantic data have comparatively low isotopic signatures and lie off the 1:2.2 line (Figure 12) so it is unlikely that this process dominates their distribution. The combined effects of steady-state production and consumption was observed for *P. dentirificans* cultures whose net N_2O production was

only 15‰ lighter than the starting NO_3^-, rather than 28.6‰ lighter (Barford et al., 1999; Granger et al., 2006). These measurements were made in the presence of very low O_2 concentrations (0 to $1\mu M$) that allowed N_2O reduction to proceed at the same rate as N_2O production. Dissolved O_2 concentrations were comparatively high during the cruise, never dropping below $19\mu M$. It is possible but seems unlikely that consumption by denitrifcation was important at any of the open ocean stations. Consumption of N_2O by water column denitrification is typically only observed in the permanent anoxic zones of the major ODZs (Cohen and Gordon, 1978). However, sedimentary denitrification could provide a stable, anoxic environment that would allow consumption of N_2O diffusing in from the water-column. Furthermore, water exported from the Southern Ocean may contain some N_2O influenced by biological processes in the major ODZs.

4.9. NO_2^-, NO₃−, and nitrifier-denitrification.

The isotopic signatures observed of the shallow South Atlantic N_2O sources are ambiguous because some of them point to a nitrification and nitrifier-denitrification source while others point to a sedimentary denitrification source. However, the NO_2^- concentration data support a nitrifier-denitrification source while the NO_3^- concentration data suggest that sedimentary denitrification is not responsible. The primary NO_2^- maxima at the base of the euphotic zone were located at nearly the same depths as the shallow SP minimum in the outer subequatorial gyre stations and also in the AG (Figure 14a-b). They also correspond with the depth of the base of the euphotic zone (Figure 15a) and the base of the thermocline (Figure 15b). The formation of the primary NO_2^- maximum has been attributed to differences in the degree of photo-inhibition of ammonia-oxidizers versus nitrite-oxidizers, which slows surface NO_2^- oxidation relative to ammonia oxidation, allowing NO_2^- to accumulate (Olson, 1981). This suggests that nitrifiers are responsible for producing the N_2O in the shallow isotopic minimum. In contrast, $NO_3^- + NO_2^-$ concentrations remain high throughout the watercolumn below the surface at all stations, suggesting that NO_3^- consumption by denitrifiers is not important.

5. Conclusions

A large range of N_2O isotopic signatures were observed over different depths and between the more oligotrophic and eutrophic zones of the cruise track. The deep signatures (600-800m) were dominated by the Southern Ocean which mixes and redistributes subsurface N_2O from all of the major ocean basins. Based on its isotopic composition, half of the N_2O in the Southern Ocean is exported there from the major ODZs and the other half is from a combined nitrification/nitrifier-denitrification source. The SP values of the nitrification/nitrifier-denitirifcation source indicate that 50-60% of it is from nitrifier-denitrification. Long-term changes in marine N_2O production and isotopic composition will probably appear first in the Southern Ocean while short term cycles such as seasonal blooms and upwelling events probably produce isotopically light N_2O with a low SP, that escapes directly from the top of the thermocline and the surface waters.

6. Acknowledgments

References

Altabet, M. A., Pilskaln, C., Thunell, R., Pride, C., Sigman, D., Chavez, F., and Francois, R. (1999). The nitrogen isotope biogeochemistry of sinking particles from the margin of the eastern north pacific. *Deep-Sea Research I*, 46:655-679.

Barford, C. C., Montoya, J., Altabet, M. A., and Mitchell, R. (1999). Steady-state nitrogen isotope effects of n2 and n2o production in *Paracoccus denitrificans*. *Applied and Environmental Microbiology*, 65(3):989–994.

Bohlke, J. K., Smith, R. L., and Hannon, J. E. (2007). Isotopic analysis of n and o in nitrite and nitrate by sequential selective bacterial reduction to N_2O. *Analytical Chemistry*, 79:5888–5895.

Boontanon, N., Watanabe, S., Odate, T., and Yoshida, N. (2010). Production and consumption mechanisms of N_2O in the southern ocean revealed from its isotopomer ratios. *Biogeosciences Discussions*, 7:7821–7848.

Bosley, K. T. (1991). *A cyclonic gyre in the Eastern Tropical South Atlantic*. PhD thesis, Columbia University.

Bourbonnais, A., Lehmann, M. F., Waniek, J. J., and Schulz-Bull, D. E. (2009). Nitrate isotope anomalies reflect N_2 fixation in the azores front region (subtropical ne atlantic). *Journal of Geophysical Research*, 114(C03003):doi:10.1029/2007JC004617.

Brea, S., Alvarez-Salgado, X. A., Alvarez, M., Perez, F. F., Memery, L., Mercier, H., and Messias, M. J. (2004). Nutrient mineralization rates and ratios in the eastern south atlantic. *Journal of Geophysical Research*, 109(C05030):doi:10.1029/2003JC002051.

Cantrell, C. A., Shetter, R. E., and Calvert, J. G. (1994). Branching ratios for the o(^{1}D) + N_2O reaction. *Journal of Geophysical Research*, 99(D2):3739–3743.

Casciotti, K. L., Bohlke, J. K., McIlvin, M., Mroczkowski, S. J., and Hannon, J. E. (2007). Oxygen isotopes in nitrite: analysis, calibration, and equilibration. *Analytical Chemistry*, 79:2427–2436.

Casciotti, K. L. and McIlvin, M. R. (2007). Isotopic analyses of nitrate and nitrite from reference mixtures and application to eastern tropical north pacific waters. *Marine Chemistry*, 107:184–201.

Casciotti, K. L., Sigman, D. M., Hastings, M. G., Bohlke, J. K., and Hilkert, A. (2002). Measurements of the oxygen isotopic composition of nitrate in seawater and freshwater using the denitrifier method. *Analytical Chemistry*, 74:4905–4912.

Casciotti, K. L. and Ward, B. B. (2001). Dissimilatory nitrite reductase genes from autotrophic ammonia-oxidizing bacteria. *Applied and Environmental Microbiology*, 67(5):2213–2221.

Charpentier, J., Farias, L., and Pizarro, O. (2010). Nitrous oxide fluxes in the central and eastern south pacific. *Global Biogeochemical Cycles*, 24:doi:10.1029/2008GB003388.

Charpentier, J., Farias, L., Yoshida, N., Boontanon, N., and Raimbault, P. (2007). Nitrous oxide distribution and its origin in the central and eastern south pacific subtropical gyre. *Biogeosciences*, 4:729–741.

Cohen, Y. and Gordon, L. I. (1978). Nitrous oxide in the oxygen minimum of the eastern tropical north pacific: evidence for its consumption during denitrification and possible mechanisms for its production. *Deep-Sea Research*, 25:509–524.

Croteau, P., Atlas, E. L., Schauffler, S. M., Blake, D. R., Diskin, G. S., and Boering, K. A. (2010). Effect of local and regional sources on the isotopic composition of nitrous oxide in the tropical free troposphere and tropopause layer. *Journal of Geophysical Research*, 115:doi:10.1029/2009JD013117.

Dore, J. E., Popp, B. N., Karl, D. M., and Sansone, F. J. (1998). A large source of atmospheric nitrous oxide from subtropical north pacific surface waters. *Nature*, 396:63–66.

Firestone, M. K. and Tiedje, J. M. (1979). Temporal change in nitrous oxide and dinitrogen from denitrification following onset of anaerobiosis. *Applied and Environmental Microbiology*, 38(4):673–679.

Fofonoff, N. P. (1985). Physical properties of seawater: a new salinity scale and equation of state of seawater. *Journal of Geophysical Research*, 90(C2):3332–3342.

Frame, C. H. and Casciotti, K. L. (2010). Biogeochemical controls and isotopic signatures of nitrous oxide production by a marine ammonia-oxidizing bacterium. *Biogeosciences*, 7:2695–2709.

Freing, A., Wallace, D. W. R., Tanhua, T., Walter, S., and Bange, H. W. (2009). North Atlantic production of nitrous oxide in the context of changing atmospheric levels. *Global Biogeochemical Cycles*, 23(GB4015):doi:10.1029/2009GB003472.

Gordon, A. L. and Bosley, K. T. (1991). Cyclonic gyre in the tropical south atlantic. *Deep-Sea Research*, 38(Suppl. 1):S323–S343.

Granger, J., Sigman, D. M., Prokopenko, M. G., Lehmann, M. F., and Tortell, Philippe, D. (2006). A method of nitrite removal in nitrate N and O isotope analyses. *Limnology and Oceanography Methods*, 4:205–212.

Griffith, D. W. T., Parkes, S. D., Haverd, V., Paton-Walsh, C., and Wilson, S. R. (2009). Absolute calibration of the intramolecular site preference of ^{15}N fractionation in tropospheric N_2O by ft-ir spectroscopy. *Analytical Chemistry*, 81:2227–2234.

Gruber, N. and Sarmiento, J. L. (1997). Global patterns of marine nitrogen fixation and denitrification. *Global Biogeochemical Cycles*, 11(2):235–266.

Hanisco, T. F. and Kummel, A. C. (1993). State-resolved photodissociation of N_2O. *Journal of Physical Chemistry*, 97:7242–7246.

Hooper, A. B. and Terry, K. R. (1979). Hydroxylamine oxidoreductase of *Nitrosomonas* production of nitric oxide from hydroxylamine. *Biochimica et Biophysica Acta*, 571:12–20.

Kiddon, J., Bender, M. L., and Orchardo, J. (1993). Isotopic fractionation of oxygen by respiring marine organisms. *Global Biogeochemical Cycles*, 7:679–694.

Kim, K.-R. and Craig, H. (1990). Two-isotope characterization of N_2O in the pacific ocean and constraints on its origin in deep water. *Nature*, 347:58–61.

Kool, D. M., Wrage, N., Oenema, O., Dolfing, J., and van Groenigen, J. W. (2007). Oxygen exchange between (de)nitrification intermediates and H_2O and its implications for source determination of NO_3^- and N_2O: a review. *Rapid Communications in Mass Spectrometry*, 21:3569–3578.

Kuypers, M. M., Lavik, G., Woebken, D., Schmid, M., Fuchs, B. M., Amann, R., Jorgensen, B. B., and Jetten, M. S. M. (2005). Massive nitrogen loss from the benguela upwelling system through anaerobic ammonium oxidation. *Proceedings of the National Academy of Science*, 102(18):6478–6483.

Law, C. S. and Owens, N. J. P. (1990). Significant flux of atmospheric nitrous oxide from the northwest indian ocean. *Nature*, 346:826–828.

Levine, N. M., Bender, M. L., and Doney, S. C. (2009). The $\delta^{18}O$ of dissoved O_2 as a tracer of mixing and respiration in the mesopelagic ocean. *Global Biogeochemical Cycles*, 23:1–12.

Lueker, T. J., Walker, S. J., Vollmer, M. K., Keeling, R. K., Nevison, C. D., and Weiss, R. F. (2003). Coastal upwelling air-sea fluxes revealed in atmospheric observations of O_2/N_2, CO_2 and N_2O. *Geophysical Research Letters*, 30(6):doi:10.1029/2002GL016615.

Luz, B. and Barkan, E. (2005). The isotopic ratios $^{17}O/^{16}O$ and $^{18}O/^{16}O$ in molecular oxygen and their significance in biogeochemistry. *Geochimica et Cosmochimica Acta*, 69(5):1099–1110.

Mariotti, A., Germon, J. C., Hubert, P., Kaiser, P., Letolle, R., Tardieux, A., and Tardieux, P. (1981). Experimental determination of nitrogen kinetic isotope fractionation: some principles; illustration for the denitrification and nitrification processes. *Plant and Soil*, 62:413–430.

McIlvin, M. M. and Casciotti, K. L. (2010). Automated stable isotopic analysis of dissolved nitrous oxide at natural abundance levels. *Limnology and Oceanography Methods*.

Naqvi, S. W. A., Jayakumar, D. A., Narvekar, P. V., Naik, H., Sarma, V. V. S. S., D'Souza, W., Joseph, S., and George, M. D. (2000). Increased marine production of N_2O due to intensifying anoxia on the indian continental shelf. *Nature*, 408:346–349.

Naqvi, S. W. A., Naik, H., Pratihary, A., D'Souza, W., Narvekar, P. V., Jayakumar, D. A., Devol, A. H., Yoshinari, T., and Saino, T. (2006). Coastal versus open-ocean denitrification in the arabian sea. *Biogeosciences*, 3:621–633.

Naqvi, S. W. A. and Noronha, R. J. (1991). Nitrous oxide in the arabian sea. *Deep-Sea Research*, 38(7):871–890.

Naqvi, S. W. A., Yoshinari, T., Jayakumar, D. A., Altabet, M. A., Narvekar, P. V., Devol, A. H., Brandes, J. A., and Codispoti, L. A. (1998). Budgetary and biogeochemical implications of n2o isotope signatures in the arabian sea. *Nature*, (462-464).

Nevison, C., Butler, J. H., and Elkins, J. W. (2003). Global distribution of N_2O and the ΔN_2O - aou yield in the subsurface ocean. *Global Biogeochemical Cycles*, 17(4):30-1–18.

117

Nevison, C. D., Lueker, T. J., and Weiss, R. F. (2004). Quantifying the nitrous oxide source from coastal upwelling. *Global Biogeochemical Cycles*, 18(GB1018):doi:10.1029/2003GB002110.

Nevison, C. D., Weiss, R. F., and Erickson III, D. J. (1995). Global oceanic emissions of nitrous oxide. *Journal of Geophysical Research*, 100(C8):15809–15820.

Noble, A. E., Saito, M. A., Lamborg, C., Lam, Phoebe annd Ohnemus, D., Goepfert, T. J., Frame, C., Casciotti, K., and Jennings, J. (2011). Basin-scale inputs of cobalt, iron, and manganese from the benguela-angola front into the south atlantic ocean. *Limnology and Oceanography*, submitted.

Olson, R. J. (1981). Differential photoinhibition of marine nitrifying bacteria-a possible mechanism for the formation of the primary nitrite maximum. *Journal of Marine Research*, 39(2):227–238.

Ostrom, N. E., Pitt, A., Ostrom, P. H., Grandy, A. S., Huizinga, K. M., and Robertson, G. P. (2007). Isotopologue effects during N_2O reduction in soils and in pure cultures of denitrifiers. *Journal of Geophysical Research*, 112:1–12.

Ostrom, N. E., Russ, M. E., Popp, B., Rust, T. M., and Karl, D. M. (2000). Mechanisms of nitrous oxide production in the subtropical north pacific based on determinations of the isotopic abundances of nitrous oxide and di-oxygen. *Chemosphere-Global Change Science*, 2:281–290.

Poole, R. and Tomczak, M. (1999). Optimum multiparameter analysis of the water mass structure in the atlantic ocean thermocline. *Deep-Sea Research I*, 46:1895–1921.

Popp, B. N., Westley, M. B., Toyoda, S., Miwa, T., Dore, J. E., Yoshida, N., Rust, T. M., Sansone, F. J., Russ, M. E., Ostrom, N. E., and Ostrom, P. H. (2002). Nitrogen and oxygen isotopomeric constraints on the origins and sea-to-air flux of N_2O in the oligotrophic subtropical north pacific gyre. *Global Biogeochemical Cycles*, 16(4):12-1-10.

Poth, M. and Focht, D. (1985). [15]N kinetic analysis of N_2O production by *Nitrosomonas europaea*: an examination of nitrifier denitrification. *Applied and Environmental Microbiology*, 49(5):1134–1141.

Preston, K. F. and Barr, R. F. (1971). Primary processes in the photolysis of nitrous oxide. *The Journal of Chemical Physics*, 54(8):3347–3348.

Quay, P. D., Emerson, S., Wilbur, D. O., and Stump, C. (1993). The $\delta^{18}O$ of dissolved O_2 in the surface waters of the subarctic pacific: a tracer of biological productivity. *Journal of Geophysical Research*, 98(C5):8447–8458.

Ritchie, G. A. F. and Nicholas, D. J. D. (1972). Identification of the sources of nitrous oxide produced by oxidative and reductive processes in *Nitrosomonas europaea*. *Biochemistry Journal*, 126:1181–1191.

Shaw, L. J., Nicol, G. W., Smith, Z., Fear, J., Prosser, J., and Baggs, E. M. (2006). *Nitrosospira* spp. can produce nitrous oxide via a nitrifier denitrification pathway. *Environmental Microbiology*, 8(2):214–222.

Sigman, D. M., Casciotti, K. L., Andreani, M., Barford, C., Galanter, M., and Bohlke, J. K. (2001). A bacterial method for the nitrogen isotopic analysis of nitrate in seawater and freshwater. *Analytical Chemistry*, 73:4145–4153.

Solomon, S., Qin, M., Manning, M., Chen, Z., Marquis, M., Averyt, K., Tignor, M., and Miller, H. (2007). *Climate Change 2007: The Physical Science Basis*. Cambridge University Press, New York, NY, USA.

Sowers, T., Rodebaugh, A., Yoshida, N., and Toyoda, S. (2002). Extending records of the isotopic composition of atmospheric N_2O back to 1800 a.d. from air trapped in snow at the south pole and the greenland ice sheet project ii ice core. *Global Biogeochemical Cycles*, 16(4):doi:10.1029/2002GB001911.

Stramma, L. and England, M. (1999). On the water masses and mean circulation of the south atlantic ocean. *Journal of Geophysical Research*, 104(C9):20863–20883.

Stramma, L., Johnson, G. C., Sprintall, J., and Mohrholz, V. (2008). Expanding oxygen-minimum zones in the tropical oceans. *Science*, 320:655–658.

Stramma, L. and Schott, F. (1999). The mean flow field of the tropical atlantic ocean. *Deep-Sea Research II*, 46:279–303.

Suntharalingam, P. and Sarmiento, J. L. (2000). Factors governing the oceanic nitrous oxide distribution: simulations with an ocean general circulation model. *Global Biogeochemical*

Cycles, 14(1):429–454.

Sutka, R. L., Ostrom, N. E., Ostrom, P. H., Gandhi, H., and Breznak, J. A. (2003). Nitrogen isotopomer site preference of N_2O produced by *Nitrosomonas europaea* and *Methylococcus capsulatus* bath. *Rapid Communications in Mass Spectrometry*, 17:738–745.

Sutka, R. L., Ostrom, N. E., Ostrom, P. H., Gandhi, H., and Breznak, J. A. (2004). Nitrogen isotopomer site preference of N_2O produced by *Nitrosomonas europaea* and *Methylococcus capsulatus* bath. *Rapid Communications in Mass Spectrometry*, 18:1411–1412.

Toyoda, S., Mutobe, H., Yamagishi, H., Yoshida, N., and Tanji, Y. (2005). Fractionation of N_2O isotopomers during production by denitrifier. *Soil Biology and Biochemistry*, 37:1535–1545.

Toyoda, S., Yoshida, N., Miwa, T., Matsui, Y., Yamagishi, H., and Tsunogai, U. (2002). Production mechanism and global budget of N_2O inferred from its isotopomers in the western north pacific. *Geophysical Research Letters*, 29(3):7-1–4.

van Bennekom, A. J. and Berger, G. W. (1984). Hydrography and silica budget of the angola basin. *Netherlands Journal of Sea Research*, 17(2-4):149–200.

Walker, C. B., de la Torre, J. R., Klotz, M. G., H, U., Pinel, N., Arp, D. J., Brochier-Armanet, C., Chain, P. S. G., Chan, P. P., Gollabgir, A., and Hemp (2010). *Nitrosopumilus maritimus* genome reveals unique mechanisms for nitrification and autotrophy in globally distributed marine crenarchaea. *Proceedings of the National Academy of Science*, 107(19):8818–8823.

Walter, S., Bange, H. W., Breitenbach, U., and Wallace, D. W. R. (2006). Nitrous oxide in the north atlantic ocean. *Biogeosciences*, 3:607–619.

Westley, M. B., Yamagishi, H., Popp, B. N., and Yoshida, N. (2006). Nitrous oxide cycling in the black sea inferred from stable isotope and isotopomer distributions. *Deep-Sea Research-II*, 53:1802–1816.

Yamagishi, H., Westley, M. B., Popp, B., Toyoda, S., Yoshida, N., Watanabe, S., and Koba, K. (2007). Role of nitrification and denitrification on the nitrous oxide cycle in the eastern tropical north pacific and gulf of california. *Journal of Geophysical Research*, 112(G02015):doi:10.1029/2006JG000227.

Yoshida, N. (1988). ^{15}N-depleted N_2O as a product of nitrification. *Nature*, 335:528–529.

Yoshida, N., Morimoto, H., Hirano, M., Koike, I., Matsuo, S., Wada, E., Saino, T., and Hattori, A. (1989). Nitrification rates and ^{15}N abundances of N_2O and NO_3^- in the western north pacific. *Nature*, 342:895–897.

Yoshida, N. and Toyoda, S. (2000). Constraining the atmospheric N_2O budget from intramolecular site preference in N_2O isotopomers. *Nature*, 405:330–334.

Yoshinari, T., Altabet, M. A., Naqvi, S. W. A., Codispoti, L., Jayakumar, A., Kuhland, M., and Devol, A. (1997). Nitrogen and oxygen isotopic composition of n2o from suboxic waters of the eastern tropical north pacific and the arabian sea-measurement by continuous-flow isotope-ratio monitoring. *Marine Chemistry*, 56:253–264.

Yung, Y. L. and Miller, C. E. (1997). Isotopic fractionation of stratospheric nitrous oxide. *Science*, 278:1778–1780.
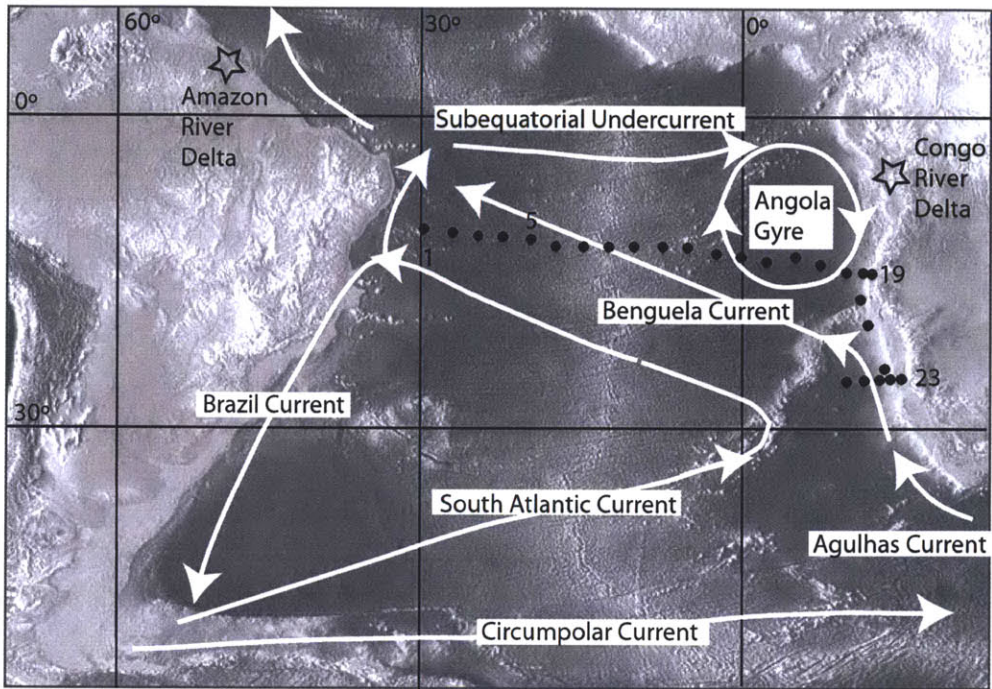
FIGURE 1. The CoFeMUG cruise track (circles) overlaid on the surface and shallow-subsurface current structure of the South Atlantic (Stramma and Schott 1999, Stramma and England 1999). Salinity, temperature, O_2, and nutrient data were collected from stations 1-27. N_2O was collected from stations 5-27 (the 23 easternmost stations).
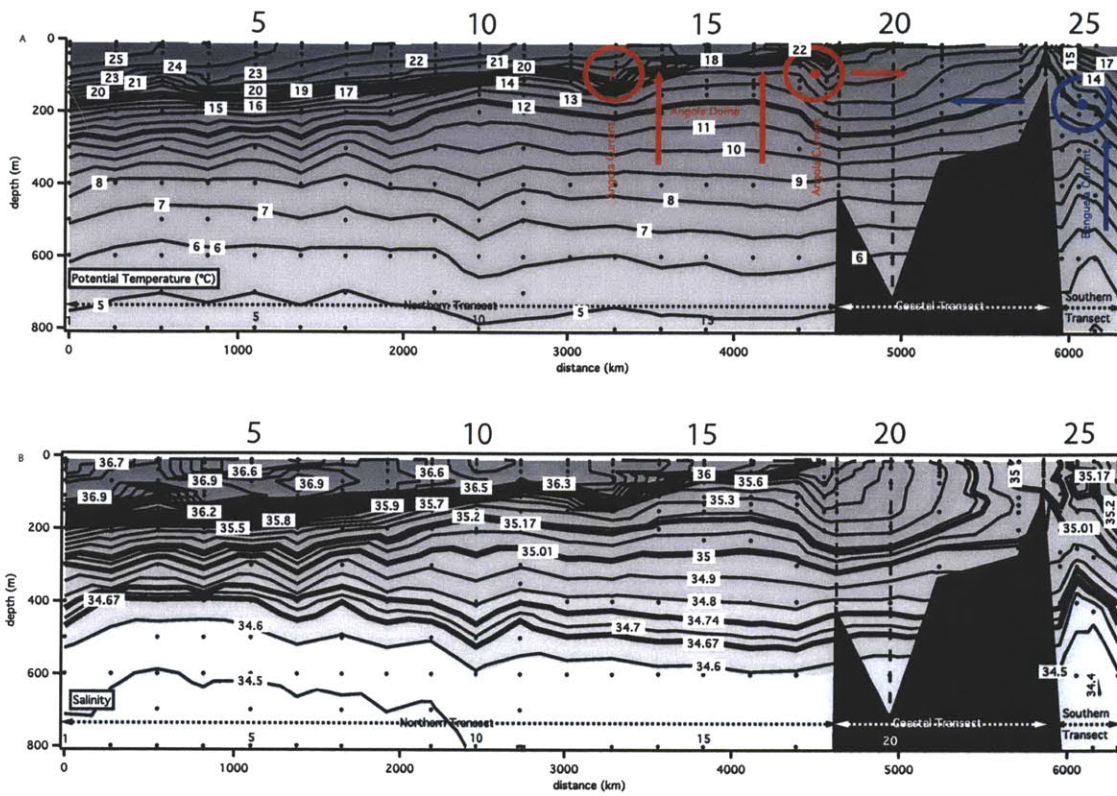
FIGURE 2. Potential temperature (a) and salinity (b). The number of every fifth station is given at the top of each transect.

FIGURE 3. O_2 (a), $NO_3^- + NO_2^-$ (b), and N_2O concentrations. The number of every fifth station is given at the top of each transect.

124
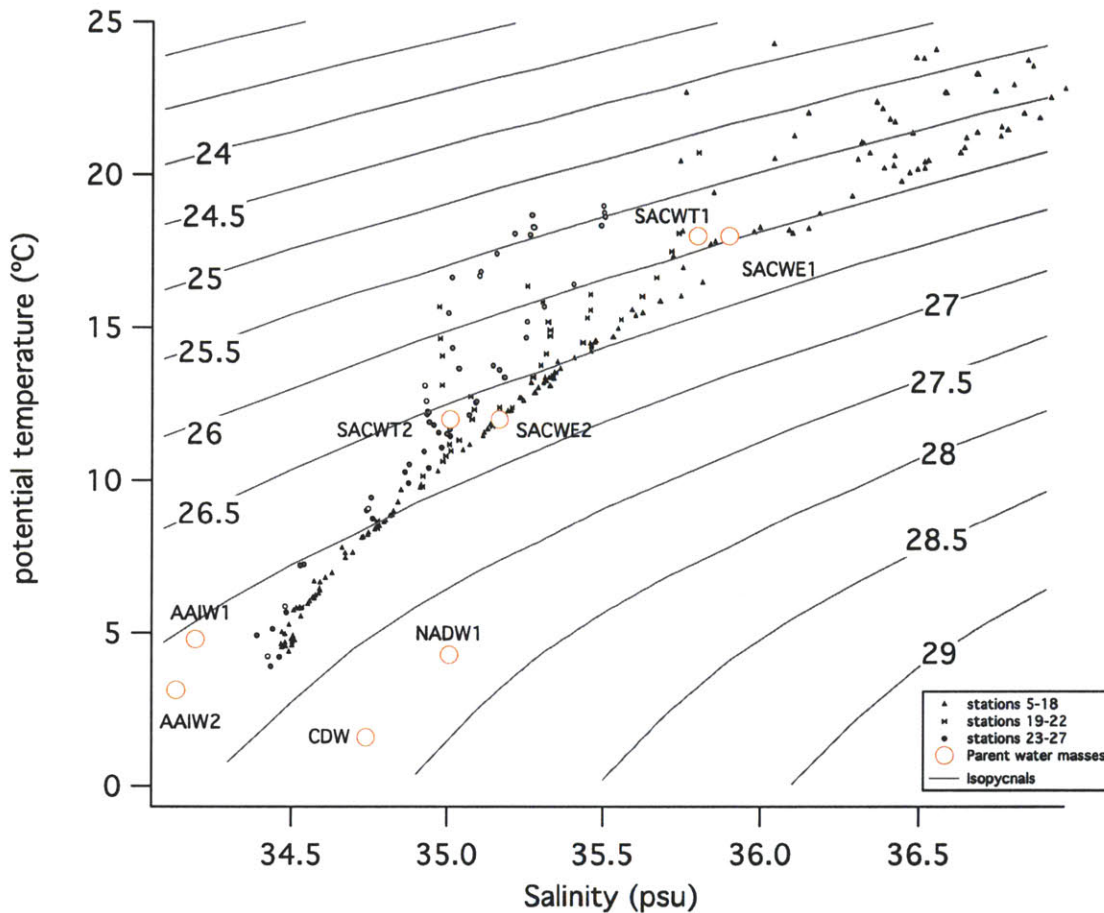
FIGURE 4. Salinity versus potential temperature for depths shallower than 800-1000m. Isopycnal lines were calculated using the equation of state for seawater of Fofonoff (1985). Markers are shaded according to N_2O concentration, with darker markers indicating more N_2O. The end-member temperatures and salinities of the relevant parent watermasses are also plotted: Antarctic Intermediate Water (AAIW), Circumpolar Deep Water (CDW), light South Atlantic Central Water (SACW1), and dense South Atlantic Central Water (SACW2). Following the analysis of Brea et al (2004), the two types of SACW are further subdivided into equatorial (SACWE) and tropical components (SACWT), each with slightly more saline equatorial components. The densest water samples were mixtures of Antarctic Intermediate Water (AAIW) and Circumpolar Deepwater (CDW). North Atlantic Deep Water (NADW) is also important watermass crossing in the South Atlantic but its contribution at the depths sampled is negligible (Stramma and England, 1999).

FIGURE 5. N₂O isotope distributions for the northern, coastal, and southern transects.

A
n = 38
depth = 169 ± 56 m
$\delta^{15}N\alpha-N_2O = 9.2 \pm 0.7‰$
$\delta^{15}N\beta-N_2O = 1.3 \pm 0.4‰$
$\delta^{18}O-N_2O = 38.8 \pm 0.5‰$
SP = 7.9 ± 1.0
$\delta^{15}Nbulk-N_2O = 5.2 \pm 0.2‰$
potential temperature = 13 ± 1.6 °C
salinity = 35.3 ± 0.2 psu
$N_2O = 36.2 \pm 7.3$ nM
$O_2 = 61 \pm 39$ µM
$NO_3^- + NO_2^- = 28 \pm 6$ µM

B
n = 5
depth = 58 ± 13 m
$\delta^{15}N\alpha-N_2O = 7.6 \pm 0.4‰$
$\delta^{15}N\beta-N_2O = 1.1 \pm 0.1‰$
$\delta^{18}O-N_2O = 38.2 \pm 0.4‰$
SP = 6.5 ± 0.5‰
$\delta^{15}Nbulk-N_2O = 4.4 \pm 0.1$
potential temperature = 15.9 ± 1.4 °C
salinity = 35.6 ± 0.2 psu
$N_2O = 30.4 \pm 3.0$ nM
$O_2 = 103 \pm 52$ µM
$NO_3^- + NO_2^- = 26 \pm 2$ µM

C
n = 4
depth = 325 ± 65 m
$\delta^{15}N\alpha-N_2O = 10.3 \pm 0.4‰$
$\delta^{15}N\beta-N_2O = 0.9 \pm 0.2‰$
$\delta^{18}O-N_2O = 40.6 \pm 0.4‰$
SP = 9.4 ± 0.5
$\delta^{15}Nbulk-N_2O = 5.6 \pm 0.2‰$
potential temperature = 10.0 ± 1.0 °C
salinity = 34.9 ± 0.1 psu
$N_2O = 39.3 \pm 5.9$ nM
O2 = 45 ± 21 µM
$NO_3^- + NO_2^- = 35 \pm 5$ µM

D
n = 9
depth = 34 ± 30 m
$\delta^{15}N\alpha-N_2O = 15.1 \pm 0.2‰$
$\delta^{15}N\beta-N_2O = -1.5 \pm 0.2‰$
$\delta^{18}O-N_2O = 45.3 \pm 0.3‰$
SP = 16.6 ± 0.3‰
$\delta^{15}Nbulk-N_2O = 6.8 \pm 0.1‰$
potential temperature = 20.8 ± 1.5 °C
salinity = 36.2 ± 0.5 psu
$N_2O = 7.5 \pm 0.5$ nM
$O_2 = 226 \pm 11$ µM
$NO_3^- + NO_2^- = 1 \pm 2$ µM

E
n = 7
depth = 56 ± 26 m
$\delta^{15}N\alpha-N_2O = 14.0 \pm 0.2‰$
$\delta^{15}N\beta-N_2O = -1.0 \pm 1.0‰$
$\delta^{18}O-N_2O = 44.6 \pm 0.4‰$
SP 14.9 ± 1.1‰
$\delta^{15}Nbulk-N_2O = 6.5 \pm 0.5‰$
potential temperature = 19.9 ± 1.8 °C
salinity = 36.2 ± 0.6 psu
$N_2O = 8.6 \pm 0.9$ nM
$O_2 = 229 \pm 17$ µM
$NO_3^- + NO_2^- = 4 \pm 3$ µM

F
n = 11
depth = 42 ± 30 m
$\delta^{15}N\alpha-N_2O = 14.0 \pm 0.3‰$
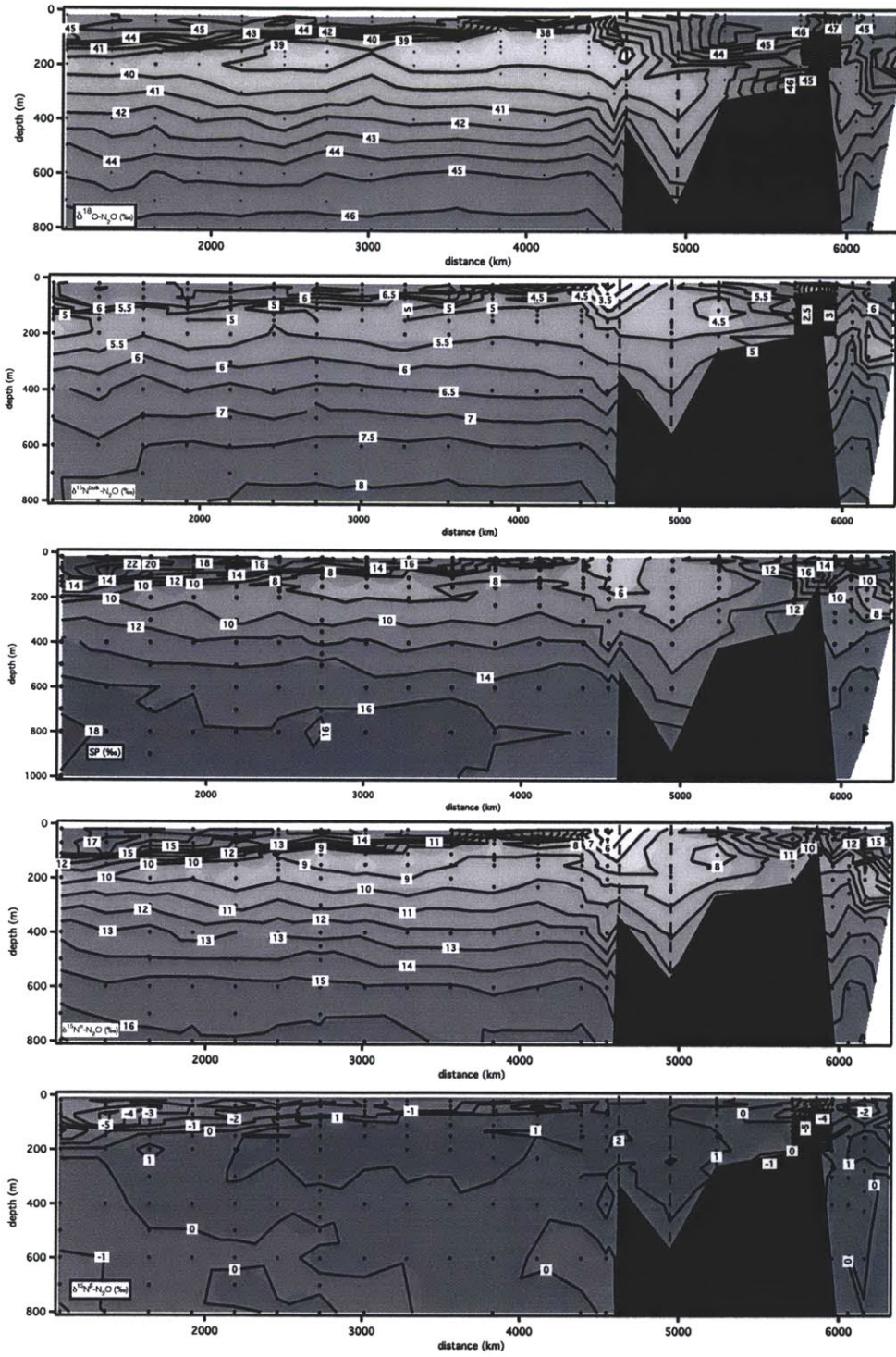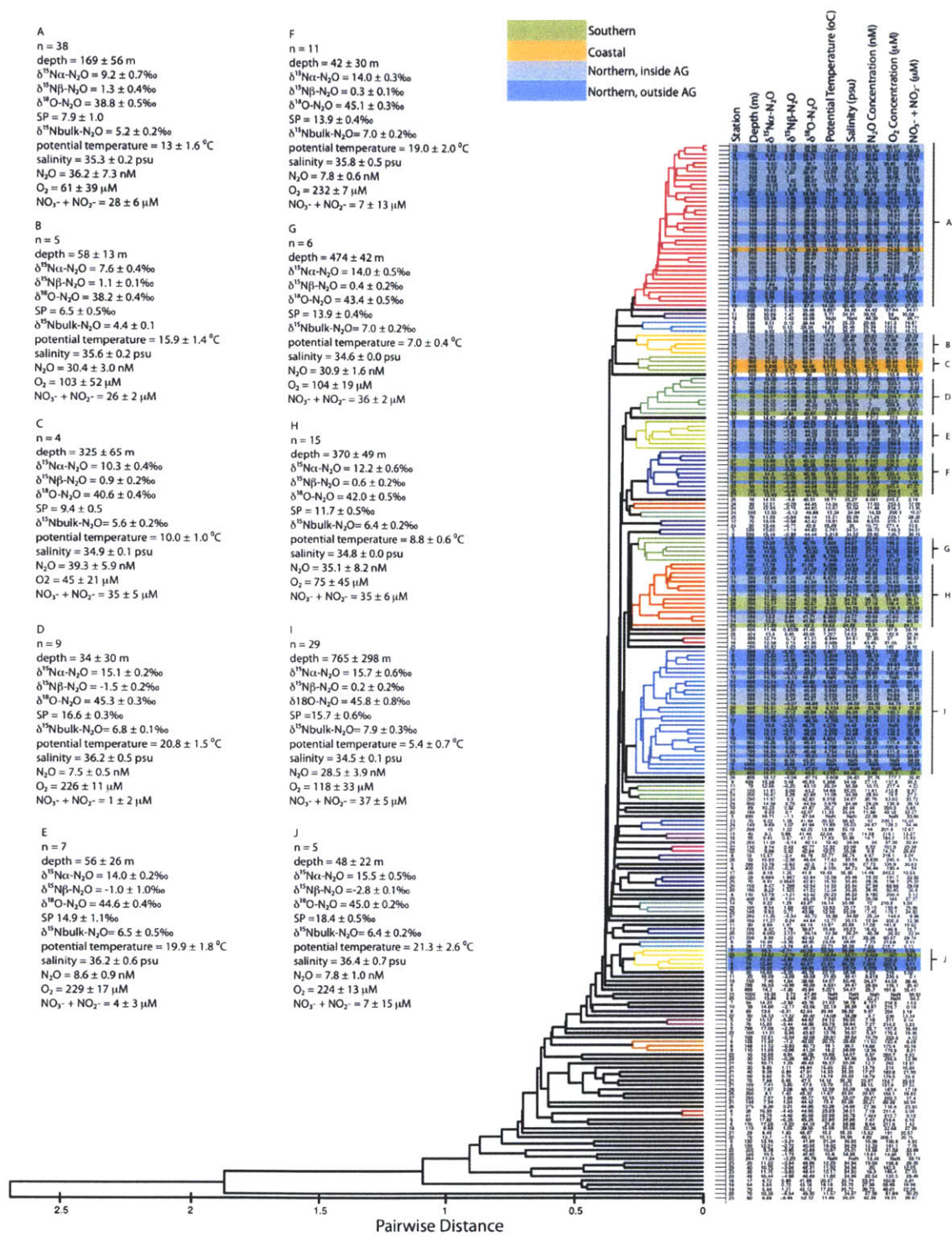$\delta^{15}N\beta-N_2O = 0.3 \pm 0.1‰$
$\delta^{18}O-N_2O = 45.1 \pm 0.3‰$
SP = 13.9 ± 0.4‰
$\delta^{15}Nbulk-N_2O = 7.0 \pm 0.2‰$
potential temperature = 19.0 ± 2.0 °C
salinity = 35.8 ± 0.5 psu
$N_2O = 7.8 \pm 0.6$ nM
$O_2 = 232 \pm 7$ µM
$NO_3^- + NO_2^- = 7 \pm 13$ µM

G
n = 6
depth = 474 ± 42 m
$\delta^{15}N\alpha-N_2O = 14.0 \pm 0.5‰$
$\delta^{15}N\beta-N_2O = 0.4 \pm 0.2‰$
$\delta^{18}O-N_2O = 43.4 \pm 0.5‰$
SP = 13.9 ± 0.4‰
$\delta^{15}Nbulk-N_2O = 7.0 \pm 0.2‰$
potential temperature = 7.0 ± 0.4 °C
salinity = 34.6 ± 0.0 psu
$N_2O = 30.9 \pm 1.6$ nM
$O_2 = 104 \pm 19$ µM
$NO_3^- + NO_2^- = 36 \pm 2$ µM

H
n = 15
depth = 370 ± 49 m
$\delta^{15}N\alpha-N_2O = 12.2 \pm 0.6‰$
$\delta^{15}N\beta-N_2O = 0.6 \pm 0.2‰$
$\delta^{18}O-N_2O = 42.0 \pm 0.5‰$
SP = 11.7 ± 0.5‰
$\delta^{15}Nbulk-N_2O = 6.4 \pm 0.2‰$
potential temperature = 8.8 ± 0.6 °C
salinity = 34.8 ± 0.0 psu
$N_2O = 35.1 \pm 8.2$ nM
$O_2 = 75 \pm 45$ µM
$NO_3^- + NO_2^- = 35 \pm 6$ µM

I
n = 29
depth = 765 ± 298 m
$\delta^{15}N\alpha-N_2O = 15.7 \pm 0.6‰$
$\delta^{15}N\beta-N_2O = 0.2 \pm 0.2‰$
$\delta 18O-N_2O = 45.8 \pm 0.8‰$
SP = 15.7 ± 0.6‰
$\delta^{15}Nbulk-N_2O = 7.9 \pm 0.3‰$
potential temperature = 5.4 ± 0.7 °C
salinity = 34.5 ± 0.1 psu
$N_2O = 28.5 \pm 3.9$ nM
$O_2 = 118 \pm 33$ µM
$NO_3^- + NO_2^- = 37 \pm 5$ µM

J
n = 5
depth = 48 ± 22 m
$\delta^{15}N\alpha-N_2O = 15.5 \pm 0.5‰$
$\delta^{15}N\beta-N_2O = -2.8 \pm 0.1‰$
$\delta^{18}O-N_2O = 45.0 \pm 0.2‰$
SP = 18.4 ± 0.5‰
$\delta^{15}Nbulk-N_2O = 6.4 \pm 0.2‰$
potential temperature = 21.3 ± 2.6 °C
salinity = 36.4 ± 0.7 psu
$N_2O = 7.8 \pm 1.0$ nM
$O_2 = 224 \pm 13$ µM
$NO_3^- + NO_2^- = 7 \pm 15$ µM

Southern
Coastal
Northern, inside AG
Northern, outside AG

Station
Depth (m)
$\delta^{15}N\alpha-N_2O$
$\delta^{15}N\beta-N_2O$
$\delta^{18}O-N_2O$
Potential Temperature (oC)
Salinity (psu)
N_2O Concentration (nM)
O_2 Concentration (nM)
$NO_3^- + NO_2^-$ (µM)

Pairwise Distance

FIGURE 6

127

Figure 6 (previous page). Dendrogram representing the hierarchical classification of N_2O samples based on their standardized $\delta^{15}N^{\alpha}$-N_2O and $\delta^{15}N^{\beta}$-N_2O, and $\delta^{18}O$-N_2O values. Data (n = 241) were paired hierarchically based on their covariances. Colored clusters have linkage values above the average value for the dendrogram. The cluster averages for other chemical parameters are indicated to the left of the tree.
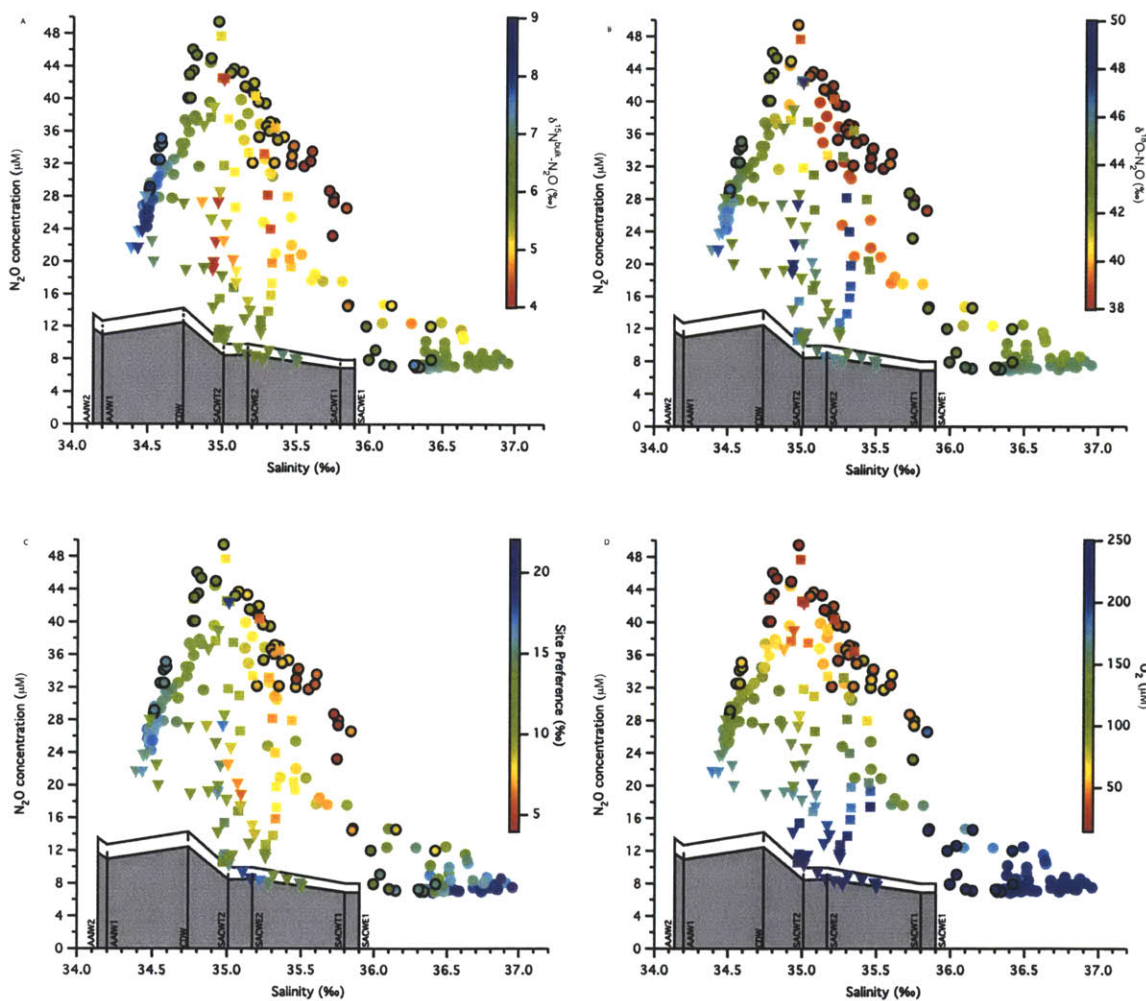

FIGURE 7. N_2O versus salinity. Data from the northern transect are circles, the coastal transect data are squares, and the southern transect data are triangles. Bold circles represent northern transect data from inside the AG. Data points are colored according to the $\delta^{15}N^{bulk}$-N_2O (a), $\delta^{18}O$-N_2O (b), and SP (c) of the N_2O. The salinities of the parent watermasses are taken from Brea et al. (2004). The atmospheric equilibrium N_2O concentrations for these parent watermasses are indicated for a 275 ppb atmosphere (gray) and 319 ppb atmosphere (white).
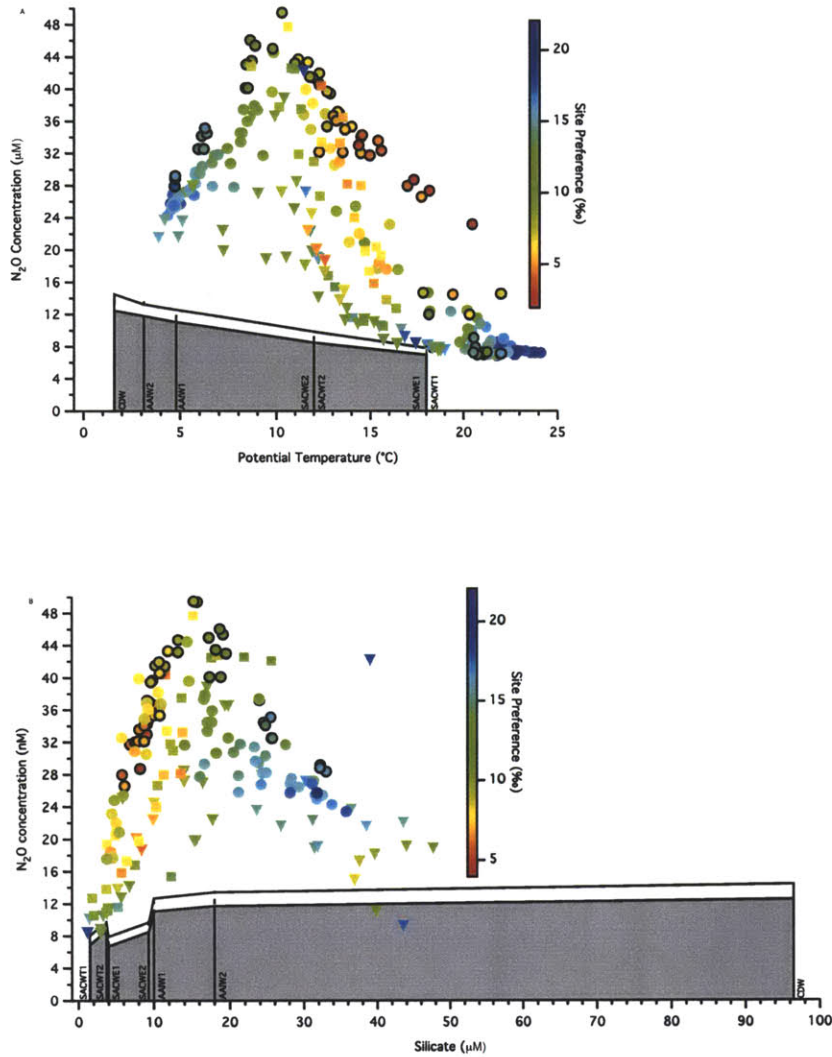
FIGURE 8. N_2O versus potential temperature (a) and silicate concentration (b). Data from the northern transect are circles, the coastal transect data are squares, and the southern transect data are triangles. Bold circles represent northern transect data from inside the AG. Color scales correspond to the SP values of the N_2O. The potential temperatures and silicate concentrations of each parent watermass are taken from Brea et al. (2004). The atmospheric equilibrium N_2O concentrations for these parent watermasses are indicated for a 275 ppb atmosphere (gray) and 319 ppb atmosphere (white).
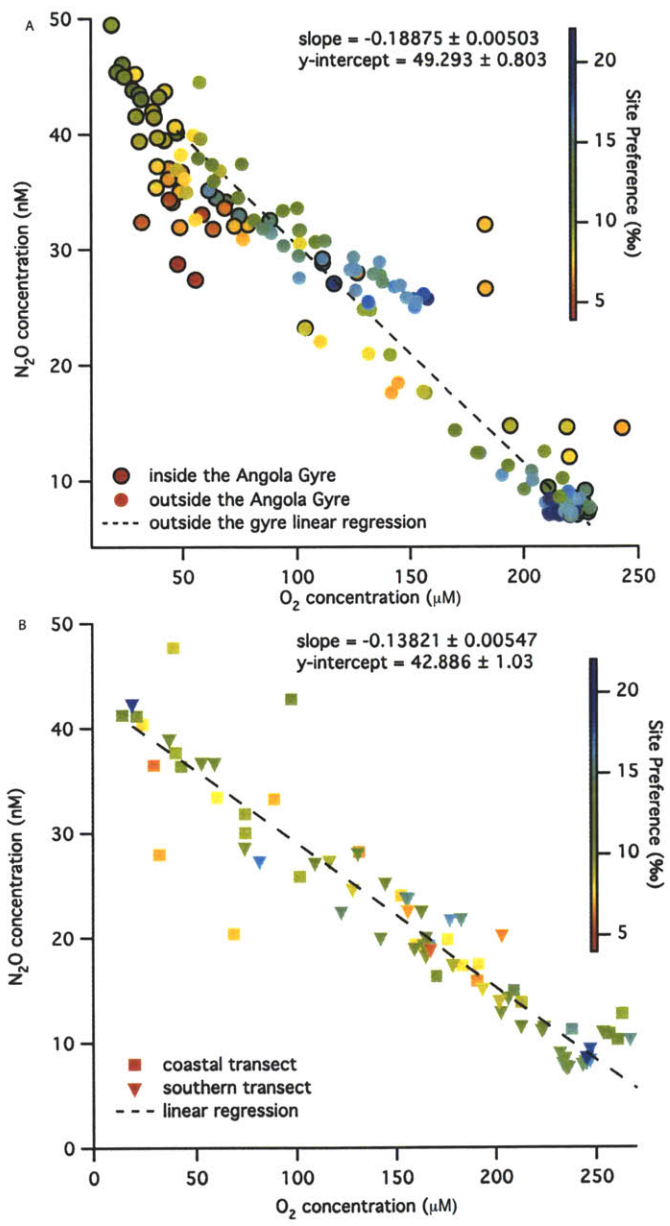
FIGURE 9. O_2 versus N_2O concentration in the northern transect outside and inside the Angola Gyre (a) and in the coastal and southern transects (b). All data in (a) are from the northern transect. The low-SP N_2O (less than 5‰) that is found only inside the AG falls off the regression line for data from outside the gyre. This suggests that N_2O with this signature is formed in the gyre and stays there until it ventilates to the atmosphere, making it one of the more important sources of N_2O to the atmosphere. In contrast, the O_2 and N_2O concentrations in (b) appear to be dominated by a single linear relationship.
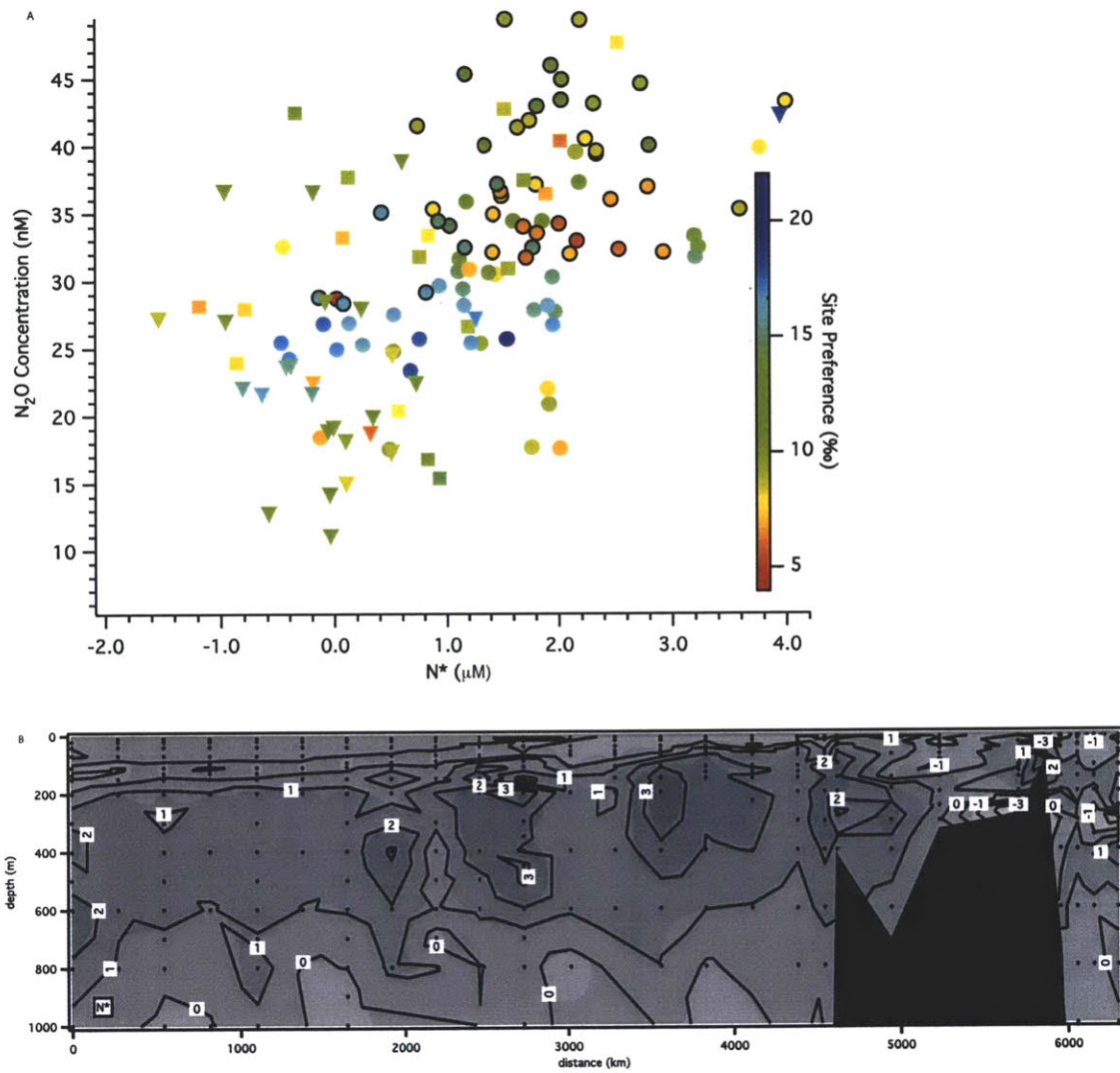
130

FIGURE 10. N* (μM) versus N_2O concentration for depths below the thermocline (a) and N* fields for the northern, coastal, and southern cruise transects (b).
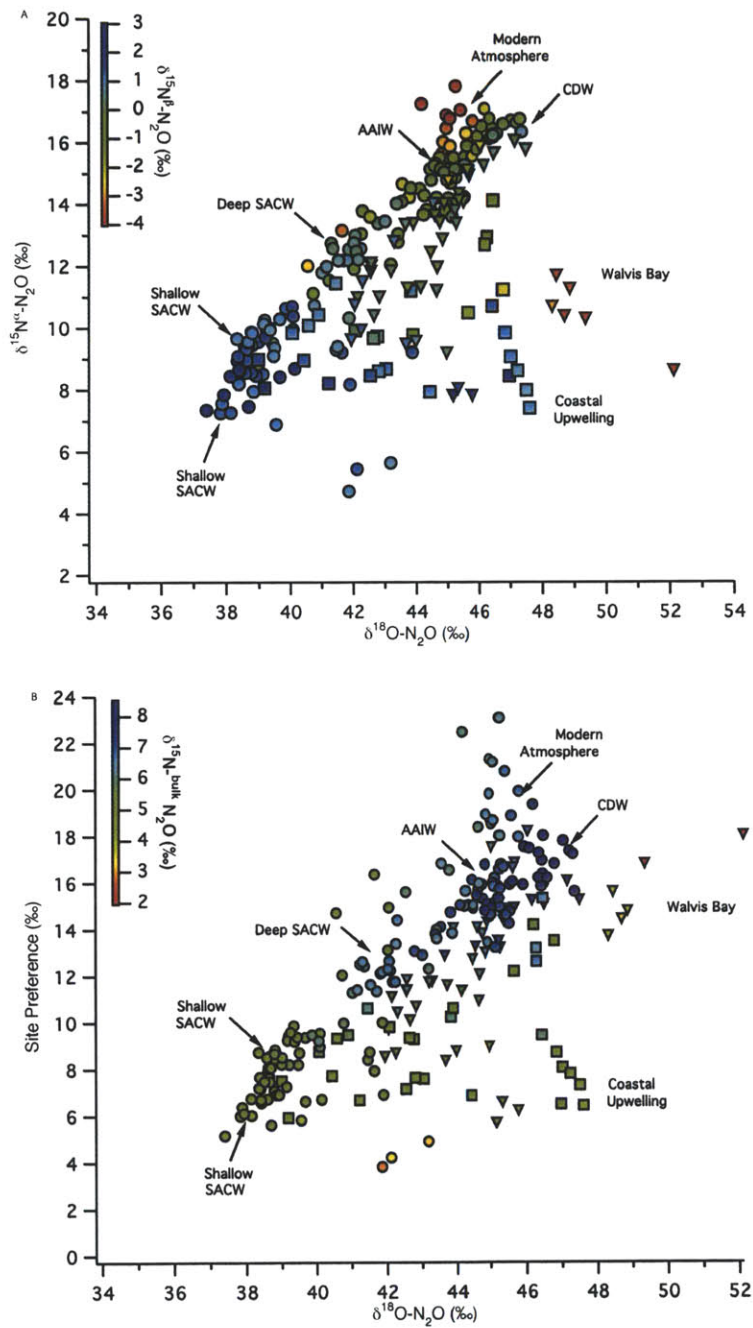
FIGURE 11. $\delta^{15}N^{\alpha}$-N_2O versus $\delta^{18}O$-N_2O (a), Site Preference versus $\delta^{18}O$-N_2O (b). Circles represent northern transect data, squares represent the coastal transect data, and triangles represent the southern transect data. Bold circles represent stations inside the AG.
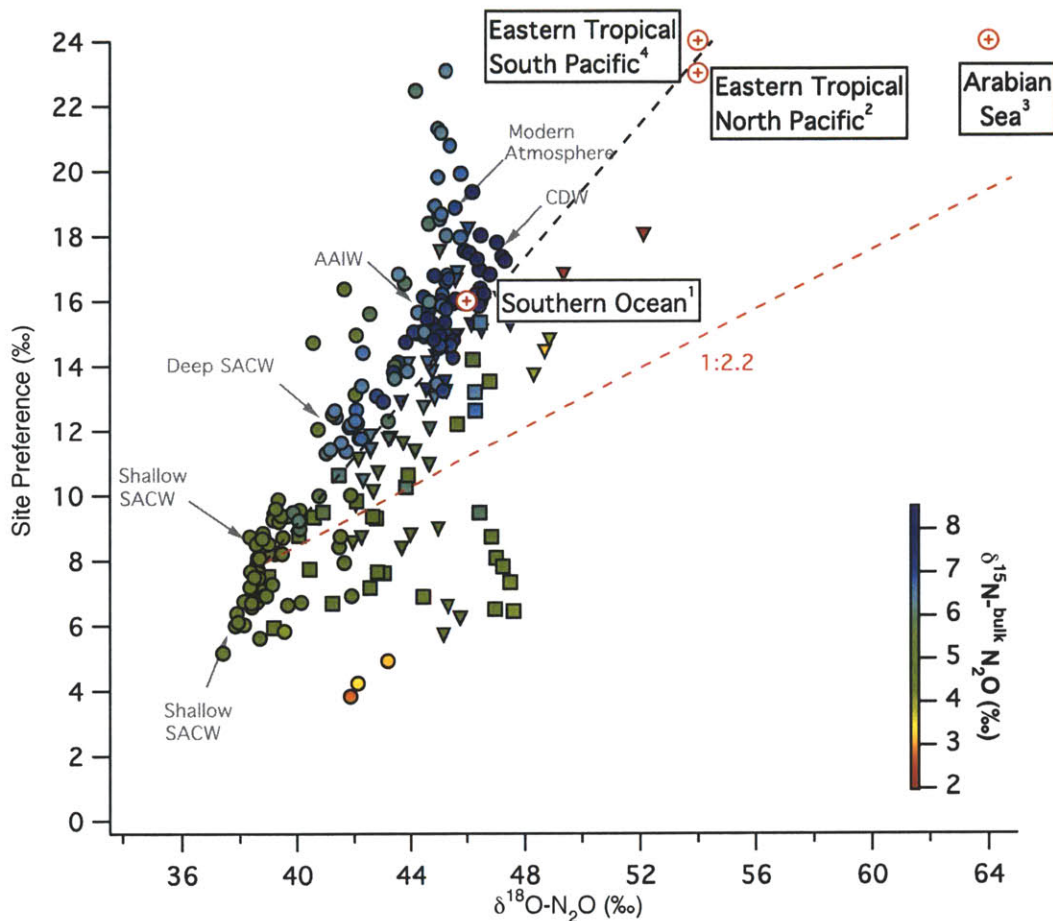
FIGURE 12. Site Preference versus $\delta^{18}O$-N_2O. The same data from Figure 11 have been included on rescaled axes that show data from two major ODZs and the Southern Ocean. Export from the deep N_2O concentration maxima in the Eastern Tropical North Pacific and the Arabian Sea contribute isotopically enriched, high SP N_2O to the total marine signal. The 1:2.2 line indicates the isotopic impact of N_2O consumption by denitrifiers, as measured by Ostrom et al. (2007). 1. Boontanon et al (submitted), 2. Popp et al 2002, Yamagishi et al 2007, 3. Mcilvin and Casciotti 2010, 4. Charpentier et al 2007.
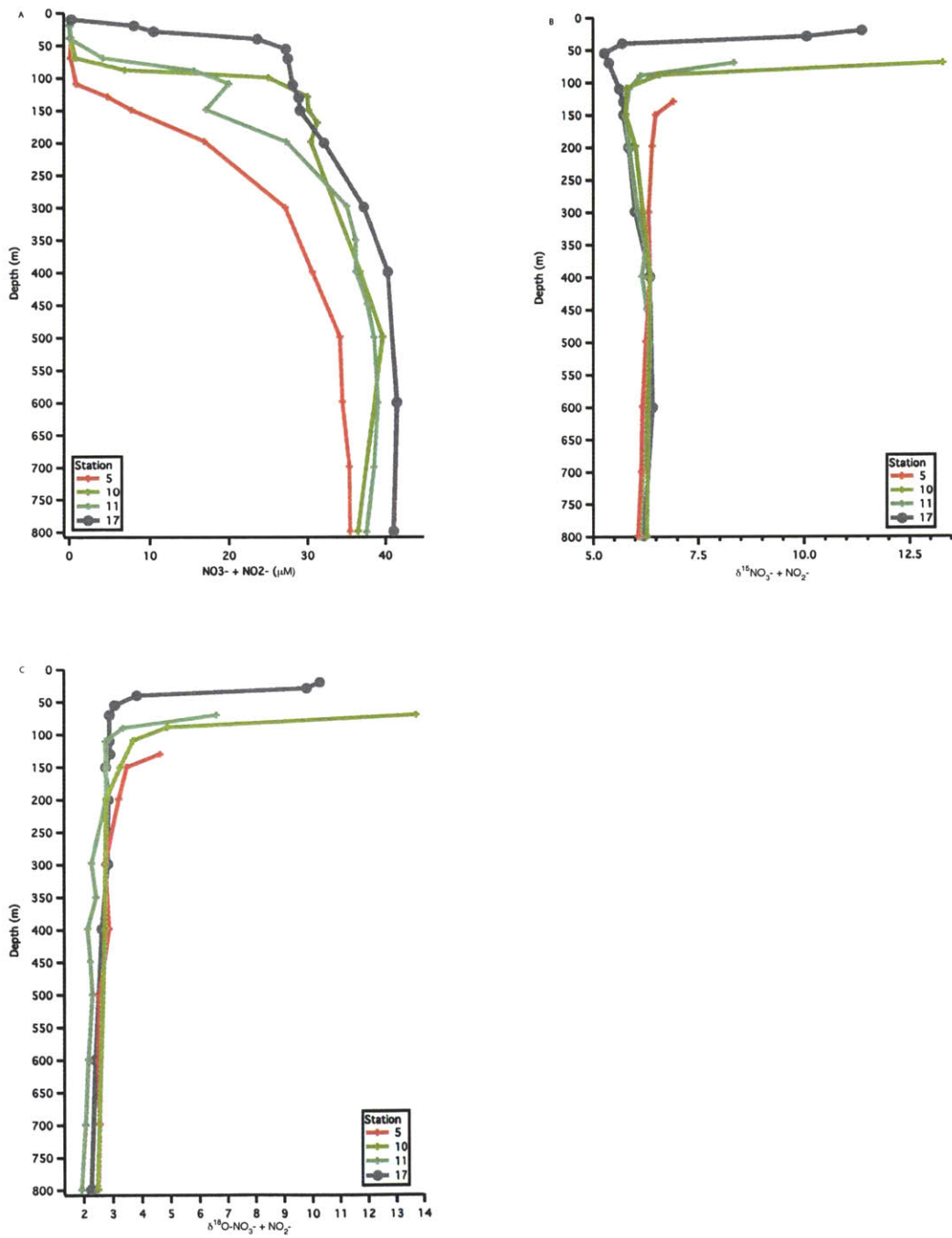
FIGURE 13. $NO_3^- + NO_2^-$ concentration profiles from stations 5, 10, 11, and 17 of the northern transect (a). $\delta^{15}N\text{-}NO_3^- + NO_2^-$ (b) and $\delta^{18}O\text{-}NO_3^- + NO_2^-$ (c) at the same stations.
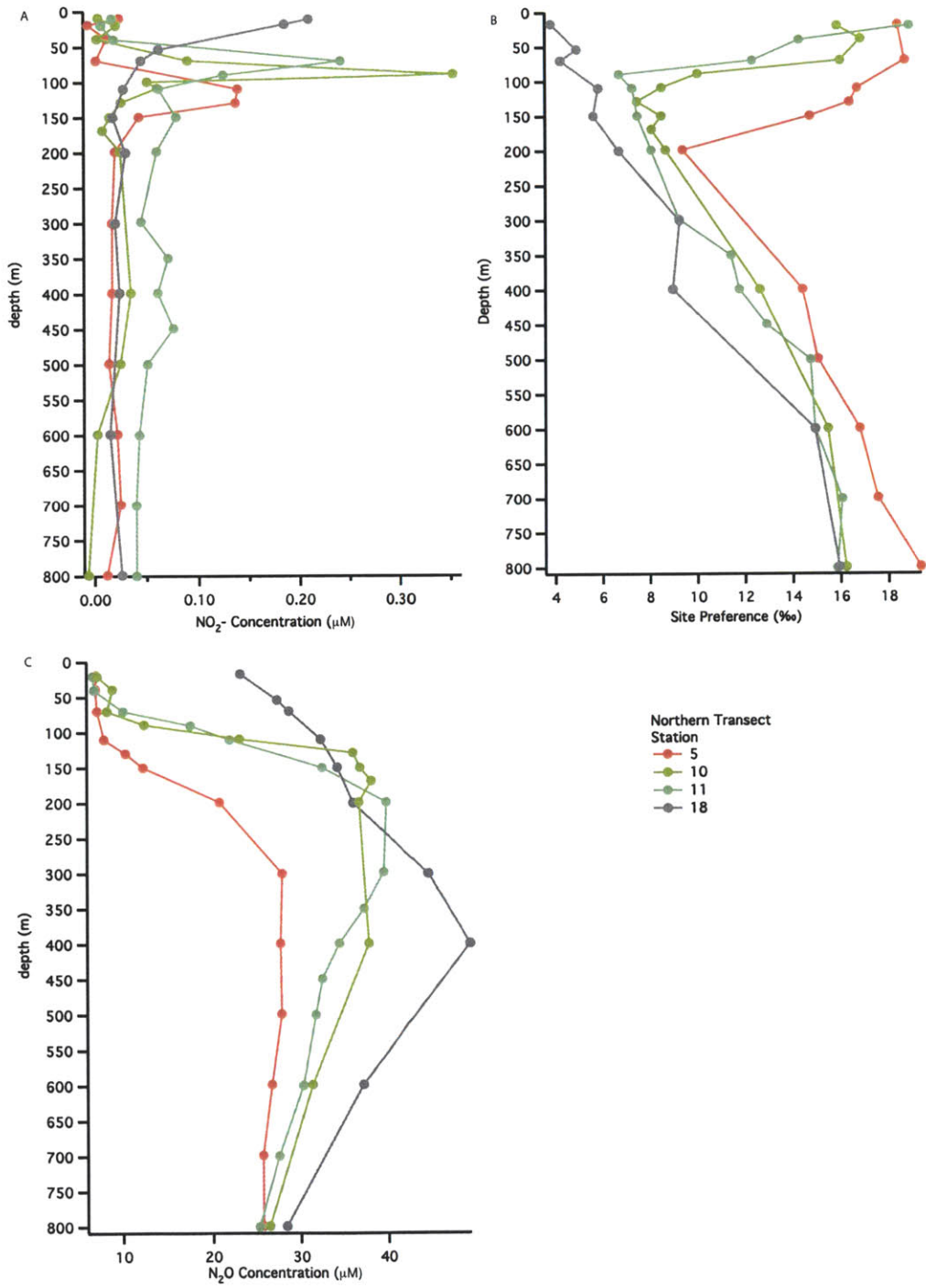
FIGURE 14. NO_2^- concentration (a), SP (b), and N_2O concentration (c) for stations sampled during the day.

135
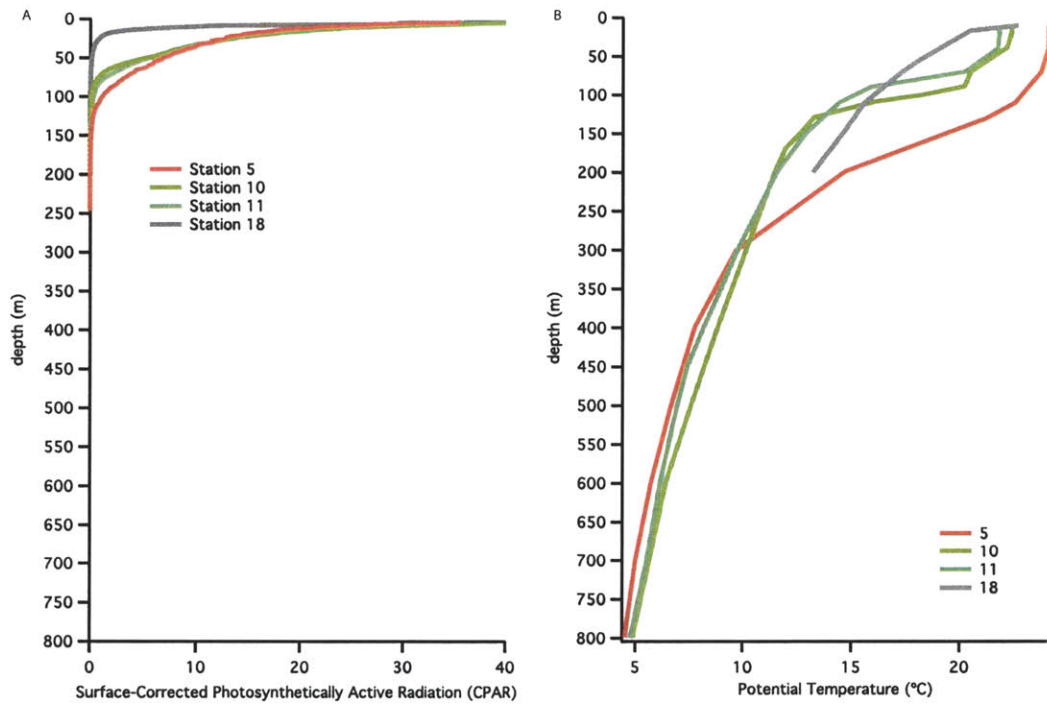
FIGURE 15. CPAR (a) and potential temperature (b) profiles at stations 5, 10, 11, and 18.

TABLE 1. AG upwelling N_2O remineralization stoichiometries. N_2O concentrations are in nM, O_2 concentrations are in μM

Source	ΔN_2O	ΔO_2	$\Delta N_2O/\Delta O_2$	AG [O_2]
Shallow (Cluster A)	3.7	-14.6	-0.25	39
Conc. Max. (Cluster H)	3.7	-38.2	-0.17	31
Deep (Cluster I)	3.7	-33.5	-0.11	83

TABLE 2. O_2 and N_2O isotopic signatures (in ‰) when the fractionation factor of respiration (α) = 0.981

$O_{2_{measured}}/O_{2_{initial}}$	$\delta^{18}O\text{-}N_2O$	$\delta^{18}O\text{-}O_2$
0.0	42.5	-
0.1	38.0	68.2
0.5	29.4	36.8
1.0	-	23.5

TABLE 3. O_2 and N_2O isotopic signatures (in ‰) when the fractionation factor of respiration (α) = 0.990

$O_{2_{measured}}/O_{2_{initial}}$	$\delta^{18}O\text{-}N_2O$	$\delta^{18}O\text{-}O_2$
0.0	33.4	-
0.1	31.0	46.8
0.5	26.6	30.5
1.0	-	23.5

FIGURE 16

TABLE 4. Isotope effects for N_2O production by denitrification. Under "system," open and closed refer to whether the system is open or closed with respect to NO_3^-

signature	$\epsilon_{expressed}$ (‰)	NO_3^- consumption	system	N_2O consumption	citation
$\delta^{15}N$	-23.5 − -28.6	steady-state	open	no	Granger et al. (22); Barford et al. (2)
$\delta^{15}N$	-15	steady-state	open	steady-state	Barford et al. (2)
$\delta^{15}N$	0	complete	closed	-	
$\delta^{15}N$	>-15	−	−	partial	Ostrom et al. (46) w/ Barford et al. (2)
$\delta^{18}O$	+18	steady-state	open	no	Granger et al. (22); Casciotti et al. (8)
$\delta^{18}O$	+29 − +33	steady-state	open	steady-state	Granger et al. (22); Ostrom et al. (46)
$\delta^{18}O$	+40	complete	closed	no	Casciotti et al. (8)
$\delta^{18}O$	>+40	−	−	partial	Ostrom et al. (46) w/ Casciotti et al. (8)

5. CONCLUSIONS

1. SUMMARY

Humans have more than doubled the global fixed nitrogen budget (Galloway et al., 1995). About 2% of this added nitrogen is converted to N_2O by microbial processes in soil and the ocean (Nevison et al., 1996). These processes, nitrification and denitrification, are both known to produce N_2O, but neither their relative contributions to the total annual source nor the environmental conditions that control their N_2O output are well understood. Marine nitrification and N_2O production rates are difficult to quantify because they are often low and highly variable. Furthermore, the temporal and spatial coverage of the measurements that have been made are low (Yool et al., 2007). Isotopic tracer incubations provide a sensitive way of tracking and quantifying the biological processes that produce N_2O but they are labor intensive and provide information about only a single location and time. Natural abundance isotopic signatures record the effects of processes over longer temporal and spatial scales. However, the trade-off made relying on these data is in the ease and certainty of interpreting their meaning. As we pointed out in the discussions of Chapter 2 and Chapter 4, different biological processes can produce N_2O with the same isotopic signatures. Furthermore, physical mixing between isotopically distinct sources and co-location of isotopically distinct biological sources could result in N_2O types that appear isotopically similar even though their origins are unrelated.

Three separate approaches to quantifying N_2O production were taken in the preceding chapters. In Chapter 2, pure cultures of the marine ammonia-oxidizing bacterium *Nitrosomonas marina* C113-a were used as a model for N_2O production by nitrifying microorganisms. While Chapter 2 tested some of the chemical factors already known to enhance N_2O yields from nitrifiers (such as low ambient O_2 and high NO_2^- concentrations) we found that the abundance or density of nitrifier cells in the growth medium actually has a substantial impact on N_2O yields–with denser cultures producing higher yields. At the lower cell densities that we tested, measured yields were lower than had been previously reported (Goreau et al., 1980). It was only when cell densities were extremely high that we observed the dramatic increases in yield previously noted when cultures were grown under low O_2

conditions. Our work suggests that future efforts to model marine N_2O production might be improved with additional biological information such as microbial or nitrifier cell counts, or overall biological activity or biomass concentrations.

The second half of Chapter 2 focused on finding ways to distinguish different biological sources of N_2O using stable isotopic measurements. To do this, the two biochemical pathways that produce N_2O in ammonia-oxidizing bacteria were separated by manipulating culture conditions to promote the production of N_2O from one pathway relative to the other and then using a model to fully resolve the end-member nitrogen and oxygen signatures of both pathways. This work is important because it demonstrates that a single bacterial nitrifier species can produce N_2O with a range of isotopic signatures that is quite broad given the variation observed in the ocean. However, this variation follows some patterns that may be useful in future efforts to identify nitrifier-dependent sources of N_2O in the ocean. In particular, the incorporation of oxygen atoms into N_2O from isotopically distinct source molecules (i.e. H_2O and O_2) is biochemically linked to the abundance and distribution of ^{15}N atoms in N_2O. Future work pairing these oxygen and nitrogen natural abundance isotopic measurements with rate measurements of the major N_2O producing processes would help us determine whether what we observe in culture is also playing out in the environment.

In Chapter 3 we also investigated the size of nitrification N_2O yields and possible environmental controls on this size. However, here the system under scrutiny was an actual microbial community from the coastal waters of Cape Cod. Potential nitrification rate measurements were paired with N_2O production rate measurements during a spring bloom of the cyanobacteria *Synechococcus*. While potential nitrification rates were low and did not change significantly over the course of the bloom, the rates of N_2O production did rise with the density of the bloom. Interestingly, N_2O yields measured in this way were about ten times higher than those measured in Chapter 2 for ammonia-oxidizing bacteria. Additional rate measurements, as well as other types of data would be helpful in resolving whether this relationship is robust and if so, what the underlying chemical or biological mechanisms might be. Ideally, in addition to the rates, we would also have data on nitrifier cell

144

abundances and phylogenetic affinities, as well as dissolved and particulate organic matter concentrations, other phytoplankton species abundances, and chlorophyll-a concentrations. As they stand now, the results of this chapter suggest that we may need to consider other environmental factors beyond ambient NO_2^- and O_2 concentrations when investigating what controls N_2O production by nitrifiers.

In Chapter 4, N_2O measurements made in a coastal upwelling zone off of southwestern Africa were used to investigate possible environmental controls and mechanisms of marine N_2O production. In this region, N_2O concentrations increased as O_2 concentrations dropped and nutrient concentrations increased along the transition from the oligotrophic subtropical gyre to the highly productive waters of the Angola Dome and Benguela upwelling off the African coast. Relative to O_2 consumption, the highest yields of N_2O were observed at shallower depths, just below the top of the thermocline. The bulk and site specific isotopic signatures of this N_2O were consistent with a nitrifier-denitrification or denitrification source. In the deeper concentration maximum, where yields were lower, these N_2O signatures were consistent with a contribution from nitrification. Although N_2O consumption by denitrification was probably not an important process in the upwelling environment itself, subsurface water recirculating from the major oxygen deficient zones into the Southern Ocean may have been recirculated into the South Atlantic and upwelled along the the African coast.

2. OUTLOOK

There are a number of approaches to measuring N_2O yields in the ocean. This thesis has focused on bottom-up approaches, which quantify the sizes and isotopic signatures of individual N_2O sources. The approach of Freing et al. (2009) pushed this half of the field forward by using transient chemical tracers to couple N_2O concentration measurements to water mass age distributions, allowing them to calculate subsurface N_2O production rates and O_2 consumption rates independently of each other. However, this method can only be applied below the depths that are in direct exchange with the atmosphere and it does not provide mechanistic information about N_2O formation. Other approaches will be needed to

measure the N_2O fluxes resulting from nitrification in the top of the thermocline or within the euphotic zone.

The bottom-up approach to flux estimation also awaits yield and isotopic signature data for archaeal nitrifiers. These organisms are abundant in the oceans, often outnumbering bacterial ammonia oxidizers, and are now thought to be responsible for much of the ammonia oxidation in the ocean (Agogue et al., 2008; Martens-Habbena et al., 2009). Only one representative of this group has been successfully isolated to date (Konneke et al., 2005). Genomic and metatranscriptomic evidence indicates that in addition to the ammonia oxidation enzyme, these organisms may also produce an enzyme homologous to NirK (Walker et al., 2010; Hollibaugh et al., 2010), which carries out the first step of nitrifier-denitrification. Information on the production of N_2O by these organisms may explain some of the discrepancies observed between N_2O made by bacterial ammonia oxidizers in Chapter 2 and the observations that we made in the South Atlantic in Chapter 4.

Top-down approaches to identifying and measuring N_2O sources are also gaining attention. These methods, which use atmospheric models and continuous measurements of atmospheric N_2O concentrations, were originally geared towards estimating regional anthropogenic N_2O emissions (Prinn et al., 1990). However, they are now being used to identify seasonal and inter annual patterns in marine N_2O fluxes. As these methods are refined, they will be able to isolate small seasonal changes in biological fluxes from larger, physically driven fluxes such as air-sea gas exchange (Nevison et al., 2005, 2007). Isotopic measurements now being added to these studies may provide additional information on source identities and sizes. In the geological past, atmospheric N_2O concentrations changed rapidly during glacial-interglacial transitions (Fluckiger et al., 1999, 2004). Human perturbation of the nitrogen cycle has moved the earth into another period of rapid N_2O increase. Understanding the underlying biogeochemistry of this increase will allow meaningful predictions of the impacts of climate change on future atmospheric N_2O concentrations.

Although the focus of much N_2O research has been on the impact of human activities, another question that remains is what other drivers are responsible for the increases

146

in atmospheric N_2O concentrations during glacial-interglacial transitions (Sowers and Galbraith, 2008). N_2O may behave like another biogenic greenhouse gas, methane (CH_4), whose glacial-interglacial atmospheric concentration changes have been attributed to changes in wetland CH_4 emissions. However, recent efforts to reconstruct the geological N_2O record using modeling have shown that changes in meridional overturning circulation in the ocean can also reproduce the increase in N_2O concentration observed during rapid warming and cooling events (Schmittner et al., 2008). Further oceanographic work will help elucidate how changes in primary production and thermocline oxygen budgets influence the current and past N_2O budget.

REFERENCES

Agogue, H., Brink, M., J, D., and Herndl, G. J. (2008). Major gradients in putatively nitrifying and non-nitrifying archaea in the deep north atlantic. *Nature*, 456(788-791).

Fluckiger, J., Blunier, T., Stauffer, B., Chappellaz, J., Spahni, R., Kawamura, K., Schwander, J., Stocker, T. F., and Dahl-Jensen, D. (2004). N_2O and CH_4 variations during the last glacial epoch: insight into global processes. *Global Biogeochemical Cycles*, 18(GB1020):doi:10.1029/2003GB002122.

Fluckiger, J., Dallenbach, A., Blunier, T., Stauffer, B., Stocker, T. F., Raynaud, D., and Barnola, J.-M. (1999). Variations in atmospheric N_2O concentration during abrupt climatic changes. *Science*, 285:227–230.

Freing, A., Wallace, D. W. R., Tanhua, T., Walter, S., and Bange, H. W. (2009). North Atlantic production of nitrous oxide in the context of changing atmospheric levels. *Global Biogeochemical Cycles*, 23(GB4015):doi:10.1029/2009GB003472.

Galloway, J. N., Schlesinger, W. H., Levy II, H., Michaels, A., and Schnoor, J. L. (1995). Nitrogen fixation: anthropogenic enhancement-environmental response. *Global Biogeochemical Cycles*, 9(2):235–252.

Goreau, T. J., Kaplan, W. A., Wofsy, S. C., McElroy, M. B., Valois, F. W., and Watson, S. W. (1980). Production of NO_2^- and N_2O by nitrifying bacteria at reduced concentrations of oxygen. *Applied and Environmental Microbiology*, 40(3):526–532.

Hollibaugh, J. T., Gifford, S., Sharma, S., Bano, N., and Moran, M. A. (2010). Meta-transcriptomic analysis of ammonia-oxidizing organisms in an estuarine bacterioplankton assemblage. *ISME Journal*, pages 1–13.

Konneke, M., Bernhard, A. E., de la Torre, J. R., Walker, C. B., Waterbury, J. B., and Stahl, D. A. (2005). Isolation of an autotrophic ammonia-oxidizing marine archaeon. *Nature*, 437(543-546).

Martens-Habbena, W., Berube, P. M., Urakawa, H., de la Torre, J. R., and Stahl, D. A. (2009). Ammonia oxidation kinetics determine niche separation of nitrifying archaea and bacteria. *Nature*, 461:976–981.

Nevison, C. D., Esser, G., and Holland, E. A. (1996). A global model of changing N_2O emissions from natural and perturbed soils. *Climate Change*, 32:327–378.

Nevison, C. D., Keeling, R. F., Weiss, R. F., Popp, B. N., Jin, X., Fraser, P. J., Porter, L. W., and Hess, P. G. (2005). Southern ocean ventilation inferred from seasonal cycles of atmospheric N_2O and O_2/N_2 at Cape Grim, Tasmania. *Tellus*, 57B(3):218–229.

Nevison, C. D., Mahowald, N. M., Weiss, R. F., and Prinn, R. G. (2007). Inter-annual and seasonal variability in atmospheric N_2O. *Global Biogeochemical Cycles*, 21(GB3017):doi:10.1029/2006GB002755.

Prinn, R., Cunnold, D., Rasmussen, R., Simmonds, P., Alyea, F., Crawford, A., Fraser, P., and Rosen, R. (1990). Atmospheric emissions and trends of nitrous oxide deduced from 10 years of ALE − GAGE data. *Journal of Geophysical Research*, 95(D11):18369–18385.

Schmittner, A., Oschlies, A., Matthews, H. D., and Galbraith, E. D. (2008). Future changes in climate, ocean circulation, ecosystems, and biogeochemical cycling simulated for a business-as-usual co2 emission scenario until year 4000 ad. *Global Biogeochemical Cycles*, 22(GB1013):doi:10.1029/2007GB002953.

Sowers, T. and Galbraith, E. (2008). Glacial greenhouse-gas fluctuations controlled by ocean circulation changes. *Nature*, 456(373-376).

Walker, C. B., de la Torre, J. R., Klotz, M. G., H, U., Pinel, N., Arp, D. J., Brochier-Armanet, C., Chain, P. S. G., Chan, P. P., Gollabgir, A., and Hemp (2010). *Nitrosop-umilus maritimus* genome reveals unique mechanisms for nitrification and autotrophy in

globally distributed marine crenarchaea. *Proceedings of the National Academy of Science*, 107(19):8818–8823.

Yool, A., Martin, A., Fernandez, C., and Clark, D. (2007). The significance of nitrification for oceanic new production. *Nature*, 447:999–1002.